How G-quadruplex ligands enhance the innate immune response in BRCA1/2-deficient cells and tumours

Yanti De Visser

St Cross College



A thesis submitted to the University of Oxford for the degree of MSc by Research

Genome Stability and Tumourigenesis Group

Department of Oncology

University of Oxford

Michaelmas Term 2020

Contents

Acknowledgements **v**

Abstract **vi**

List of Abbreviations **vii**

List of Tables **xii**

List of Figures **xiii**

List of Supplementary Figures **xv**

1 Introduction **1**

1.1 DNA repair 1

1.1.1 Homologous recombination 2

1.1.2 Non-homologous end-joining 4

1.2 BRCA-deficiency in tumours 5

1.2.1 Consequences of BRCA-deficiency in tumourigenesis 5

1.3 G-quadruplexes as a tool for cancer treatment 7

1.3.1 G-quadruplex 7

1.3.2 Occurrence in the human genome 8

1.3.3 G-quadruplex ligands . . . 9

1.3.4 G4 ligands as cancer therapy . . . 9

1.4 Innate immune response . . . 10

1.4.1 Immune response caused by DNA-damage . . . 11

1.4.2 Immune response activation . . . 11

1.4.3 Antitumour immunity . . . 12

1.5 Paclitaxel . . . 13

1.5.1 Origin . . . 13

1.5.2 Application . . . 13

2 Aim **14**

3 Material and methods **15**

3.1 Cell lines . . . 15

3.2 Viability assay . . . 15

3.3 Western blot . . . 17

3.4 Immunofluorescence . . . 19

3.5 RT-qPCR . . . 20

3.5.1 RNA extraction and cDNA synthesis . . . 20

3.5.2 qPCR . . . 20

3.5.3 Calculations . . . 21

3.6 Flow cytometry . . . 22

3.6.1 Apoptotic assay . . . 22

3.6.2 Propidium iodide staining . . . 22

4 Results **23**

4.1 Pyridostatin induced immune response . . . 23

4.2 Combination treatment of paclitaxel and PDS . . . 27

4.3 Characterisation of HAP1 *p53*$^{-/-}$ *BRCA2*$^{-/-}$ cell line . . . 39

5 Discussions **43**

5.1 Pyridostatin activates the innate immune response . . . 44

5.2 Influence of paclitaxel on BRCA1/2-deficient cells . . . 45

5.3 PDS and paclitaxel synergism . . . 46

5.4 Unsuccessful BRCA2 knockout in HAP1 . . . 48

6 Conclusions **50**

7 Future perspectives **51**

8 Appendix **72**

Acknowledgements

While writing these last words, I would like to thank Madalena Tarsounas for welcoming me into her laboratory and guiding me through the project. This gave me the opportunity to develop myself more in every scientific aspect. I also like to thank my secondary supervisor Anderson Ryan for his guidance and availability.

Next, I would like to thank Florian Groelly for his close support and guidance, his availability at any time and his help with my Western blots. My appreciation to you, Rebecca, for your enormous amount of technical help and patience to explain me everything I needed to know to become the scientist that I currently am. Giuliana, your wise advise taught me more than only science and our lab parties will be a precious memory for me. Even though our time together was not as long as I hoped for, thank you Emilia for being there whenever I needed G-quadruplex advise or a coffee/crisps-break. I also want to thank you Yuri for your care and friendship. In general, I would like to show my appreciation to everyone in the Tarsounas lab who helped me in the past year and by proofreading this thesis.

Finally, I am extremely grateful for my parents' support, both emotionally and financially. Without you, I would not have been able to be here in Oxford and achieve what we could only dream of. Thank you Jonas, Jirina and Jorne for your everlasting love and support, your motivational calls and faith in me. Tobias, I am blessed to have you by my side. Without your love and encouragement I would not have been able to complete this work.

How G4 ligands enhance the innate immune response in BRCA1/2-deficient cells and tumours

A thesis submitted to the University of Oxford for the degree of MSc by Research

Yanti De Visser

St Cross College, Michaelmas Term 2020

G-quadruplex binding ligands, like pyridostatin, are known to cause DNA damage and eventually trigger apoptosis (Rodriguez et al., 2012; Zimmer et al., 2016). The stabilisation of G-quadruplexes causes replication fork stalling resulting in DNA damage accumulation and subsequent activation of DNA damage repair pathways such as homologous recombination (Rodriguez et al., 2012). However, tumours lacking BRCA1 and BRCA2 expression, and consequently abrogation of homologous recombination, will accumulate this damage and will therefore be killed more efficiently. Nonetheless, how the pyridostatin induced damage can selectively cause apoptosis in BRCA-deficient cells is currently unknown. Here, we show that pyridostatin potentially triggers apoptosis by activating the innate immune response. We found that pyridostatin activates the innate immune response. This is likely induced by the accumulation of micronuclei, which are DNA carrying cytosolic bodies known to activate the innate immune response, ultimately leading to cell death. (Gisselsson et al., 2001). Our results demonstrate how the G-quadruplex ligand pyridostatin can selectively kill BRCA1 and BRCA2-deficient cells and tumours upon activation of the innate immune response. Additionally, the combination of pyridostatin with the chemotherapeutic paclitaxel showed a synergistic effect in tumours lacking BRCA1, resulting in more efficient induction of apoptosis.

List of Abbreviations

53BP1	p53 binding protein 1
ADB	antibody dilution buffer
ADP	adenosine diphosphate
AMP	adenosine monophosphate
aNHEJ	alternative non-homologous end-joining
APC	antigen presenting cell
ATM	ataxia telangiectasia mutated
ATP	adenosine triphosphate
BARD1	BRCA1 associated RING-domain
Bcl-2	B-cell lymphoma 2
BER	base excision repair
BLM	Bloom syndrome protein
BRCA1	breast cancer 1
BRCA2	breast cancer 2
BSA	bovine serum albumin
cGAMP	cyclic GMP-AMP
cGAS	cyclic GMP-AMP synthase
CHK2	checkpoint kinase 2
clPARP	cleaved PARP

cNHEJ	classic non-homologous end-joining
C^t	threshold cycle
CtIP	CtBP interacting protein
DAPI	4', 6-diamidino-2-phenylindole
DMEM	Dulbecco's modified Eagle's medium
DMSO	Dimethyl sulfoxide
DNA-PKcs	DNA-dependent protein kinase catalytic subunits
DNA2	DNA replication helicase/nuclease 2
DOX	doxycycline
DSB	double-strand break
dsDNA	double-stranded DNA
DTT	dithiothreitol
EdU	5-ethynyl-2' deoxyuridine
EXO1	exonuclease 1
FBS	foetal bovine serum
G4	G-quadruplex
GAPDH	Glyceraldehyde 3-phosphate dehydrogenase
GDP	guanosine diphosphate
γH2AX	phosphorylated H2AX
GMP	guanosine monophosphate

GTP	guanosine triphosphate
Gy	gray
HR	homologous recombination
IFIT2	interferon induced protein with tetratricopeptide repeats 2
IFN	interferon
IgG	immunoglobulin G
IM	intramuscular
IMDM	Iscove's modified Dulbecco's medium
IP	interperitonial
IRF3	IFN regulatory factor 3
ISG	interferon stimulated gene
IV	intravenous
MDC1	mediator of DNA damage checkpoint protein 1
MDM2	mouse double minute 2
MMR	mismatch repair
MOPS	3-(N-morpholino) propanesulfonic acid
MRN	MRE11-RAD50-NBS1
NBS1	Nijmegen breakage syndrome 1
NER	nucleotide excision repair
NHEJ	non-homologous end-joining

OAS2	2'-5'-oligoadenylate synthetase 2
PALB2	partner and localiser of BRCA2
PARP1	poly-[ADP-ribose]polymerase 1
PBS	phosphate-buffered saline
PBST	0.05% Tween in PBS
PCR	polymerase chain reaction
PDS	pyridostatin
PI	propidium iodide
pIRF3	phosphorylated IRF3
pKAP1	phosphorylated KAP1
RNF8	ring finger protein 8
RPA	replication protein A
SD	standard deviation
SCID	severe combined immunodeficient
SDS	sodium dodecyl sulphate
SEM	standard error of the mean
SMC1	Structural maintenance of chromosomes protein 1
SSA	single strand annealing
SSB	single-strand break
ssDNA	single-stranded DNA

STING stimulator of IFN gene

TBK1 TANK-binding kinase 1

UV ultraviolet

XLF XRCC4-like factor

XRCC4 X-ray repair cross-complementing protein 4

List of Tables

3.1 Primary antibodies used for Western blot 18

3.2 Secondary antibodies used for Western blot 19

3.3 Antibodies used for immunofluorescence staining 19

3.4 Primers used for RT-qPCR 21

3.5 Programme for RT-qPCR reaction 21

List of Figures

1.1 Illustration of homologous recombination 3

1.2 Illustration of classic non-homologous end joining 6

1.3 G-quadruplex formation 8

1.4 Illustration of cGAS-STING pathway activation 12

3.1 Cell seeding layout for viability assay 16

3.2 Treatment layout for viability assay 17

4.1 DLD1 *BRCA2*$^{-/-}$ cells are sensitive to the DNA damaging agents PDS and olaparib . 24

4.2 Innate immune response is activated in H1299 upon treatment with PDS or olaparib 26

4.3 PDS and paclitaxel combination treatment *in vivo* kills BRCA1-deficient tumours more effectively 28

4.4 Paclitaxel unable to activate the innate immune response in BRCA2-deficient cells. . 29

4.5 Combination treatment does not trigger more apoptosis *in vitro* compared to single agent treatments 30

4.6 Paclitaxel induces cell cycle changes in BRCA-deficient cells 32

4.7 Innate immune response activation upon combination treatment in H1299 and MDA-MB-436. 34

4.8 Paclitaxel treated cells accumulate in G2/M, resulting in abnormal chromosomal content 36

4.9 Paclitaxel and combination treatment cause abnormal chromosomal content 38

4.10 Sensitivity of HAP1 cells for olaparib 40

4.11 No full length BRCA2 is detected using Western blot 41

4.12 Confirmation of BRCA2 status via immunofluorescence 42

List of Supplementary Figures

1 Innate immune response activation in H1299 upon treatment with olaparib 72

2 No synergistic effect on triggering apoptosis *in vitro* upon combination treatment . . 73

3 The influence of single and combination treatment on the cell cycle and chromosomal content of H1299 - Replicate 1 74

4 The influence of single and combination treatment on the cell cycle and chromosomal content of H1299 - Replicate 2. 75

5 The influence of single and combination treatment on the cell cycle and chromosomal content of H1299 - Replicate 3 76

6 The influence of single or combination treatment on the chromosomal content of H1299 - Replicate 1 77

7 The influence of single or combination treatment on the chromosomal content of H1299 - Replicate 2 78

8 The influence of single or combination treatment on the chromosomal content of H1299 - Replicate 3 79

9 The influence of single or combination treatment on the chromosomal content of MDA-MB-436 - Replicate 1 80

10 The influence of single or combination treatment on the chromosomal content of MDA-MB-436 - Replicate 2 81

11 The influence of single or combination treatment on the chromosomal content of MDA-MB-436 - Replicate 3 82

1 Introduction

When a cell duplicates, 6 x 10^9 nucleotides have to be replicated (Heyer et al., 2010; Tubbs and Nussenzweig, 2017b). This process is among other things carried out by polymerases, which are not error-proof. They cause DNA damage at a low but constant speed and ultimately result in about 70,000 lesions per cell and per day (Lindahl and Barnes, 2000; Tubbs and Nussenzweig, 2017b). Each of these lesions can increase the risk of cancer development if they are not dealt with by the mismatch repair system (Aaltonen et al., 2007). Another form of DNA damage with high tumourigenesis potential is DNA breaks. This can be a single-strand break (SSB) or a double-strand break (DSB), induced by for example ionising or ultraviolet (UV)-irradiation or DNA-damaging agents (Featherstone and Jackson, 1999; Negritto, 2010). Even though SSBs are the most frequently observed lesions, they can easily transform into DSBs, resulting in genomic instability that predisposes people to cancer and other diseases (Fedor et al., 2013). Consequently, it is essential that cells repair these lesions and restore genome integrity.

1.1 DNA repair

It was already known since the early 1940's that exposure to certain exogenous agents like UV or X-ray introduces mutations in the DNA causing genome instability (Hollaender and Curtis, 1935; Friedberg, 2008). At this time, one still presumed that DNA was intrinsically stable but could not handle the exogenous introduction of mutations. However, it was only after discovering the double helix structure of DNA that scientists found evidence of endogenous DNA damage accumulation (Tubbs and Nussenzweig, 2017a) and precise mechanisms for what was later termed as "DNA-repair". There are various DNA repair mechanisms, all active during different cell cycle stages and dependant on the nature of the DNA damage. For SSB repair, pathways like nucleotide excision repair (NER), base excision repair (BER) or mismatch repair (MMR) are known (De Laat et al., 1999; Schärer, 2013; Krokan and Bjørås, 2013). These pathways were reviewed in detail elsewhere (Kunkel and Erie, 2005; Zharkov, 2008; Spivak, 2015) and are out of this thesis' scope. This work,

will focus on the two key pathways for DSB repair: homologous recombination (HR) and classic non-homologous end-joining (cNHEJ).

1.1.1 Homologous recombination

HR's most acknowledged activity is the repair of DSBs, but it also plays a role in protecting and restarting stalled replication forks (Carr, 2002; Feng and Jasin, 2017; Rickman and Smogorzewska, 2019). If DSBs are not accurately repaired, the genome's integrity will be affected with an enhanced risk of cancer development (Mills et al., 2003; Wang et al., 2013). HR is considered an error-free pathway for the repair of DSBs (Porteus, 2007). It is a slow mechanism compared to other DNA-repair mechanisms and requires a template to complete its task. This constraint explains the restriction of HR activity only to the late-S and G2 phases when sister chromatids are present to be used as a template (Aylon et al., 2004; Ira et al., 2004; Zhao et al., 2017b). In rare cases, the homologous chromosome can be used as a template for HR during G1.

When DSBs occur, the MRN complex consisting of MRE11, RAD50 and Nijmegen breakage syndrome 1 (NBS1) forms and binds ataxia telangiectasia mutated (ATM) (Jazayeri et al., 2006; Williams et al., 2009), as shown in Figure 1.1. Auto-phosphorylation activates the complex and binds on either side of the DSBs (Kozlov et al., 2011). Next, ATM phosphorylates H2AX, known as γH2AX, and checkpoint kinase 2 (CHK2) resulting in activation of the protein which subsequently phosphorylates p53 (Delia et al., 2000; Jazayeri et al., 2006; Williams et al., 2009). At the same time, the mediator of DNA damage checkpoint protein 1 (MDC1) binds γH2AX and will also be phosphorylated by ATM (Williams et al., 2009; Stracker and Petrini, 2011), which can recruit the E3 ubiquitin ligase ring finger protein 8 (RNF8) (Dickey et al., 2010; Hustedt and Durocher, 2017). RNF8 performs ligation of the K63 poly-ubiquitin chains onto histones adjacent to the DSB. It activates the recruitment of DSB factors like breast cancer 1 (BRCA1) and p53 binding protein 1 (53BP1) to the position of damage (Hustedt and Durocher, 2017).

Simultaneously with the phosphorylation of p53 by CHK2, ATM also phosphorylates mouse double

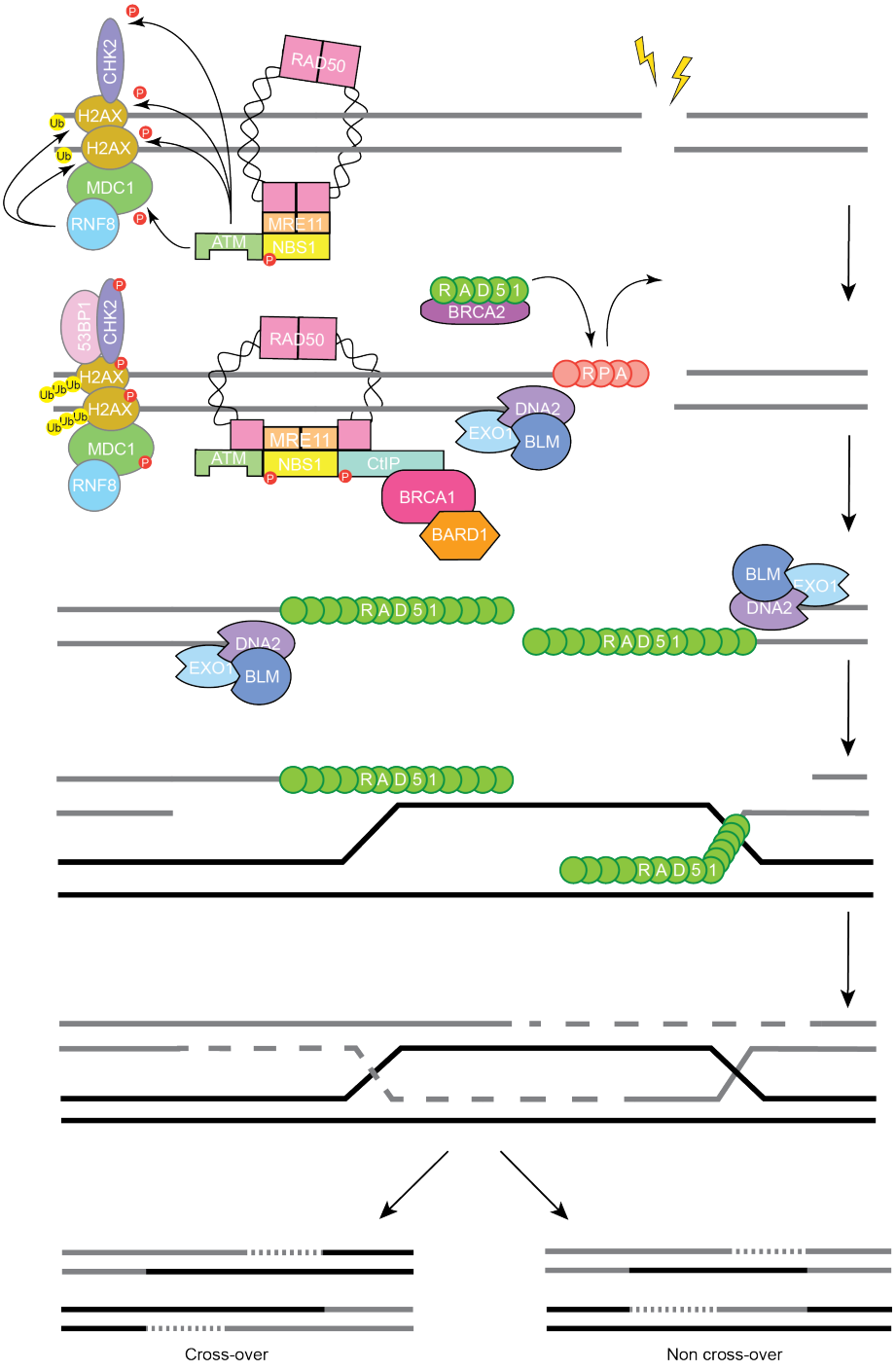


Figure 1.1: Illustration of homologous recombination

minute 2 (MDM2) and p53 to avoid their heterodimerisation and subsequent activation (Canman et al., 1998; Khosravi et al., 1999; Delia et al., 2000). After that, CtBP interacting protein (CtIP) binds onto NBS1 at the MRN complex together with the previously recruited BRCA1, in complex with BRCA1 associated RING-domain (BARD1) (Williams et al., 2009; Wang et al., 2013). Subsequently, exonuclease 1 (EXO1), and the helicase-nuclease complex Bloom syndrome protein (BLM)-DNA replication helicase/nuclease 2 (DNA2) create a 3' overhang up to ± 1000 base-pairs (Nimonkar et al., 2008; Karanja et al., 2012). To prevent the single-stranded DNA (ssDNA) to form secondary structures or being degraded by other nucleases, replication protein A (RPA) binds on the ssDNA 3' overhang (Krogh and Symington, 2004; Stracker and Petrini, 2011). Then, breast cancer 2 (BRCA2) is recruited by BRCA1 and replaces RPA with RAD51 forming nucleoprotein filaments (Krogh and Symington, 2004; Nimonkar et al., 2008; Hustedt and Durocher, 2017). When BRCA1 and RAD51 filaments interact, they can search and recruit the sister chromatid's matching DNA strand (Krogh and Symington, 2004). Strand invasion occurs, RAD51 leaves the 3' overhang, the displacement-loop is set up, and the Holliday junction is formed (Pâques and Haber, 1999; Heyer et al., 2010). The resolution of the latter structure by resolvases is responsible for introducing genetic diversity by cross-over (Whitby, 2007). DNA polymerases are now required to extend the 3' overhang. The last nucleotide to close the gap will be inserted by DNA ligase.

1.1.2 Non-homologous end-joining

Because of HR's restriction to the late-S and G2 phases, cells need an alternative way to repair DNA damage occurring during other phases of the cell cycle (Aylon et al., 2004; Symington and Gautier, 2011). The pathway responsible for this is known as cNHEJ. It can repair DSBs fast ($t_{1/2}$ = 10-30 min) and efficiently but is error-prone compared to HR (Dueva and Iliakis, 2013). cNHEJ does not require a template for repair but instead joins DNA ends, possibly inserting alterations or causing translocations when multiple DSBs coincide (Khanna and Jackson, 2001; Aylon et al., 2004). When DSBs are detected, ATM phosphorylates the serine 139 residue of H2AX, resulting in γH2AX (Figure 1.2). Subsequently, the non-catalytic heterodimer Ku, a complex of

Ku70 and Ku80, binds the DSBs on both sides (Dynan and Yoo, 1998). DNA-dependent protein kinase catalytic subunits (DNA-PKcs) are subsequently recruited and interact with the Ku-complex resulting in the DNA-PK holoenzyme. Auto-phosphorylation of DN-PKcs promotes DNA-end tethering. Thereafter, Artemis is recruited and phosphorylated by DNA-PKcs while X-ray repair cross-complementing protein 4 (XRCC4) and XRCC4-like factor (XLF) guides Ligase IV onto the DNA to help to align, process and ligate both ends of the DSB (Khanna and Jackson, 2001; Lieber, 2010). Another related pathway for DSB repair is alternative non-homologous end-joining (aNHEJ). Even though the names are similar, the pathways are very different from each other. aNHEJ uses short homologous sequences to align the broken strands and is, therefore considered more accurate (Bennardo et al., 2008; Chang et al., 2017). The pathway is mainly active during the S and G2-phase of the cell cycle, similar to HR (Truong et al., 2013). Due to the higher accuracy of HR over aNHEJ, HR is preferred and even suppresses activation of aNHEJ (Ahrabi et al., 2016).

1.2 BRCA-deficiency in tumours

1.2.1 Consequences of BRCA-deficiency in tumourigenesis

BRCA1 and BRCA2 play an essential role in DNA repair of DSBs by HR. Deficiencies in these proteins are mostly correlated with cancer but in two different ways. First, heterozygous loss of BRCA1 or BRCA2 predisposes a patient to breast, ovarian and other cancers (Daly et al., 2010). Homozygous loss causes HR failure (Gudmundsdottir and Ashworth, 2006) and back-up pathways, such as single strand annealing (SSA) and NHEJ, have to repair the DSBs instead (Tutt et al., 2001). Error-prone repair of DSBs by these pathways induce mutations and translocations, resulting in genomic instability (Cerbinskaite et al., 2012), leading to tumourigenesis. Lack of BRCA1 or BRCA2 in mice also causes early embryonic lethality, confirming that the accumulation of DNA damage leads to cell death (Sharan et al., 1997). Normal cells prevent themselves from becoming a transformed cell by activating p53-dependant DNA-damage response upon BRCA1 or BRCA2 inactivation (Levine, 1997). This response blocks the cell cycle and decides if the cell can be repaired

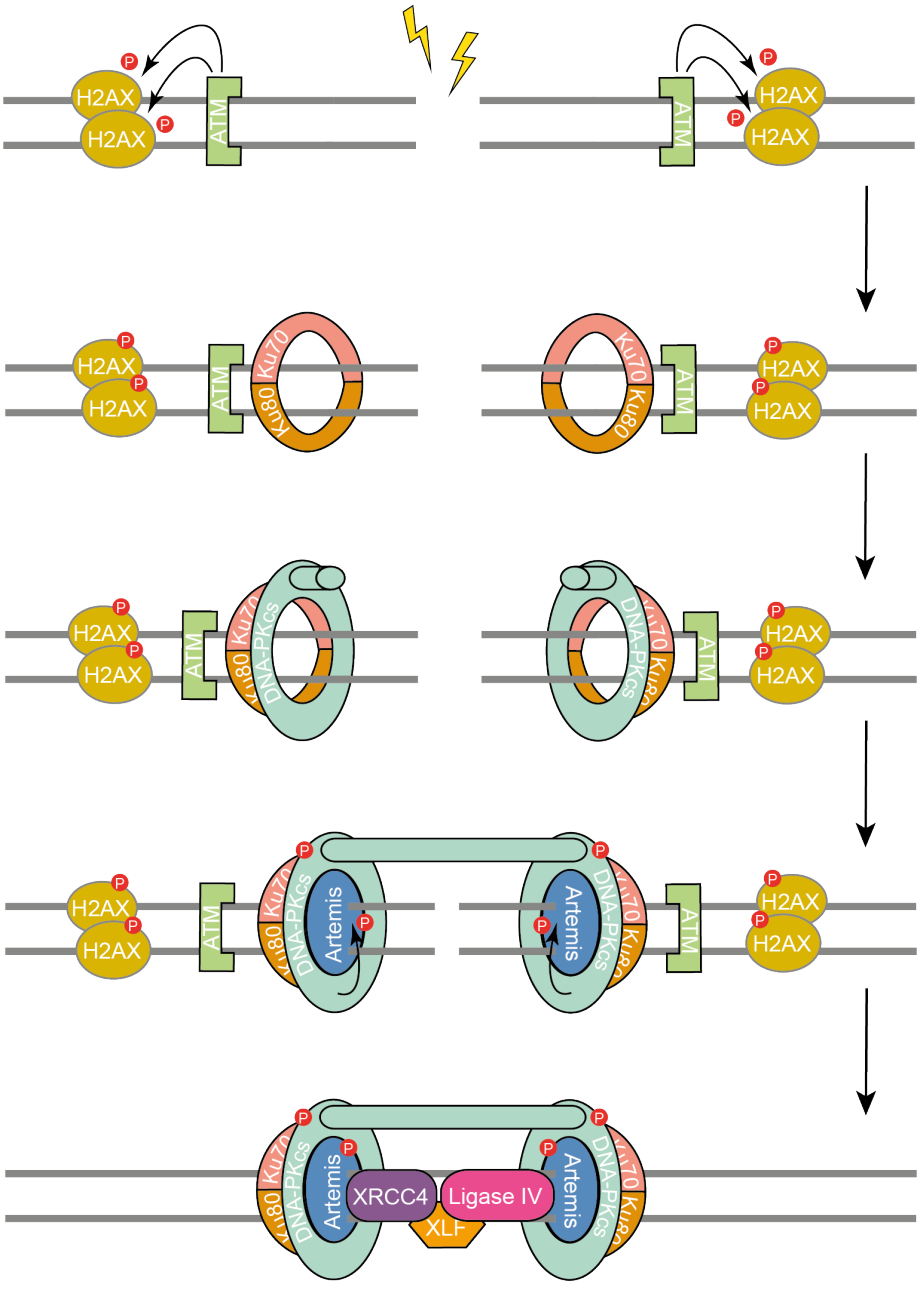


Figure 1.2: Illustration of classic non-homologous end joining

or apoptosis needs to be induced, resulting from a DNA damage overload. For the cell to become a transformed cell, loss of p53 or other DNA-damage signalling components is required (Vousden and Lu, 2002; Attardi, 2005). In this way, loss of BRCA1 or BRCA2 indicates severe risks in the development of cancer.

Likewise, it has been described that BRCA1 or BRCA2-deficient tumours are hypersensitive to DNA-damage inducing agents like cisplatin (Lohse et al., 2015). This drug induces a large quantity of DNA-damage, by crosslinking with purine bases, which cannot be repaired in the absence of HR and forces the cell into apoptosis (Im et al., 2016; Siddik, 2003). Another discovery related to the treatment of BRCA-deficient tumours has been termed 'synthetic lethality'. This is when the loss of expression of at least two genes leads to cell death, whereas the loss of only one gene has no implications. Indeed, blocking one of the alternative pathways for DNA-repair, in particular, BER by inhibition of poly-[ADP-ribose]polymerase 1 (PARP1), is lethal to HR-compromised cells (Hoeijmakers, 2001). Specific secondary structures in the DNA, like G-quadruplex (G4) (see 3.1, below), have recently been considered as potential targets for cancer treatment in a BRCA-deficient context. Stabilisation of these structures results in DNA damage accumulation and subsequent induction of apoptosis by the absence of HR. These discoveries highlight the vulnerability of BRCA1 or BRCA2-deficient cancer cells. Ultimately, loss of BRCA1 or BRCA2 will act as a double-edged sword towards cancer.

1.3 G-quadruplexes as a tool for cancer treatment

1.3.1 G-quadruplex

A G4 is a non-canonical secondary structure formed in guanine-rich regions of DNA when helicases transiently unwind the double helix (for instance, during replication or transcription), or in RNA (Huppert, 2010). Four guanines interact via their non-canonical Hoogsteen base pairing side to form a planar structure known as a G-quartet. The stacking of at least two of these quartets is required

to form the G4 structure (Figure 1.3) (Todd et al., 2005). These G-quartets are stabilised by the interaction of monovalent cations, like potassium or sodium, with the oxygen from the guanine (Schultze et al., 1999; Črnugelj et al., 2003). Via their Hoogsteen oxygen and nitrogen, every guanine has the capacity to be a donor and acceptor of two hydrogen bonds. The G4 consensus motif is described as $G_3N_{1-7}G_3N_{1-7}G_3N_{1-7}G{-}3N_{1-7}$, where every guanine is separated by a loop of N_{1-7}, indicating any combination of 1 up to 7 bases (Todd et al., 2005; Tippana et al., 2014).

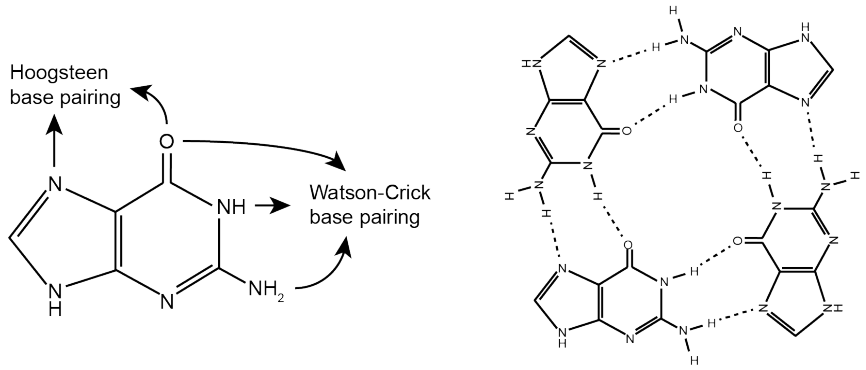


Figure 1.3: G-quadruplex formation Left: Hoogsteen and Watson-Crick base paring positions of guanine. Right: Interaction of four guanines, referred to as G-quartet, in the formation of a G-quadruplex

1.3.2 Occurrence in the human genome

Bioinformatics studies have revealed that regions with the potential to form G4s are widespread throughout the whole genome, but their presence is more abundant at specific locations. For example, in transcription, start sites or telomeres where they are thought to have a potential regulatory role (Besnard et al., 2012; Lam et al., 2013; Sun et al., 2019). If G4s form in mRNA, they might act as translational regulators (Sun et al., 2019). Correlated with these potential properties of G4s, failure to resolve these secondary structures has adverse effects on DNA replication and thus leads to genomic instability. It has also been shown that G4s have a role in regulating transcription as G4 sequences are enriched in the promoters of oncogenes (Huppert and Balasubramanian, 2005; Rodriguez et al., 2012). They can cause changes in the transcription profile of these genes by

blocking the transcription machinery. Therefore, G4s have become an attractive target for potential anti-cancer treatments (McLuckie et al., 2013; Wang et al., 2019).

1.3.3 G-quadruplex ligands

A G4 ligand is a compound that can bind a G4 and stabilises the secondary structure by impeding the unwinding of the G4 by specific helicases. There are three well-defined binding locations on which a variety of G4 ligands can bind. The most common one is binding onto the quartet. The ligand, e.g., pyridostatin (PDS), needs to have a large aromatic surface in order to bind the large hydrophobic surface of the quartets constructed by the interacting guanines (Rodriguez et al., 2012; Bidzinska et al., 2013). Other ligands, of which Distamycin A is the most famous one, bind into the groove of the G4. However, it is really challenging to find a molecule that binds specifically on G4s instead of the DNA-helix (Cocco et al., 2003; Nguyen et al., 2017). The last interaction point is inside the ion channel. This implies that the ligand needs to be small enough, like the metal ion Ni-salphene, to fit inside the ion channel (Campbell et al., 2012).

1.3.4 G4 ligands as cancer therapy

As mentioned earlier in this chapter, G4s and their stabilisation by G4 ligands have a great potential for novel anti-cancer therapies by inducing genomic instability. However, how G4 ligands induce this DNA damage is still not elucidated. Up to date, only a few mechanisms of action are hypothesised.

The first one suggests that DNA-damage is induced upon replication fork stalling and collapse. Binding of G4 ligands onto their substrates during replication has been suggested to cause replication fork stalling or even collapse on both leading and lagging strand (Weitzmann et al., 1996; Bryan, 2019). Besides being part of HR, BRCA1 and BRCA2 are also responsible for repairing and restarting stalled replication forks (Zimmer et al., 2016; Bryan, 2019). However, this restart comes with the cost of DSB introductions by structure-specific endonucleases as MUS81 or XPF (Ciccia

et al., 2008; Pepe and West, 2014; Bétous et al., 2018). This phenomenon was first discovered in telomeres (Rizzo et al., 2009). Later on, studies demonstrated that this is reoccurring across the whole genome, accentuating the reliance on replication or S-phase in general (Rodriguez et al., 2012).

It is worth pointing out that the use of G4 ligands in BRCA1 and BRCA2-deficient cells will enhance its tumour killing ability. In the absence of BRCA1 or BRCA2 and the subsequent failure of HR, stalled or collapsed replication forks and induced DSBs will accumulate. Non-effective repair of the DSB accumulation drives the cell into apoptosis (Chatzinikolaou et al., 2014). This suggests that G4 ligands like PDS can target specific HR-deficient cells and tumours (Zimmer et al., 2016).

The second mechanism predicts direct cleavage of the DNA. G4s will be recognised by factors like DNA2, a DNA replication adenosine triphosphate (ATP)-dependent helicase/nuclease important for Okazaki fragment processing and telomere replication (Lin et al., 2013). Its endonuclease activity is activated upon interaction with RPA, and it is believed that DNA damage accumulates by cleaving the DNA directly at the G4s (Masuda-Sasa et al., 2008).

Finally, the hypothesis for the last mechanism is transcription-related DNA damage induction upon G4 stabilisation. It has been suggested that G4s form simultaneously with the DNA:RNA hybrid, known as R-loops, during transcription. Binding of the G4 ligands in the displacement strand of the R-loop will stabilise the whole G4/R-loop structure causing replication fork stalling (De Magis et al., 2019).

The lack of knowledge about the mechanism of action is an important reason why none of the developed G4 ligands has been clinically approved.

1.4 Innate immune response

The body's immune system has the capacity to recognise external RNA and DNA and is, therefore, able to detect various pathogens (Sun et al., 2013). It has recently been suggested that genomic

instability could also trigger immune responses (Chatzinikolaou et al., 2014; Mackenzie et al., 2017; Gonzalo and Coll-Bonfill, 2019). The cGAS-STING pathway is the driving force behind the activation of the immune responses in both cases.

1.4.1 Immune response caused by DNA-damage

When DNA damage occurs as a consequence of DNA-damaging agents, radiation or by the absence of HR, DNA will accumulate in the cytoplasm as micronuclei. This is a small nucleus formed next to the primary nucleus when chromosomes are damaged, or miss-segregation occurred during the cell cycle (Fenech et al., 2011). Micronuclei have a nuclear envelope but the majority of them rip during interphase, exposing double-stranded DNA (dsDNA) to cyclic GMP-AMP synthase (cGAS) in the cytoplasm (Hatch et al., 2013; Mackenzie et al., 2017). Binding of cGAS onto the DNA will activate the cGAS-STING pathway, inducing an innate immune response.

1.4.2 Immune response activation

cGAS acts as the sensor for dsDNA detection (Sun et al., 2013). cGAS binds the sugar backbone of the DNA implying that DNA binding occurs in a sequence-independent manner (Civril et al., 2013). After binding, cGAS undergoes conformational changes allowing the conversion of guanosine triphosphate (GTP) and ATP into cyclic GMP-AMP (cGAMP) (Figure 1.4 (Sun et al., 2013)). This second messenger experiences high affinity for stimulator of IFN gene (STING) (Zhong et al., 2008). Binding of cGAMP onto STING induces conformational changes in STING, activating this adaptor protein at the endoplasmic reticulum and initiating translocation to the Golgi apparatus (Dobbs et al., 2015). During this translocation, the carboxyl terminus recruits and activates TANK-binding kinase 1 (TBK1), which in turn activates IFN regulatory factor 3 (IRF3) by phosphorylation (Dobbs et al., 2015; Saitoh et al., 2009). Phosphorylated IRF3 subsequently dimerises and translocates to the nucleus. STING also phosphorylates IκB, which degrades and results in the release of NF-κB, entering the nucleus. Both NF-κB and phosphorylated IRF3 activate transcription of type I

interferon (IFN) and cytokines (Tanaka and Chen, 2012).

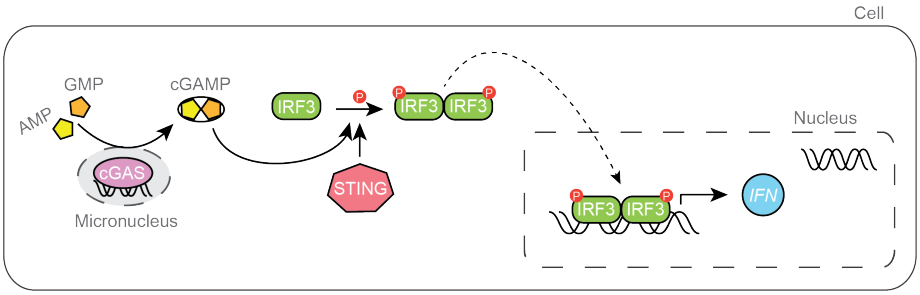


Figure 1.4: Illustration of cGAS-STING pathway activation

1.4.3 Antitumour immunity

The cGAS-cGAMP-STING pathway also links DNA damage to cancer (Mackenzie et al., 2017). The antitumour immunity is stimulated by DNA damage, but at the same time, genomic instability is one of the important hallmarks of cancer (Hanahan and Weinberg, 2000; Woo et al., 2015; Sen et al., 2019). cGAS-STING is important for activation of antigen presenting cell (APC)s via type I IFN signalling (Diamond et al., 2011). Those in turn induce the activation of immune surveillance. Other antitumour mechanisms such as cell senescence and cell death are mediated by cGAS-STING (Yang et al., 2017; Zierhut et al., 2019). Inducing an antitumour immune response is a recent and highly novel strategy for fighting cancer. Our group has been studying the link between prolonged BRCA2-deficiency and the activation of the innate immune response. Additionally, we showed that treatment with PARP1 inhibitor olaparib enhances the immune response's activation (Reisländer et al., 2019).

1.5 Paclitaxel

1.5.1 Origin

In 1962, researchers from the US Department of Agriculture collected samples from the Pacific yew, aiming to find natural compounds with anti-cancer properties (Weaver, 2014; Walsh and Goodman, 2002). A few years later, Drs Wall and Wani identified the cytotoxic activity of the compound (Wani et al., 1971). It was extracted from the bark of *Taxus brevifolia*. Only in 1978, the National Cancer Institute was able to confirm its anti-cancer property and advised for a clinical trial (Wall and Warn, 1995; Walsh and Goodman, 2002). Nowadays, paclitaxel (Taxol) and docetaxel (Taxotere) are proven to be effective in the clinic for the treatment of ovarian, breast and various other cancers (van Oosterom, 1995; Günthert et al., 1999; Ten Tije et al., 2004; Weaver, 2014).

1.5.2 Application

Paclitaxel influences proliferation of the cell by binding the β-tubulin, the building blocks of the microtubules (Horwitz, 1992). This prevents the microtubules from depolymerising during the anaphase stage of mitosis, obstructing the mitotic spindle figure formation and inhibiting chromosome segregation (Schiff et al., 1979). As shown by Zierhut et al. (2019), chromosomes stay in the cytosol during mitotic arrest. The dsDNA is sensed by cGAS, resulting in a slow accumulation of phosphorylated IRF3, via the build-up of cGAMP (Tanaka and Chen, 2012; Motwani et al., 2019). Once the mitotic concentration of phosphorylated IRF3 reaches the threshold, transcription-independent apoptosis is induced (Zierhut et al., 2019) (Figure 1.4). Further research has discovered that paclitaxel can also bind onto B-cell lymphoma 2 (Bcl-2), inhibiting its anti-apoptotic property and again inducing programmed cell death (Ferlini et al., 2009).

2 Aim

Previous studies from our group showed that the G4 ligand PDS has the ability to selectively kill BRCA1 and BRCA2-deficient cells and tumours (Zimmer et al., 2016). In the current work, we aimed to further explore the mechanisms of action for PDS's specific cell killing property. Techniques used to investigate this are based on Reisländer et al. (2019) who showed that prolonged BRCA2-deficiency can activate the innate immune response and how treatment with PARP1 inhibitor olaparib can enhance this activation. We hypothesise based on the same principles that PDS has the potential to activate the innate immune response similar to olaparib and therefore kills BRCA1 and BRCA2-deficient cells. Subsequently, we also wanted to examine the observed synergy between PDS and paclitaxel during *in vivo* combination treatments. We hypothesise that the DNA-damage induced by PDS will activate the innate immune response. As paclitaxel will also activate the innate immune response due to the induced mitotic block, the combination of both drugs will therefore lead to a cumulative effect leading to more toxicity. We expect that our results help elucidate the connection between DNA-damage and the activation of the innate immune response.

3 Material and methods

3.1 Cell lines

The colorectal adenocarcinoma cell line DLD1, of which both parental and BRCA2$^{-/-}$ mutant was used, and the breast adenocarcinoma MDA-MB-436 BRCA1$^{5396G>A}$ were grown in Dulbecco's modified Eagle's medium (DMEM) (#D5796, Sigma-Aldrich) supplemented with 10% filter sterilised foetal bovine serum (FBS) (#F7524-500ML, Merck). The human non-small cell lung carcinoma H1299 with p53 deficiency has a doxycycline (DOX)-inducible shBRCA2 and was grown in DMEM supplemented with 10% filter sterilised tetracycline free FBS (#631106, Clontech). 2 µg/mL DOX (#D9891, Sigma-Aldrich) was added to activate the shRNA expression. HAP1 *TP53*$^{-/-}$, HAP1 *TP53*$^{-/-}$ *BRCA1*$^{-/-}$ and HAP1 *TP53*$^{-/-}$ *BRCA2*$^{-/-}$ are near-haploid human cell lines and were kindly provided by the lab of Serena Nik-Zainal (University of Cambridge, UK). All HAP1 cell lines were maintained in Iscove's modified Dulbecco's medium (IMDM) (#21980-065, Sigma-Aldrich) substituted with 10% filter sterilised FBS. All cells were grown at 37°C, 5% CO_2.

3.2 Viability assay

A resazurin-based assay was used to assess the effect of PDS, paclitaxel or olaparib on the viability of different cell lines and determine the right treatment concentration. Cells were grown in a T75 flask until 70-80% confluency. The media was aspirated, the cells were washed once with phosphate-buffered saline (PBS) (#BR0014G, Thermo Fisher Scientific) and 3 mL of trypsin (#T4799-5G, Sigma-Aldrich) was then used to remove the cells from the culture flask. The cells were resuspended in the media and well mixed to ensure the cell suspension to be single cell. With the help of a hemacytometer, two different cell suspensions were prepared to plate into a 96-well plate with 100 µL per well. The first one is the desired seeding concentrations that will result in 80% confluency after 6 days growth. The second cell suspension was half the concentration of the initial one. An example layout is shown in Figure 3.1. Note that the cells were not plated in the wells at the edge

(red) of the plate to prevent biased results due to evaporation in these wells.

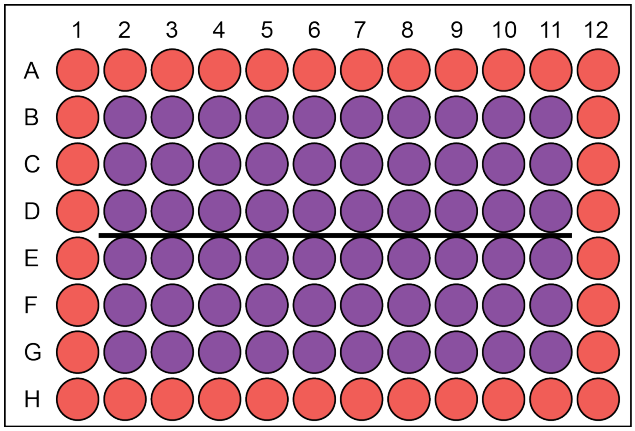


Figure 3.1: Cell seeding layout for viability assay. Two different cell concentrations are seeded in the purple wells. The red wells are filled up with PBS to protect from evaporation.

While seeding this assay, a cell pellet was collected as well to check the presence of BRCA1 or BRCA2 with Western blot in case a DOX-inducible cell line was used. The cells were kept in the incubator overnight. After 24 hours, the cells were treated in triplicate. At least two sets of triplicates were used as controls and treated with drug vehicle, e.g. Dimethyl sulfoxide (DMSO) for paclitaxel or sterile milli-Q water for PDS. The other cells were treated with 1:2 serial dilution of the drug of interest. An example of the treatment layout is given in Figure 3.2. Subsequently, the cells were incubated for 6 days at 37°C, 5% CO_2.

To determine cell viability, 10 µg/mL resazurin (#R7017, Sigma-Aldrich) was added in the growth media of the cells to make up a 1X working solution. The media in the 96-well plate was removed, and 100 µL of 1x resazurin working solution was added to the wells, including 3 blank wells in the top row indicated as dark red in Figure 3.2. The plate was incubated for 2 hours at 37°C, 5% CO_2 and the fluorescence of the plates was measured using the POLARstar OMEGA (BMG Labtech) plate reader (544 nm excitation and 590 nm emission). The fluorescence measurement is proportional to the number of living cells in the samples.

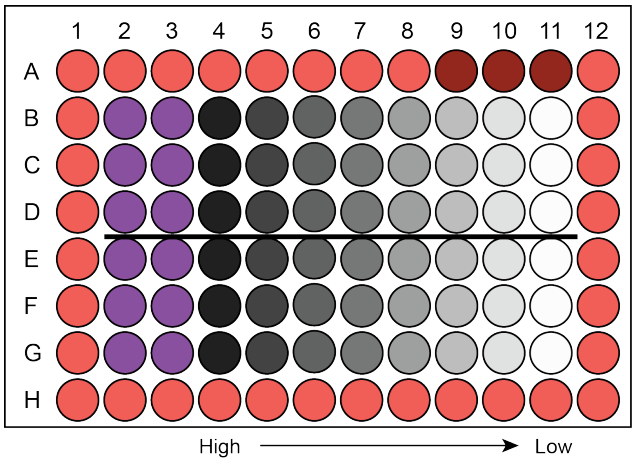


Figure 3.2: Treatment layout for viability assay. The first two columns are only treated with the vehicle. The upfollowing columns are treated with 1:2 serial drug dilutions. Wells A9-11 were used to blank the POLARstar OMEGA during fluorescence measurements.

3.3 Western blot

Cells from a 6 cm-dish were collected in 1.5 mL tubes and centrifuged at 250 *g* for 5 minutes to form a solid cell pellet. The media was aspirated, and the cell pellet was washed with PBS by centrifuging again for 5 minutes at 250 *g*. The cell pellet was lysed in sodium dodecyl sulphate (SDS) lysis buffer (4% SDS (#BP1311-200, Thermo Fisher Scientific), 0.16 M Tris pH 8 (#BPE1762-1, Thermo Fisher Scientific), 20% glycerol (#02193996, MP Biomedical), 0.01% bromophenol blue (#B392-5, Thermo Fisher Scientific), 100 mM dithiothreitol (DTT) (#441494N, VWR Chemicals)). Protease inhibitor (#04 693 159 001, Roche) and phosphatase inhibitor (#04 906845 001, Roche) was added following manufacturers guidelines to inhibit protease and phosphatase degradation. Thereafter, the cells were sonicated for 5 seconds to fragment the DNA and incubated for 10 minutes at 70°C to denature the proteins. To remove the cellular debris, the samples were centrifuged for 7 minutes at 18,000 *g*. The protein concentration was measured using the Spectrophotometer ND-1000 (NanoDrop Technologies Inc.). Equal concentrations of the samples were loaded onto Tris-acetate gel or Bis-Tris (#EA03752, #EA03785, #NP0322 or #NP0336 Thermo Fisher Scientific) submerged in Tris-acetate (#LA0041, Thermo Fisher Scientific) or 3-(N-morpholino) propanesulfonic

acid (MOPS) (#N0001, Thermo Fisher Scientific) running buffer. The XCell SureLock™ Mini-Cell (#EI0001, Thermo Fisher Scientific) was used for electrophoresis and run at 180 V. After electrophoresis, proteins were transferred to a nitrocellulose membrane (#10600001, GE Healthcare Life Sciences) with 1X NuPAGE™ transfer buffer at 30 V at room temperature. To block free sites, the membrane was incubated for 1 hour at room temperature with 5% dry skimmed milk in 1X PBST (PBS(#BR0014G, Thermo Fisher Scientific), 0.05% Tween 20 (#P7949, Sigma-Aldrich)). Membranes were then incubated with primary antibodies (Table 3.1) diluted in 2% bovine serum albumin (BSA) (#A7906, Sigma-Aldrich) and 0.05% azide (#S2002-100G, Sigma-Aldrich) in PBST overnight at 4°C.

Table 3.1: Primary antibodies used for Western blot

Target	Host and isotype	Dilution	Target size (kDa)	Catalog number	Supplier
BRCA1	Mouse IgG	1:1,000	220	OP92	Merck
BRCA2	Mouse IgG2b	1:1,000	384	OP95	Merck
Cleaved PARP	Rabbit IgG	1:1,000	89	9541S	Cell Signaling Technology
GAPDH	Mouse IgG1	1:30,000	36	NB600-502	Novus Biologicals
IRF3	Rabbit IgG	1:1,000	47	AB76409	Abcam
IRF3(p-S386)	Rabbit IgG	1:1,000	47	AB76493	Abcam
KAP1	Rabbit IgG	1:1,000	89	A300-274A	Bethyl Laboratories
KAP1(p-S824)	Rabbit IgG	1:1,000	89	A300-767A	Bethyl Laboratories
SMC1	Rabbit IgG	1:10,000	143	A300-055A	Bethyl Laboratories

The next day, the membranes were washed 3 times for 10 minutes with 1X PBST and incubated at room temperature for 1 hour in secondary antibodies (1:5,000) (Table 3.2) coupled to horseradish peroxidase. After washing 3 times with 1X PBST, the signal was visualised by applying enhanced chemiluminescence Western blot detection reagent (#32106, Thermo Fisher Scientific; #WBKLS0100, Millipore; #RPN2235GE, Healthcare) onto the membrane and followed by detection on CL-XPosure™ Film (#34089, Thermo Fisher Scientific) using the X-ray film processor ECOMAX™(#1186-3-4000, PROTEC).

Table 3.2: Secondary antibodies used for Western blot

Target	Host and isotype	Dilution	Catalog number	Supplier
Mouse	Goat IgG	1:5,000	P0447	Dako
Rabbit	Goat IgG	1:5,000	P0448	Dako

3.4 Immunofluorescence

This experiment was conducted to check for RAD51 foci formation, which indicates the presence of BRCA2 and the activation of HR. Cells were seeded onto coverslips in 6-well plates at the appropriate density for the coverslips to be 50-60% confluent the following day. Half of the coverslips were irradiated with 10 gray (Gy), the other half was used as a control. Subsequently, they were left aside to recover for 2 hours and were then transferred into a 24-well plate and washed with 1X PBS. Next, the coverslips were incubated in hypotonic solution (85.5 mM NaCl, 5 mM MgCl2 solution, pH 7.0) at room temperature for 5 minutes and followed by incubation for 10 minutes at room temperature in fixation solution (4% paraformaldehyde (#15710, Electron Microscopy Sciences) in double-distilled H_2O (ddH_2O), pH 8.5-9). Permeabilisation solution (1X PBS + 0.5% Triton-X (#X100, Sigma-Aldrich)) was used to permeabilise the coverslips by incubation for 20 minutes at room temperature. During the next step, the coverslips were washed twice for 5 minutes in 1X PBS supplemented with 0.4% Photoflo 200 (#P7417-1PT, Sigma-Aldrich) and subsequently blocked with 1X antibody dilution buffer (ADB) (10X: 10% goat-serum (#G6767, Sigma-Aldrich), 3% BSA (#A7906, Sigma-Aldrich), 0.05% Triton X-100™ in PBS) for 15-30 minutes at room temperature.

Table 3.3: Antibodies used for immunofluorescence staining

Target	Host and isotype	Dilution	Target size (kDa)	Catalog number	Supplier
BRCA1	Mouse IgG	1:1,000	220	OP92	Merck
Phospho-H2AX	Mouse IgG1	1:2,000	17	05-636	Merck
RAD51	Rabbit IgG	1:2,000	37	sc-8349	Santa Cruz Biotechnology
RAD51	Rabbit IgG	1:5,000	37	70-001	Bio Academia
53BP1	Rabbit IgG	1:5,000	214	NB100-304	Novus Biologicals

The primary antibodies were diluted in 200 µL 1X ADB according to Table 3.3 and incubated

overnight. Thereafter, the coverslips were washed for 5-10 minutes on a rotating platform (Grant-bio™ PMR-30) with wash buffer 1 (1X ADB supplemented with 0.4% Photoflo), then with wash buffer 2 (1X ADB/0.005% Triton X-100) and the third time with wash buffer 1 again. The secondary antibody was diluted 1:1,000 in 1X ADB and incubated for 1 hour at room temperature in the dark. The coverslips were once again washed with wash buffer 1, while rotating in the dark. Finally, the coverslips were washed for 1 minute with wash buffer 3 (ddH_2O/0.4% Photoflo) while rotating in the dark. In the next step, the coverslips were transferred carefully onto filter paper to let them dry by air, completely covered from light. A drop of Prolong Gold AntiFade with 4', 6-diamidino-2-phenylindole (DAPI) (#P36935, Thermo Fisher Scientific) was added onto a microscope slide (#12372098, Thermo Fisher Scientific) to mount the coverslips on top. The following day, the slides were analysed using the Leica wide field fluorescent microscope.

3.5 RT-qPCR

3.5.1 RNA extraction and cDNA synthesis

The SYBR™ Green Cells-to-CT™ Kit (#4402954, Thermo Fisher Scientific) kit was used according to manufacturer's instructions for RNA extraction and reverse transcription to cDNA. The cDNA was synthesized in a reaction of 25 µL consisting of 12.5 µL 2X SYBR® RT Buffer, 1.25 µL 20X RT Enzyme Mix, 6.25 µL nuclease-free water and 5 µL RNA.

3.5.2 qPCR

Subsequently, the Power SYBR™ Green PCR Master Mix (#4367659, Applied Biosystems) for the qPCR reaction was prepared according to the kit's instructions. The reactions are performed in 10 µL containing 5 µL Power SYBR® Green PCR MasterMix, 400 nM primers, 2.2 µL nuclease-free water and 2 µL 1:10 diluted cDNA. The primers used in these experiments are listed in Table 3.4.

Table 3.4: Primers used for RT-qPCR

Target	Sense	Sequence
GAPDH	Forward	GAC AGT CAG CCG CAT CTT CT
	Reverse	ACC AAA TCC GTT GAC TCC GA
IFIT1	Forward	TAC CTG GAC AAG GTG GAG AA
	Reverse	GTG AGG ACA TGT TGG CTA GA
IFIT2	Forward	TGT GCA ACC TAC TGG CCT AT
	Reverse	TTG CCA GTC CAG AGG TGA AT
ISG15	Forward	GCG AAC TCA TCT TTG CCA GTA
	Reverse	CCA GCA TCT TCA CCG TCA G
OAS2	Forward	TCC AGG GAG TGG CCA TAG
	Reverse	TCT GAT CCT GGA ATT GTT TTA AGT C

The newly synthesised cDNA was diluted 1:10 with DNase/RNase-free water (#B003000WB100, Thermo Fisher Scientific) before adding to the reactions. Every reaction was conducted in technical triplicate on the StepOnePlus™ Real-Time PCR System (#4376600, Thermo Fisher Scientific). The cycling program can be found in Table 3.5.

Table 3.5: Programme for RT-qPCR reaction

Cycle stage	Cycles	Ramp rate (°C/s)	Temperature (°C)	Hold Time
Enzyme activation	1x	1.6	95	10 min
PCR cycle	40x	1.6	95	15 s
		1.6	60	60 s
Dissociation curve	1x	1.6	95	15 s
		1.6	60	60 s
		0.075	95	15 s

3.5.3 Calculations

The normalisation of the gene expression was conducted using the housekeeping gene Glyceraldehyde 3-phosphate dehydrogenase (*GAPDH*). Therefore, the threshold cycle (C^t) – values of all triplicates were used to the following calculations of differential expression between two genes.

$$Average\ C^t = \frac{C^t replicate\ 1\ + C^t replicate\ 2\ + C^t replicate\ 3}{3}$$

$$\Delta C^t = Average\ C^t(sample) - Average\ C^t(GAPDH)$$

$$\Delta\Delta C^t = \Delta C^t(sample1) - \Delta C^t(sample2)$$

$$Differential\ expression = 2^{-\Delta\Delta C^t}$$

3.6 Flow cytometry

3.6.1 Apoptotic assay

Cells were treated according to the desired drug treatment scheme and collected afterwards. The Dead Cell Apoptosis Kit with Annexin V Alexa Fluor™ 488 (#V13245, Invitrogen) and propidium iodide (PI) (#P4864-10ml, Sigma-Aldrich) kit was used according to the manufacturer's guidelines and instructions. The BD FACSCalibur flow cytometer (#342975, BD Biosciences) was used to process the samples measuring the fluorescence emission at 530 nm (for Alexa 488) and 585 nm (for PI) using 488 nm laser. Per condition, 30,000 events were analysed using FlowJo® software.

3.6.2 Propidium iodide staining

After the desired drug treatment for the cells, they were harvested and centrifuged for 5 minutes at 350 *g*. The cell pellet was washed with 1X PBS and subsequently fixed with ice cold 99% ethanol (#E/0650DF/17, Fisher Chemicals), added dropwise to the cells whilst vortexing. The cells were stored at 4°C overnight. The next day, the samples were spun down for 5 min at 350 *g*, and afterwards, the ethanol was removed. The cells were washed once again with PBS and resuspended in propidium iodide-mix. A total volume of 0.5 mL of propidium iodide-mix was prepared per sample, containing 480 µL PBS, 10 µL PI and 10 µL RNase A (#12091-021, Invitrogen). The samples were analysed by the BD FACSCalibur flow cytometer (BD Biosciences) measuring the fluorescence emission at 585 nm using 488 nm excitation. Per condition, a minimum of 10 000 events were analysed using FlowJo® software

4 Results

4.1 Pyridostatin induced immune response

From the literature we know that G4 ligands cause replication fork stalling resulting in DSBs in BRCA1 and BRCA2 deficient cells. However, how PDS induces lethal levels of DNA damage in BRCA-deficient cells remains unknown. Recent work has established that BRCA-inactivation leads to an innate immune response and that this is further induced by treatment with compounds such as PARP1 inhibitors (Reisländer et al., 2019; Ding et al., 2018; Kim et al., 2020). Consequently, one hypothesis is that PDS triggers the innate immune response in BRCA1/2 inactivated cells, and it is this pathway that leads to the cell death observed in these cells.

First, we confirmed the sensitivity of BRCA1 and BRCA2-deficient cells to PDS and PARP inhibitors, another type of DNA-damage inducing agents. The sensitivity of isogenic human colorectal cancer DLD1 cell lines, which were either BRCA2 wild type (WT; $BRCA2^{+/+}$) or BRCA2 knockout ($BRCA2^{-/-}$), to treatment with PDS was measured using a viability assay as in Zimmer et al. (2016). DLD1 WT and DLD1 $BRCA2^{-/-}$ cells were seeded and treated with different concentrations of PDS. After 6 days, the viability of the cells was determined using resazurin. In order to observe the effect of BRCA2 knockout, DLD1 WT cells were used as a control. DLD1 $BRCA2^{-/-}$ cells are more sensitive to increasing PDS concentrations than the WT, as expected (Figure 4.1A). In Figure 4.1B, the assay is conducted under similar circumstances using olaparib. This PARP inhibitor is already used in the clinic for the treatment of BRCA1 and 2 deficient tumours (Kim et al., 2015). It is a control used to confirm that BRCA-deficient cells behave as expected and are sensitive to PARP inhibitors. PDS treatment did not impact on the survival of WT cells to the same extent as $BRCA2^{-/-}$ cells which can be seen as 2.5 µM PDS led to 27% viability in $BRCA2^{-/-}$ cells compared to 64% viability in WT cells treated with the same dose. This indicates selective sensitivity of BRCA2-deficient cells to PDS. In parallel with the viability assays, Western blotting was used to confirm the BRCA2-deficiency of the DLD1 $BRCA2^{-/-}$ cell line (Figure 4.1C).

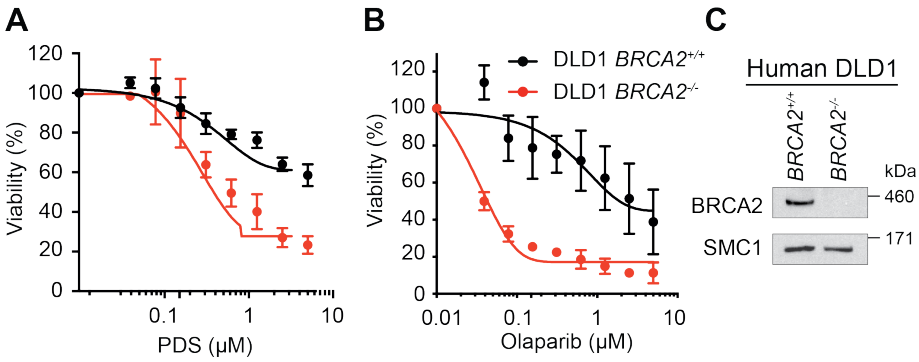


Figure 4.1: DLD1 *BRCA2*$^{-/-}$ cells are sensitive to the DNA damaging agents PDS and olaparib. A. Viability of *BRCA2*$^{+/+}$ and *BRCA2*$^{-/-}$ cells after increased PDS treatment. DLD1 WT and DLD1 *BRCA2*$^{-/-}$ were cultured in a series of PDS doses (5, 2.5, 1.25, 0.625, 0.3125, 0.156, 0.0781, 0.0391 µM) for 6 days. Error bars represent standard deviation (SD) of n = 3 independent experiments, each performed in technical triplicate. B. Viability of *BRCA2*$^{+/+}$ and *BRCA2*$^{-/-}$ cells after increased olaparib treatment. DLD1 WT and DLD1 *BRCA2*$^{-/-}$ were cultured in a series of olaparib doses (5, 2.5, 1.25, 0.625, 0.3125, 0.156, 0.0781, 0.0391 µM) for 6 days. Error bars represent SD of n = 3 independent experiments, each performed in technical triplicate. C. BRCA2 depletion control via Western blot. Untreated cell pellet was collected during seeding of viability experiment to check the absence of BRCA2 in DLD1 *BRCA2*$^{-/-}$ cell line. The membrane is probed with an anti-BRCA2 antibody, and SMC1 was used as a loading control.

Next, I wanted to test if PDS can activate the innate immune response. The human non-small cell lung carcinoma cell line H1299 with a homozygous partial deletion of p53 and a DOX-induced shRNA against BRCA2, referred to as H1299 shBRCA2$^{\text{DOX}}$, was used to examine the expression of innate immunity proteins by Western blot. Treatment of this cell line with 2 µg/mL DOX for 2-4 days is sufficient to downregulate BRCA2. Untreated cells were used as a control. The immune response is a downstream effect of cGAS sensing the presence of naked DNA in the cytoplasm, mainly in the form of micronuclei (Harding et al., 2017). As previously reported in Reisländer et al. (2019) activation of the innate immune response is induced by olaparib (Figure 4.2A). An apparent dose dependent increase in the protein concentration of pIRF3 is visible and illustrates the elevated levels of innate immune response activation. Olaparib also caused the induction of DNA damage, of which phosphorylation of serine residue 824 of KAP1 (pKAP1) is the used biomarker (White et al., 2006). The increased expression of pKAP1, therefore indicates higher levels of DNA damage with increasing olaparib concentration. Subsequently, we assessed whether PDS could

activate the innate immune response similar to olaparib. Therefore, cells were seeded and first treated with or without 2 µg/mL DOX for 4 days to ensure BRCA2 depletion and thereafter treated for 3 days with 0, 5 or 10 µM of PDS. In Figure 4.2B, we again observed an elevation of pIRF3 levels with increasing PDS concentrations in the BRCA2-deficient (-BRCA2) cells. This indicates that PDS has the ability to activate the cGAS-STING pathway. Higher doses of PDS caused elevated levels of DNA damage, similar to olaparib, as seen by the increased protein levels of pKAP1. The BRCA2-depletion of the DOX-inducible cell lines was confirmed by probing the immunoblot with an anti-BRCA2 antibody. Hence, we have determined PDS treatment leads to the activation of the cGAS-STING pathway and that this corresponds to increased levels of DNA damage.

Next, we determined the mRNA expression levels of downstream regulator genes (interferon induced protein with tetratricopeptide repeats 2 (*IFIT2*) and 2'-5'-oligoadenylate synthetase 2 (*OAS2*)) of the innate immune response, known as interferon stimulated gene (ISG) due to their association with the type I IFN response (De Veer et al., 1998; Chawla-Sarkar et al., 2003; Vanpouille-Box et al., 2018). Quantitative reverse transcription PCR (RT-qPCR) was performed using H1299 shBRCA2$^{\mathrm{DOX}}$ cells treated under the same conditions as the Western blot: pre-treatment with or without 2 µg/mL DOX for 4 days and subsequently treated with 0 or 10 µM PDS for 3 days (Figure 4.2C). In accordance with previous results, *IFIT2* and *OAS2* were significantly upregulated in PDS treated cells with a p-value of 0.03 and <0.001, respectively, indicating the activation of the innate immune response. A small non-significant upregulation was observed in the untreated (-PDS) BRCA2-deficient cells compared to untreated BRCA2-proficient cells for both *IFIT2* and *OAS2*. As previously reported in Reisländer et al. (2019), BRCA2-deficient cells activate the innate immune response upon prolonged BRCA2-loss (28 days). Therefore, we suspect that short-term BRCA2 depletion (4 days) can already affect the mRNA levels, although not yet in a statistically significantly way. Similarly, treatment with 5 µM olaparib shows a significant upregulation of *IFIT2* and *ISG15* in BRCA2-deficient cells by RT-qPCR (Supplementary Figure 1), as described in Reisländer et al. (2019).

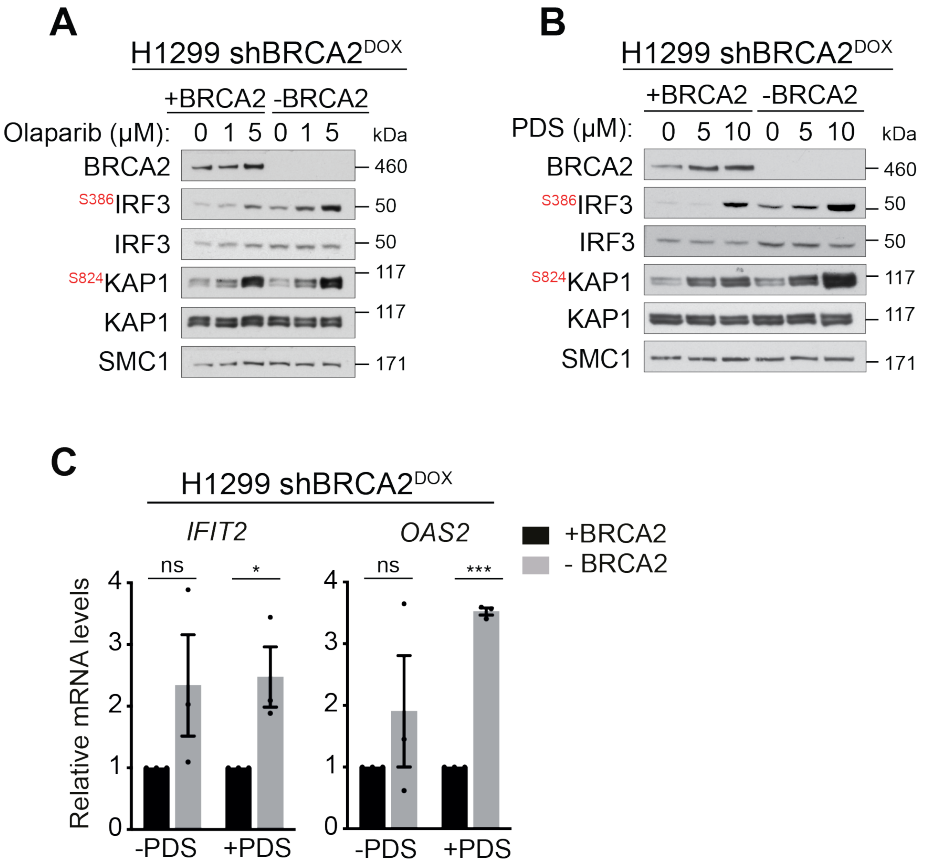


Figure 4.2: Innate immune response is activated in H1299 upon treatment with PDS or olaparib. A. Innate immune response activation after olaparib treatment. H1299 shBRCA2^{DOX} were pre-treated for 4 days with or without 2 µg/mL DOX prior to further treatment. Subsequently, the cells were treated for 3 days with 1 or 5 µM of olaparib and 2 µg/mL DOX as indicated, and whole-cell extracts were immunoblotted. SMC1 is used as a loading control. This experiment is done with the help of Florian Groelly. B. Innate immune response activation after PDS treatment. H1299 shBRCA2^{DOX} were pre-treated for 4 days with or without 2 µg/mL DOX prior to further treatment. Subsequently, the cells were treated for 3 days with 5 or 10 µM of PDS and 2 µg/mL DOX as indicated, and whole-cell extracts were immunoblotted. SMC1 is used as a loading control. This experiment is done with the help of Florian Groelly. C. H1299 shBRCA2^{DOX} were pre-treated for 4 days with or without 2 µg/mL DOX prior to further treatment. Subsequently, the cells were cultured in the absence (-PDS) of PDS or with 10 µM (+PDS) for 3 days. RNA was extracted, reverse transcribed to cDNA and used for qPCR analysis using specific primers for the indicated genes. The mRNA levels were normalised to the mRNA levels of *GAPDH* and the +BRCA2 samples. The graphs represent the $2^{-\Delta\Delta C^t}$ value. Error bars represent SEM of n = 3 independent experiments, each performed in technical triplicate. NS: $p > 0.05$; *: $p < 0.05$; **: $p \leq 0.01$; ***: $p \leq 0.001$ (unpaired two-tailed t-test).

4.2 Combination treatment of paclitaxel and PDS

Paclitaxel is part of the taxane drugs family and is used in the clinic for the treatment of ovarian, breast and many other cancers (Rowinsky et al., 1993; Verweij et al., 1994; Singla et al., 2002). It blocks mitosis progression by stabilising the microtubules and prolonging mitotic checkpoint activation, which subsequently triggers apoptosis (Verweij et al., 1994; Blagosklonny and Fojo, 1999; Dalton and Yang, 2009). A mini pharmacological drug screen conducted by Dr Annamaria Biroccio (Regina Elena National Cancer Institute, Rome), in collaboration with our lab, led to the discovery of a new potential anti-cancer combination therapy utilising PDS and paclitaxel (unpublished data). For this screen, Dr Biroccio generated a xenograft model in severe combined immunodeficient (SCID) female mice by injecting $4x10^6$ cells intramuscular (IM) with the mammary breast cancer cell line MDA-MB-436 $BRCA1^{5396G>A}$, which carry a 5396G>A mutation in the BRCA1 gene. When the tumour reaches a volume of $\pm$ 200 mm^3, on average 6 days after injection, one of three different treatment schemes started. One cohort of 5 mice was treated with a single dose of 20 mg/kg paclitaxel on day 1 and 8. Cohort two was administered 7.5 mg/kg/day PDS for 5 consecutive days. After a 2-day break, the mice were treated again for 5 days under the same conditions. The last cohort received the combination of both drugs in which the mice were daily injected with PDS from day 1 to 4, followed by a 2-day break and again from day 8 to 11. They also received two single doses of paclitaxel on day 5 and 12. All drugs were administered intravenous (IV). Both cohorts that received single-drug treatment of PDS or paclitaxel showed a reduced tumour growth speed compared to the untreated mice (Figure 4.3). The difference between the single-drug treatment of PDS or paclitaxel was small. However, the combination of both drugs together inhibited the tumour growth for up to 30 days. This is, on average, three times longer than the single drug treatments. Therefore, we suspect that there is a synergy between the two drugs that increase the efficacy of BRCA1-deficient tumour killing. Consequently, we sought to validate these results and gain insight into the mechanism of action for this novel drug combination.

First, we set out to assess the sensitivity of the human colorectal cancer cell lines DLD1 WT and

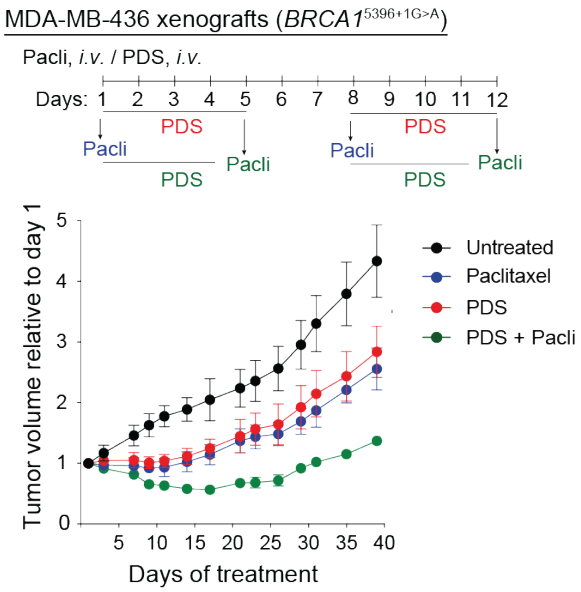


Figure 4.3: PDS and paclitaxel combination treatment *in vivo* kills BRCA1-deficient tumours more effectively. 4x10^6 MDA-MB-436 BRCA1$^{5396G>A}$ cells were injected IM in female SCID mice. 20 mg/kg/day paclitaxel was administered IV on day 1 and 8. PDS was administered IV as well at a dose of 7.5 mg/kg/day for 5 consecutive days. After a 2-day break, the mice were again treated for 5 consecutive days. For the combination treatment, mice were treated for 4 consecutive days with 7.5 mg/kg/day PDS and received a single dose of 20 mg/kg/day paclitaxel on day 5. After a 2-day break the mice were treated again following the same treatment scheme for day 8 until 12. The tumour volumes are measured using a vernier calliper on the indicated days, and it is relative to the tumour volumes at the beginning of the treatment. Error bars represent SD of n = 5 mice. This experiment is conducted by Dr Biroccio (Regina Elena National Cancer Institute, Rome).

DLD1 *BRCA2*$^{-/-}$ to paclitaxel treatment using a viability assay. Cells were seeded and exposed to increasing paclitaxel concentrations from 0.1 to 10 nM for 6 days (Figure 4.4A). Thereafter, the viability of the cells was determined using resazurin, but no difference in the viability between the WT and *BRCA2*$^{-/-}$ cells was observed. This indicates that single paclitaxel treatment cannot selectively target BRCA2-deficient cells as we observed for PDS.

Following a similar approach as for PDS, we investigated whether paclitaxel could activate the innate immune response. The cells were pre-treated with or without 2 µg/mL DOX for 4 days prior to treatment with 50, 100, 250 and 500 nM paclitaxel for 2 days. Whole cell extracts were

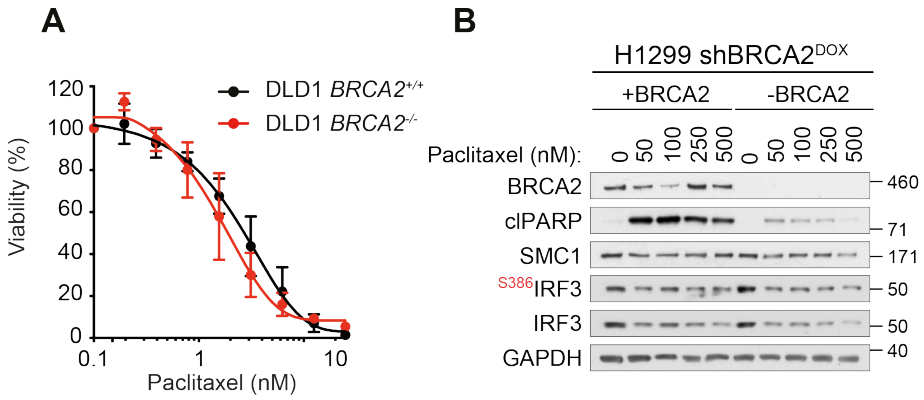


Figure 4.4: Paclitaxel unable to activate the innate immune response in BRCA2-deficient cells. A. Viability of *BRCA2*$^{+/+}$ and *BRCA2*$^{-/-}$ cells after increased paclitaxel treatment. DLD1 WT and DLD1 *BRCA2*$^{-/-}$ were cultured in a series of paclitaxel doses (10, 5, 2.5, 1.25, 0.625, 0.3125, 0.156, 0.0781 nM) for 6 days. Error bars represent SD of n = 3 independent experiments, each performed in technical triplicate. B. Innate immune response activation after paclitaxel treatment. H1299 shBRCA2^{DOX} were pre-treated for 4 days with or without 2 µg/mL DOX prior to further treatment. Subsequently, the cells were treated for 2 days with 50, 100, 250 or 500 nM of paclitaxel and 2 µg/mL DOX (-BRCA2) as indicated and whole-cell extracts were immunoblotted. SMC1 and GAPDH are used as a loading control.

prepared and immunoblotted (Figure 4.4B). We found elevated levels of cleaved PARP (clPARP) that demonstrate increased apoptosis for all treated BRCA2-proficient (+BRACA2) cells. The levels of pIRF3 remain consistent over all treated samples implying no activation of the innate immune response. This indicates that paclitaxel influences the base levels of this protein. How this is possible is not known and therefore needs to be investigated. Collectively these data suggest, that paclitaxel cannot specifically target BRCA2-deficient cells nor activate the innate immune response in these cells and with this type of treatment.

The synergy observed in the *in vivo* experiment from Dr Biroccio led us to explore the impact of PDS and paclitaxel combination treatment on the induction of apoptosis *in vitro* (Figure 4.5; Supplementary Figure 2). To assess this issue, H1299 shBRCA2^{DOX} cells were seeded and pre-treated with or without 2 µg/mL DOX for 4 days and subsequently treated with 5 µM PDS and/or 50 nM paclitaxel for 3 days. After collection, the Dead Cell Apoptosis Kit with Annexin V Alexa Fluor™ 488 was utilised following the manufacturer's guidelines to stain the cells. We determined

the distribution of living, dead or apoptotic cells via flow cytometry analysis. The effect of single PDS treatment on triggering apoptosis is minimal compared to the untreated cells for both BRCA2-proficient and deficient cells. Similarly, we did not observe an additional effect of the combination treatment compared to the single paclitaxel treatment in the two different conditions, +BRCA2 and -BRCA2. This experiment could not identify the beneficial effect of combination treatment *in vitro* for tumour growth repression, as shown *in vivo* by Dr Biroccio. Note that only one replicate of this experiment was conducted.

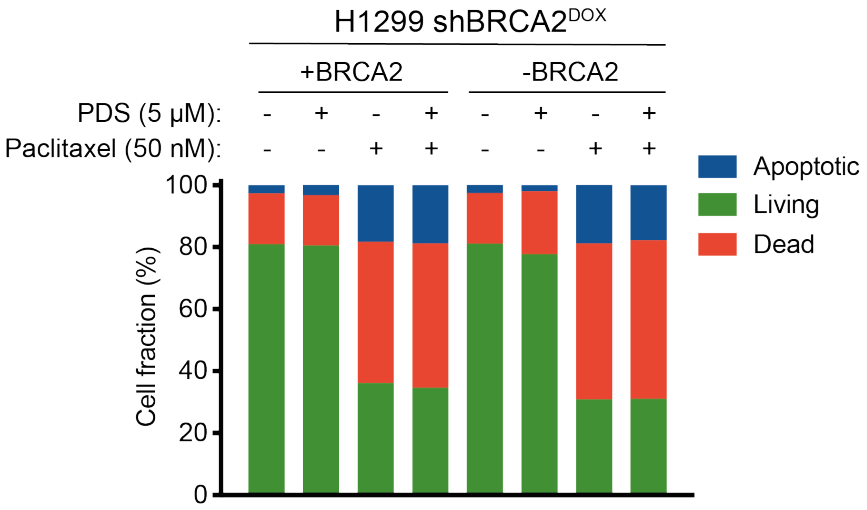


Figure 4.5: Combination treatment does not trigger more apoptosis *in vitro* compared to single agent treatments. The apoptotic cell fraction induced by single or combination treatment with PDS and paclitaxel in H1299 shBRCA2^{DOX}. Cells were pre-treated with or without 2 µg/mL DOX for 4 days prior to further treatment. Subsequently, the cells were treated for 3 days with 5 µM PDS and/or 50 nM of paclitaxel and 2 µg/mL DOX as indicated. The Dead Cell Apoptosis Kit with Annexin V Alexa Fluor™ 488 was used to stain the cells and DNA was stained with propidium iodide. The percentage of living, dead or apoptotic cells was determined via flow cytometry analysis. n = 1 independent experiment.

The above finding led us to investigate whether paclitaxel's current treatment conditions are too toxic. The determination of the right concentration and incubation time is critical to identify the synergism between the two drugs. They are both active in different phases of the cell cycle and will therefore affect the cell cycle differently. From the literature, it is known that PDS is active during S-phase while DNA is replicated (Rodriguez et al., 2012, Miglietta et al., 2020)(Rodriguez et al.,

2012; Miglietta et al., 2020). It binds on to the G4 structures, stabilises them, causes replication fork stalling and induces DSBs (Rodriguez et al., 2012). These breaks cannot be repaired efficiently due to the lack of HR as a result of BRCA2 abrogation (Zimmer et al., 2016). Instead, they are repaired by less accurate pathways that give rise to micronuclei formation (Essers et al., 2000). One hypothesis for the synergy of PDS and paclitaxel treatment observed in mice is that when the cells slip through the paclitaxel-induced arrest in mitosis, the accumulated micronuclei are sensed by cGAS during interphase, which activates the innate immune response. In order for this mechanism to work, we have to identify the duration of PDS treatment required to induce enough DNA damage under the form of micronuclei, for cGAS to activate the innate immune response after paclitaxel treatment. To address this issue, we investigated the impact of paclitaxel on the cell cycle. H1299 shBRCA2^{DOX} cells were seeded and pre-treated with 2 µg/mL DOX for 4 days and subsequently incubated with 50 nM paclitaxel for 12, 24 or 72 hours and 10 nM for 72 hours. After harvesting, the cells were treated with propidium iodide and analysed. In Figure 4.6, we observed a shift in the 2n (G1-phase) peak in the control sample towards 4n (mitosis) with 50 nM paclitaxel for 12 hours, indicating paclitaxel led to the arrest of cells in mitosis. After 24 hours paclitaxel, there was a shift in the peak from 4n back towards 2n. This indicates that the cells originally arrested in mitosis escaped the block and continue their cell cycle with failed chromosome segregation. This phenomenon is known as mitotic slippage (Zierhut et al., 2019) and causes different intermediate chromosomal contents between the normal 2n and 4n. After 72 hours for both 10 and 50 nM paclitaxel, the majority of the cells has a DNA content of 2n. When we compared 10 and 50 nM paclitaxel at 72 hours treatment, we also noticed that the 4n peak for 10 nM is more distinct than for 50 nM. The curve of 50 nM for 72 hours treatment also demonstrates a heterogenous collection of cells with different chromosomal contents, explaining the lack of unambiguous results in the previously described experiments. We thus hypothesised that the 12 and potentially 24-hour treatment is insufficient to induce the mitotic block as the cell cycle of H1299 cells takes 23.2 ± 2.5 hours (Eden et al., 2011). We believe that the majority of the cells will not be able to complete their cell cycle and therefore, will not reach the paclitaxel induced block. However, 72 hours treatment with 50 nM paclitaxel resulted in a chromosomal heterozygous cell mass. Based on these results, we

changed the paclitaxel treatment conditions to 10 nM for 72 hours to reduce the toxicity compared to 50 nM but ensuring that a large proportion of the cells are arrested in mitosis in the upcoming experiments.

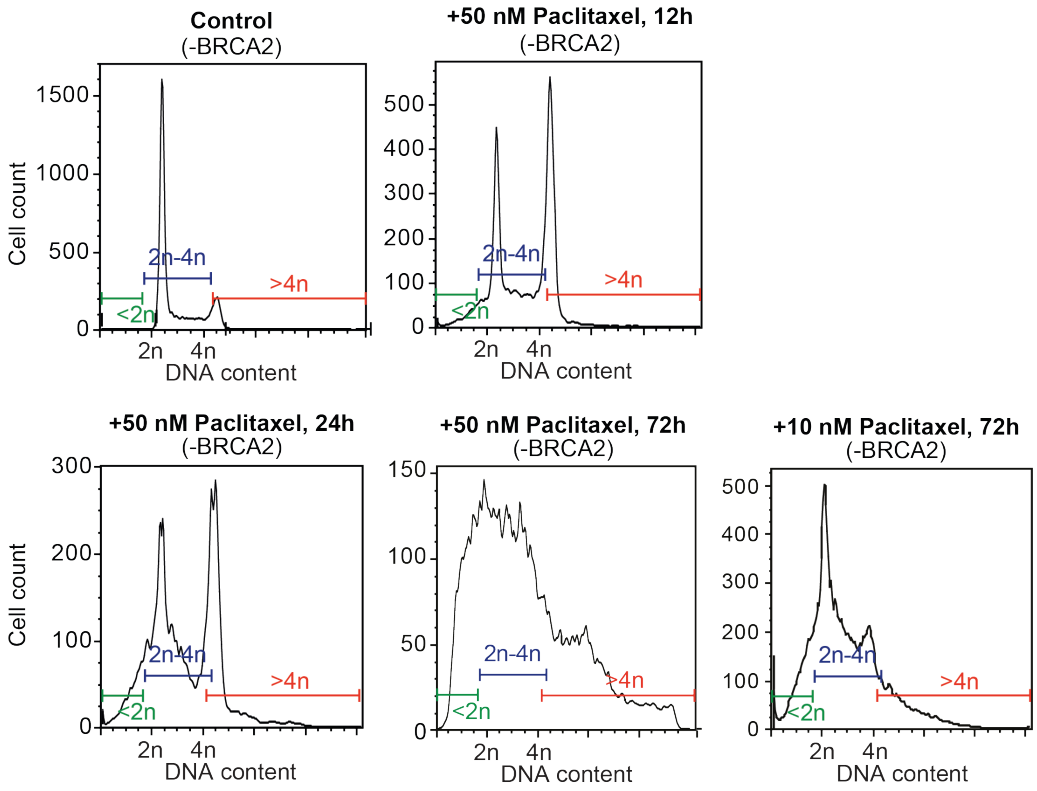


Figure 4.6: Paclitaxel induces cell cycle changes in BRCA-deficient cells. Cell cycle analysis after different paclitaxel incubation times. H1299 shBRCA2^{DOX} cells are incubated with 50 nM paclitaxel for 12, 24 or 72 hours or 10 nM for 72 hours. Subsequently, the gDNA was stained with propidium iodide and analysed using flow cytometry.

We next sought to determine whether the combination of PDS and paclitaxel can activate the innate immune response via Western blotting. H1299 shBRCA2^{DOX} cells were pre-treated with or without 2 µg/mL DOX for 2 days. Subsequently, the cells were treated with 5 µM PDS and/or 10 nM paclitaxel as indicated in the treatment scheme in Figure 4.7A for 3 days. Whole-cell extracts were immunoblotted and probed for the earlier described markers. Elevated levels of pKAP1 in single paclitaxel and combination treatment for BRCA2-deficient cells, indicates the presence of

DNA damage accumulation in these cells compared to single PDS treatment or untreated. However, the levels of pKAP1 are higher for the combination compared to paclitaxel treated samples. This is in accordance with the hypothesis that combination treatment is more effective in tumour killing by generating additional DNA damage.

To confirm that this additional DNA damage was lethal, we probed with an anti-clPARP to determine the levels of apoptosis induced by the different drug treatments. For both BRCA2-proficient and deficient cells, single paclitaxel and combination treatment trigger more apoptosis compared to the untreated or PDS treated samples. A similar effect was observed in the apoptosis analysis via flow cytometry (Figure 4.5). Activation of the cGAS-STING pathway was evaluated using pIRF3 as a marker. The protein levels of pIRF3 were only slightly higher for the single dose paclitaxel and combination treatment for both BRCA2-proficient and deficient cells compared to the untreated or single PDS samples. These results indicate there was only a modest if any, activation of the innate immune response. However, we have to take into account that the used mouse models only lack B and T-cells, implying that they are not fully immunocompromised. Therefore, we hypothesise that the previously observed synergistic effect of the combination treatment might not be based on higher levels or more efficient activation of the innate immune response as cGAS can affect the host's immune responses.

To complement the finding from Figure 4.7A the innate immune response's activation was assessed in another cell line model. To this end, the same cell line was used as for the *in vivo* experiment (Figure 4.3), the mammary breast cancer cell line MDA-MB-436 BRCA1$^{5396G>A}$. Whole-cell extracts were immunoblotted and probed for pKAP1 and pIRF3 to investigate the induced DNA damage and the activation of the innate immune response. As expected, single treatment with 10 µM paclitaxel caused high levels of DNA damage and increased levels of pIRF3, which indicated activation of the innate immune response. This is in line with the results obtained in Figure 4.7A. Single PDS treatment showed accumulation of DNA damage similar to the levels observed in the combination treatment. The blot demonstrates a similar pattern for the base levels of IRF3 as for the phosphorylated protein. This implies that the treatments, especially PDS and combination

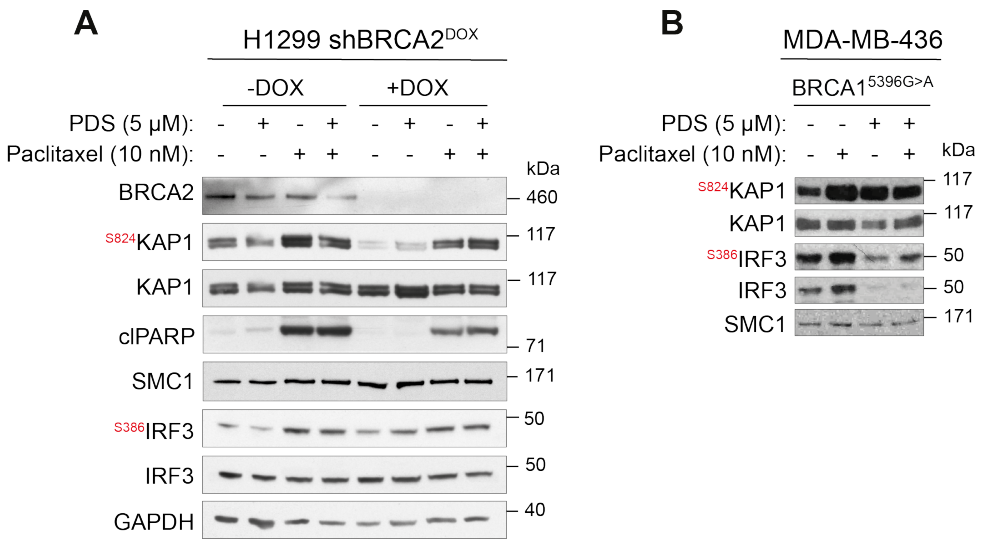


Figure 4.7: Innate immune response activation upon combination treatment in H1299 and MDA-MB-436. A. Innate immune response activation after simultaneous cotreatment of PDS and paclitaxel. H1299 shBRCA2^{DOX} were pre-treated for 2 days with or without 2 µg/mL DOX prior to further treatment. Subsequently, the cells were treated for 3 days with 5 µM PDS and/or 10 nM of paclitaxel and 2 µg/mL DOX as indicated and whole-cell extracts were immunoblotted. SMC1 and GAPDH are used as loading controls B. Innate immune response activation after simultaneous cotreatment of PDS and paclitaxel. MDA-MB-436 BRCA1$^{5396G>A}$ were treated for 3 days with 5 µM PDS and/or 10 nM of paclitaxel as indicated and whole-cell extracts were immunoblotted. SMC1 is used as a loading control.

treatment, also influence the cells' basal IRF3 levels. Since the base level of IRF3 of the paclitaxel treated sample seems similar to the control sample, we highly suspect PDS to be causing this change of basal protein expression.

From the literature, it is known that paclitaxel blocks the microtubule disassembly by binding directly onto them, resulting in a G2/M arrest and prolonged mitotic checkpoint activation which triggers apoptosis (Dalton and Yang, 2009). Consequently, we explored the influence of paclitaxel on the cell cycle. To this end, H1299 shBRCA2^{DOX} cells were used to assess the cell cycle distribution using 5-ethynyl-2' deoxyuridine (EdU) and propidium iodide. The cells were cultured in the presence or absence of 2 µg/mL DOX for 2 days followed by treatment with 5 µM PDS and/or 10 nM paclitaxel. Subsequently, the cells were labelled with EdU for 30 minutes pre-harvesting, and

the DNA was stained with propidium iodide afterwards. The cell cycle distribution was evaluated via flow cytometry analysis (Figure 4.8A; raw data Supplementary Figure 3, 4, 5). Firstly, we saw that BRCA2-deficient cells accumulate in G1, consistent with Lai et al. (2017). Paclitaxel or combination treated samples showed an increase in G2/M cells as a result of the paclitaxel-induced mitotic block, which is in line with the literature (Dalton and Yang, 2009). Interestingly, the difference between BRCA2-proficient and deficient cells is minimal, similar to the protein levels of pIRF3 and pKAP1 in the Western blots (Figure 4.7), indicating that paclitaxel does not explicitly effect BRCA2-deficient cells. Strikingly, the influence of PDS on the cell cycle for both BRCA2-proficient and BRCA2-deficient cells is minimal. The effect of PDS treated samples on the cell cycle was comparable to the control cells. Similarly, PDS does not have an additional effect on the induction of apoptosis, as seen in Figure 4.5.

Next, we sought to investigate the slippage of cells through the paclitaxel-induced mitotic block by looking at cells with an abnormal chromosomal content. The cells classified as "<G1" have a DNA content smaller than 2n, known as aneuploid and are part of the result of asymmetric cell division (Riffell et al., 2009). Polyploid cells are known to have a DNA content higher than 4n, referred to as ">G2/M" in Figure 4.8B. No additional effect of PDS was observed for both BRCA2-proficient and deficient cells when compared to the untreated samples. Treatment with 5 µM PDS did not influence the cell fractions with either a lower or higher average DNA content compared to the untreated samples. In contrast, paclitaxel treated samples demonstrated higher numbers of cells with abnormal chromosomal numbers. The total cell fraction of aneuploid cells for paclitaxel and combination treated samples increased to almost 20% in both BRCA2-proficient and deficient cells. Polyploid cells were 25-30% of the total cell fraction in these circumstances. This increase in both aneuploid and polyploid cells suggest that mitotic block induced upon paclitaxel treatment causes chromosome missegregation and cell death. Together, these findings suggest again that paclitaxel cannot selectively affect BRCA2-deficient cells. The difference observed between single paclitaxel or combination treatment is minimal. We hypothesised that this is due to the lack of PDS-induced additional effects in the combination treatment. Therefore, we increased the PDS concentration

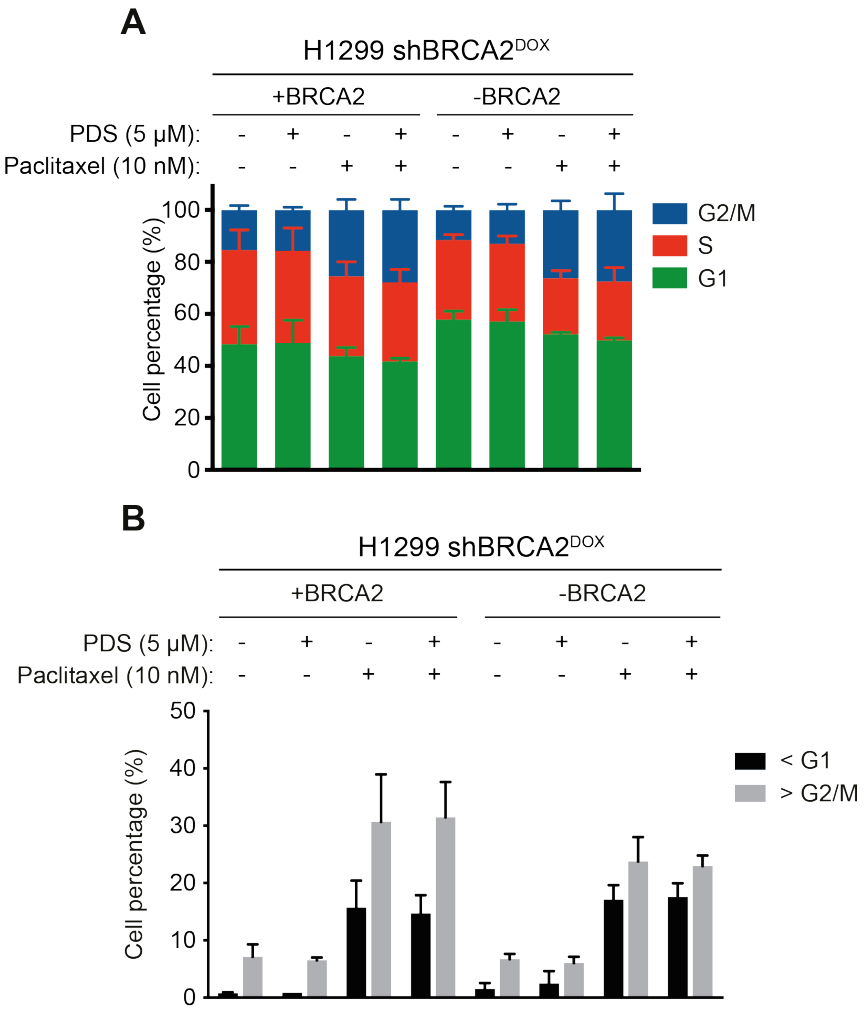


Figure 4.8: Paclitaxel treated cells accumulate in G2/M resulting, in abnormal chromosomal content. H1299 shBRCA2^{DOX} cells were pre-treated for 2 days with or without 2 µg/mL DOX prior to further treatment. Subsequently, the cells were treated for 3 days with 5 µM PDS and/or 10 nM of paclitaxel and 2 µg/mL DOX as indicated. Cells were labelled with EdU for 30 minutes prior to harvesting and the DNA was stained with propidium iodide. A. The cell cycle distribution was determined via flow cytometry analysis. Error bars represent SD of n = 3 independent experiments. B. The percentage "<G1" and ">G2/M" was determined via flow cytometry analysis. Error bars represent SD of n = 3 independent experiments.

from 5 to 10 µM using the same experimental conditions (Figure 4.9A; raw data Supplementary Figures 6, 7, 8). The cells were pre-treated with or without 2 µg/mL DOX for 2 days followed by treatment with 10 µM PDS and/or 10 nM paclitaxel for 3 days. Subsequently, the DNA was stained using propidium iodide and analysed using flow cytometry. The higher PDS concentrations reduced both the "<G1" and ">G2/M" cell fractions of PDS treated samples. However, the control and PDS treated samples had similar fractions of "<G1" and ">G2/M" where as the 5 µM PDS treated sample from Figure 4.8 showed almost no "<G1" fraction. This is not due to using a dose of PDS that is ineffective in BRCA-deficient cells, as the PDS viability (Figure 4.1) assay indicates that BRCA2-deficient cells are sensitive to these doses of PDS. The single dose paclitaxel and the combination treatment were also similar for "<G1" both BRCA2-proficient and deficient cells, whereas the ">G2/M" fraction is lower in -BRCA2 cells compared to +BRCA2 cells.

To compliment the analysis of BRCA2-deficient cells, we investigated the presence of chromosomal abnormality after treatment of PDS and/or paclitaxel using the mammary breast cancer cell line MDA-MB-436 BRCA1$^{5396G>A}$. The cells were treated with 10 µM PDS and/or 10 nM paclitaxel, and afterwards, the DNA was stained with propidium iodide. Determination of the "<G1" or ">G2/M" fraction was done using flow cytometry analysis (Figure 4.9B; raw data Supplementary Figures 9, 10, 11). The levels of ">G2/M" are higher than those recorded for H1299 shBRCA2^{DOX} cells in Figure 4.9A. This implies that more cells can slip through the paclitaxel-induced mitotic block resulting in polyploidy. These cells seem to be more stable and progress again though the cell cycle which potentially creates even higher DNA content. In contrast, the aneuploid cell fractions are much lower, indicating their instability and poor survival rates. However, there is no additional effect caused by the combination of PDS and paclitaxel so like the BRCA2-deficient cells, this is not responsible for the synergy observed in the mouse models.

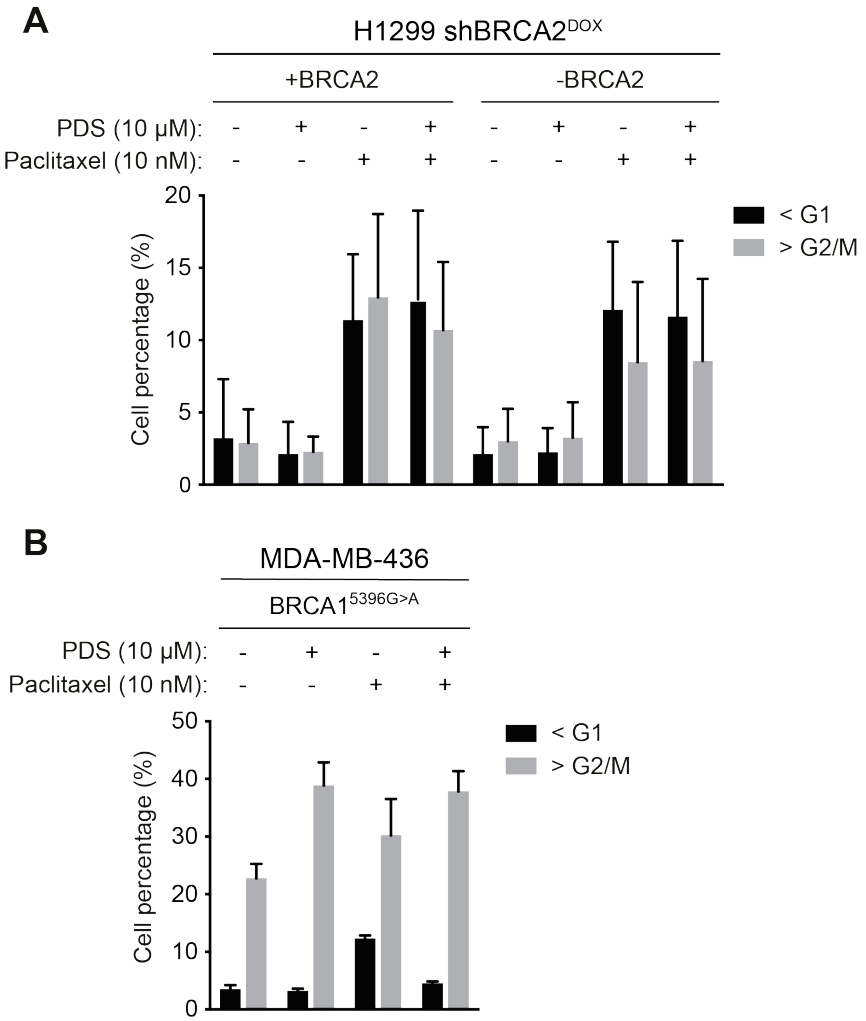


Figure 4.9: Paclitaxel and combination treatment cause abnormal chromosomal content A. H1299 shBRCA2^{DOX} cells were pre-treated for 2 days with or without 2 µg/mL DOX prior to further treatment. Subsequently, the cells were treated for 3 days with 10 µM PDS and/or 10 nM of paclitaxel and 2 µg/mL DOX as indicated. The DNA was stained with propidium iodide. The percentage "<G1" and ">G2/M" was determined via flow cytometry analysis. Error bars represent SD of n = 3 independent experiments. B. MDA-MB-436 BRCA1$^{5396G>A}$ cells were treated for 3 days with 10 µM PDS and/or 10 nM of paclitaxel. The DNA was stained with propidium iodide. The percentage "<G1" and ">G2/M" was determined via flow cytometry analysis. Error bars represent SD of n = 3 independent experiments.

4.3 Characterisation of HAP1 *p53*$^{-/-}$ *BRCA2*$^{-/-}$ cell line

A general issue in research investigating the impact of BRCA1 and BRCA2-deficient tumours is the shortage of cell models for BRCA1 and BRCA2 knockout. Additionally, no cell line has both BRCA1 and BRCA2 knockouts. Therefore, no direct comparison of the effect of BRCA1 or BRCA2 knockout in the same cell line can be made. Hence, in collaboration with the lab of Dr Serena Nik-Zainal (University of Cambridge) and other Tarsounas lab members, we wanted to generate and validate a cell line model with knockouts of both BRCA1 and BRCA2. To this end, the human near-haploid cell line HAP1 was used and carried a CRISP/Cas9-mediated BRCA2 deletion, referred to as HAP1 *TP53*$^{-/-}$ *BRCA2*$^{-/-}$. The HAP1 *TP53*$^{-/-}$ *BRCA1*$^{-/-}$ variant, used in the next experiments, was validated earlier by other lab members.

To validate whether this cell line was a functionally BRCA2 knockout, we investigated its sensitivity to the PARP inhibitor olaparib (Figure 4.10) as its is well established that BRCA-deficient cells are sensitive to PARP inhibitors (Kim et al., 2015). To this end, HAP1 *TP53*$^{-/-}$, HAP1 *TP53*$^{-/-}$ *BRCA1*$^{-/-}$ and HAP1 *TP53*$^{-/-}$ *BRCA2*$^{-/-}$ were seeded and treated with different olaparib concentrations. After 6 days, the viability of the cells was determined using resazurin. HAP1 *TP53*$^{-/-}$ *BRCA1*$^{-/-}$ cells were more sensitive to increasing olaparib concentrations than the WT, as expected (Figure 4.10). Strikingly, HAP1 *TP53*$^{-/-}$ *BRCA2*$^{-/-}$ cells did not show sensitivity for olaparib, compared to HAP1 *TP53*$^{-/-}$ *BRCA1*$^{-/-}$. This implies that HR is still active in the cells as a consequence of incomplete BRCA2 knockout.

Next, we verified the abrogation of BRCA1 and BRCA2 utilising Western blot. Cells from HAP1 *TP53*$^{-/-}$, HAP1 *TP53*$^{-/-}$ *BRCA1*$^{-/-}$ and HAP1 *TP53*$^{-/-}$ *BRCA2*$^{-/-}$ were collected simultaneously with the viability assay and whole-cell extract were prepared for immunoblotting. We probed with anti-BRCA1 and anti-BRCA2 antibodies, and no detectable full-length BRCA2 was detected for HAP1 *TP53*$^{-/-}$ *BRCA2*$^{-/-}$ (Figure 4.11). This result is in contrast with the lack of sensitivity for olaparib that was shown earlier. Next generation sequencing by the Nik-Zainal lab, identified a 2,235 bp in-frame deletion in exon 11 caused by the gRNA used in the CRISPR experiment,

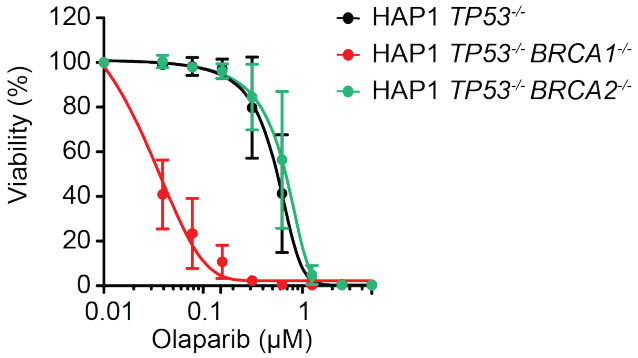


Figure 4.10: Sensitivity of HAP1 cells for olaparib. A. Viability of different HAP1 cell lines after increased olaparib treatment. HAP1 *TP53*$^{-/-}$, HAP1 *TP53*$^{-/-}$ *BRCA1*$^{-/-}$ and HAP1 *TP53*$^{-/-}$ *BRCA2*$^{-/-}$ were cultured in a series of olaparib doses (5, 2.5, 1.25, 0.625, 0.3125, 0.156, 0.0781, 0.0391 µM) for 6 days. Viability is assessed using resazurin. Error bars represent SD of n = 3 independent experiments, each performed in technical triplicate.

resulting in the loss of 5 of the 8 BRC repeats that are responsible for the loading of RAD51 during homologous recombination. The anti-BRCA2 antibody used in our Western blots has its binding epitope in the deleted section hence the absence of full-length BRCA2 in the Western blot. The lack of sensitivity for olaparib implies that loss of BRC repeats 2 to 6 does not affect RAD51 recruitment and homologous recombination remains active in the cell.

To confirm that the *BRCA2*$^{-/-}$ cells retained functional BRCA2 protein, we examined RAD51 loading in response to irradiation. We seeded cells on coverslips and let them grow overnight. Next, the cells were irradiated and left to recover for at least 2 hours. After recovery, the cells were fixed, and the coverslips were stained with DAPI, anti-γH2AX and anti-RAD51. DAPI is a fluorescent dye that selectively binds to adenine-thymine rich regions in the DNA (Kapuscinski, 1995) and thus stains the nucleus. γH2AX was used as a marker for double-stranded breaks whilst RAD51 is a protein involved in HR (Baumann and West, 1998). BRCA2 will recruit partner and localiser of BRCA2 (PALB2) and BRCA1 at a given point during HR and will load RAD51 onto the 3' ends to mediate strand invasion (Zhao et al., 2017a). The presence of RAD51 foci indicates that BRCA2 is still present and functional, and therefore HR is still active in the cell to repair

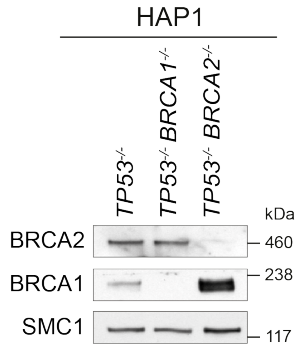


Figure 4.11: No full length BRCA2 is detected using Western blot. Whole-cell extracts of HAP1 *TP53*$^{-/-}$, HAP1 *TP53*$^{-/-}$ *BRCA1*$^{-/-}$ and HAP1 *TP53*$^{-/-}$ *BRCA2*$^{-/-}$ were prepared and immunoblotted. SMC1 is used as a loading control.

DNA damage in the most accurate way. After staining, the coverslips of HAP1 *TP53*$^{-/-}$ and HAP1 *TP53* -/- *BRCA2*$^{-/-}$ were analysed using fluorescence microscopy (Figure 4.12). We observed the presence of γH2AX foci indicating the effective introduction of DNA damage in both samples upon irradiation but importantly, we also observed RAD51 foci in both samples. As RAD51 requires BRCA2 to be loaded to ssDNA the presence of these foci indicate the BRCA2 CRISPR in the HAP1 *TP53* -/- *BRCA2*$^{-/-}$ cells did not result in a complete knockout of the functional BRCA2 protein.

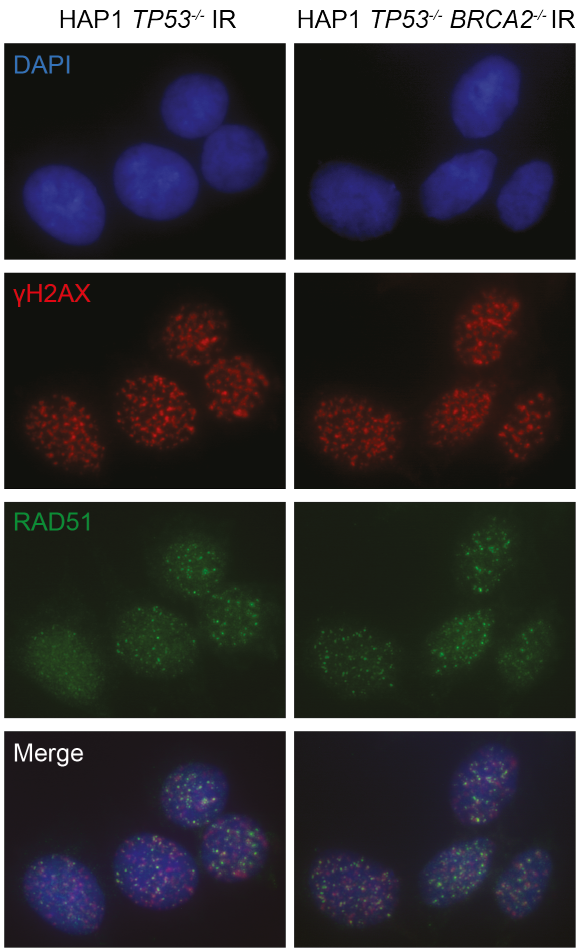


Figure 4.12: Confirmation of BRCA2 status via immunofluorescence. HAP1 *TP53*$^{-/-}$ and HAP1 *TP53*$^{-/-}$ *BRCA2*$^{-/-}$ are seeded on coverslips, irradiated with 10 Gy. After 2h of recovery, they were fixed and stained with DAPI (blue), anti-γH2AX (red) and anti-RAD51 (green) antibodies. Subsequently, the slides are analysed using fluorescence microscopy. Representative images of irradiated HAP1 *TP53*$^{-/-}$ and HAP1 *TP53*$^{-/-}$ *BRCA2*$^{-/-}$ cells are shown.

5 Discussions

Over the years, many G4 ligands have been developed to specifically target G4s with the aim to develop novel anti-cancer therapies (Asamitsu, 2019; Zuffo 2018)(Zuffo et al., 2018; Asamitsu et al., 2019). The binding of a G4 ligand and its subsequent stabilisation of the G4 structure induces DSBs, later resulting in genome instability. However, how G4 ligands induce this damage is not known yet, but different pathways are proposed. Despite *in vitro* evidence that G4 ligands induce lethal levels of DNA damage in cancer cells few have gone into clinical trials (Carvalho et al., 2020). Quarfloxin (CX-3543; (Drygin et al., 2009; Yao et al., 2018)) reached Phase II clinical trials in neuroendocrine carcinomas (NCT00780663) but had to be terminated due to a bioavailability problem. Recently, the G4 ligand CX-5461 was shown to be specifically lethal to BRCA1 and BRCA2-deficient cell and tumour models and this is currently being evaluated in patients in Phase I clinical trial (NCT02719977; (Xu et al., 2017; Yan et al., 2020)). Nevertheless, there is a discrepancy between the development of new G4 ligands and the number of clinically approved compounds. A better understanding of the mechanism of action is required for the development of more effective G4 ligands.

Cells lacking HR after the loss of BRCA1 or BRCA2 are prone to accumulating DSBs (Patel et al., 1998; Arnaudeau et al., 2001; Tutt and Ashworth, 2002). These breaks are the driving force for genome instability, as the cells lacking homologous recombination rely on less accurate repair mechanisms that often induce more DNA damage (Venkitaraman, 1999; Turner et al., 2005). The absence of HR makes the cells highly susceptible to other replication stress-inducing factors, for example, UV damage, chemotherapeutics or G4 ligands. Replication stress is defined as the event in which replication forks stall and consequently, DNA synthesis decreases (Zeman and Cimprich, 2014; Gaillard et al., 2015). This can be caused by replication fork barriers like G4s (Weitzmann et al., 1996; Hänsel-Hertsch et al., 2017). Stabilisation of a G-quadruplex by binding of a specific ligand like PDS makes this secondary structure almost unresolvable (Chen et al., 2015). BRCA1 and BRCA2 are then required to restart or repair the stalled replication fork. However, in BRCA1 and

BRCA2-deficient cells, HR mediated DNA repair is absent and prolonged replication fork stalling and collapse will induce DNA damage, eventually lead to cell death (Rizzo et al., 2009; Gauthier et al., 2012). Consequently, PDS is able to selectively kill cells lacking homologous recombination (Zimmer et al., 2016).

5.1 Pyridostatin activates the innate immune response

PDS selectively kills BRCA-deficient cells however, the exact cellular mechanism required to induce this cell death has not been elucidated. Recently, activation of the innate immune response has been described in cells in response to DNA damage caused by PARP inhibitors, IR and DNA cross-linking agents like cisplatin (Reisländer et al., 2020). Therefore, we hypothesised that the innate immune response's activation might contribute to PDS's selective killing of BRCA1 and BRCA2-deficient cells. We confirmed that *BRCA2*$^{-/-}$ cells are sensitive for PDS and therefore can be specifically targeted by the drug (Figure 4.1). *BRCA2*$^{+/+}$ cells experience less sensitivity upon PDS treatment as the presence of homologous recombination can repair most of the induced damage (Zimmer et al., 2016).

We hypothesised that PDS has the ability to enhance the innate immune response similar to that observed in BRCA2-deficient cells treated with olaparib (Reisländer et al., 2019). In Figure 4.2, the innate immune response activation upon olaparib treatment was considered as a control and used to compare against PDS treated BRCA2-proficient and deficient cells. The Western blots demonstrated elevated levels of pKAP1, indicating increased levels of DNA damage for both olaparib and PDS, as expected from the literature (Zimmer et al., 2016; Perkhofer et al., 2017). Elevated levels of pIRF3 were observed in BRCA2-deficient cells, which is a commonly used marker for the activation of the innate immune response (Servant et al., 2003; Mori et al., 2004). These observations were confirmed by measuring mRNA expression levels of downstream regulator genes of the type I IFN response. *IFIT2* and *OAS2* are examples of interferon-stimulated genes that are expressed upon type I IFN response activation. They are significantly upregulated in BRCA2-deficient

cells compared to BRCA2-proficient cells. Together, these findings suggest that the mechanism of action for PDS to target and kill HR-compromised cells specifically, is potentially based on the activation of the innate immune response. We predict that the presence of micronuclei is the link between DNA-damage accumulation and innate immune response activation. Micronuclei are cytosolic structures containing small pieces of DNA resulting from failed chromosome segregation and are considered an important marker for genomic instability (Gisselsson et al., 2001; Hatch et al., 2013). De Magis et al. (2019) has confirmed in his experiments that G4 ligands can cause the accumulation of micronuclei in an R-loop dependent way. He also found that additional micronuclei accumulation occurred upon BRCA2 knockdown (De Magis et al., 2019). Apart from R-loop dependent formation of micronuclei, it has been suggested that chromosomal bridges can trigger micronuclei formation (Hoffelder et al., 2004; Pampalona et al., 2010). These bridges occur after the fusion of two broken chromosomes that were mis-repaired and are believed to induce genomic instability in cancer. Tahara et al. (2006) showed using microscopy that G4 ligands can induce these chromosomal bridges. This implies that G4 ligands have two different potential pathways to trigger the formation of micronuclei supporting the hypothesis that PDS can activate the innate immune response by accumulating micronuclei.

5.2 Influence of paclitaxel on BRCA1/2-deficient cells

After finding the synergistic effect of pyridostatin and paclitaxel during the mini screen conducted by Dr Annamaria Biroccio, we wanted to verify this potential anti-cancer drug combination *in vitro*. Paclitaxel (Taxol) is known to arrest cells in mitosis by binding the microtubules and eventually causing cell death (Rowinsky and Donehower, 1995; Milross et al., 1996; Singla et al., 2002; Chabalier et al., 2006). We assessed the sensitivity of BRCA1/2-proficient and deficient cells for paclitaxel treatment. Viability assay in Figure 4.4A showed that in contrast to PDS, paclitaxel does not have the ability to target BRCA1/2-deficient cells selectively.

Subsequently, the ability of paclitaxel to activate the innate immune response was tested using

Western blot. Despite what was observed for PDS, paclitaxel treatment only causes slow accumulation of pIRF3 but there is no evidence of further innate immune response activation. This is in line with what Zierhut et al. (2019) showed. They observed that paclitaxel-induced arrest in mitosis led to the weak activation of cGAS which in turn causes slow pIRF3 accumulation resulting in triggering of apoptosis (Zierhut et al., 2019). For these experiments, they used a treatment concentration of 500 nM paclitaxel until cell death was observed, this is of course dependent on the cell line and paclitaxel dose (Gascoigne and Taylor, 2008). The duration before cells died varied between 2 to 60 hours. However, the majority of the control cells died after an average of 8 hours. For our experiments, concentrations of 50 – 500 nM were used for 3 days. The cell lines used in our experiments differ from the ones used by Zierhut et al. (2019).

5.3 PDS and paclitaxel synergism

Synergism between PDS and paclitaxel was originally observed in the *in vivo* experiments from the lab of Dr Biroccio (in collaboration with our lab). Using a xenograft model, we tested the difference between PDS and paclitaxel single agent treatment or the combination of both drugs. It is known from previous studies that both compounds have an antitumour effect, but the combination of both was not yet described (Khandare et al., 2006; De Magis et al., 2019). However, the combination of other G4 ligands with paclitaxel has already been investigated and demonstrated to positively affect the tumour growth suppression. Gowan et al. (2002) examined the combination of BRACO19 and paclitaxel and looked at the difference in time required by the tumour to grow to 10-fold of the starting volume. They saw that the tumour treated with the drug combination grew at a slower rate. It took 10 days longer to reach the same tumour size compared to the other treatments. Similarly, Cookson et al. (2005) examined the combination of paclitaxel with RHPS4 and found a synergistic effect between the two drugs. Strikingly, three G4 stabilising ligands, including PDS, have independently shown synergy with paclitaxel, making it essential to determine the mechanism behind the synergy of both drugs.

Based on the *in vivo* experiment of Dr Biroccio, we assessed the induction of apoptosis after combination treatment with PDS and paclitaxel. We hypothesised that the replication stress induced by PDS triggers micronuclei formation after mitosis, which would be sensed by cGAS during interphase (Glück et al., 2017; Harding et al., 2017; De Magis et al., 2019). Conversely, we did not observe an increase of apoptosis in the combination treated samples in either BRCA2-proficient or deficient cells compared to single PDS or paclitaxel (Figure 4.5). However, the amount of cell death did increase in paclitaxel treated samples as previously described by other groups (Panvichian et al., 1998; Gowan et al., 2002).

Flow cytometry analysis subsequently demonstrated that prolonged treatment of paclitaxel causes slippage of cells through the induced mitotic block. Slippage of these cells results in the accumulation of cells with abnormal chromosomal content. Jordan et al. (1996) observed that most cells exited mitosis after removing 10 nM paclitaxel and that one or more nuclei were detected in 55% of the cells. These results suggested that cells coming out of a mitotic block have an abnormal chromosomal content. Subsequent studies confirmed that cells treated with paclitaxel ultimately become tetraploid (Panvichian et al., 1998; Stewart et al., 1999; Blajeski et al., 2001). However, the effects are cell type dependent as Gascoigne and Taylor (2008) has shown. Stewart et al. (1999) suggest that cells slipped from mitosis will undergo replication again. These findings are complementary with our observations that paclitaxel blocked cells can escape with incomplete DNA-segregation resulting in polyploid cells (Riffell et al., 2009).

Based on the observation of our preliminary experiments and the literature, we reduced the concentration of paclitaxel from 50 nM to 10 nM for 3 days. We demonstrated in Figure 4.7 that the combination treatment of 5 µM PDS and 10 nM paclitaxel is able to induce the activation of the innate immune response, similarly as we observed for PDS single treatments in Figure 4.2B. Similar results were found for single PDS and paclitaxel treatment with the BRCA1 mutated cell line MDA-MB-436 that was used for the *in vivo* experiment. However, the combination of both drugs did not trigger as much DNA damage in MDA-MB-436 as observed from H1299 cells in Figure 4.7A.

Next, we sought to determine paclitaxel's impact on the cell cycle by induction of a mitotic block. We demonstrated the accumulation of cells arrested in mitosis for paclitaxel treated samples (Figure 4.8A). This is in line with the observation made by Milross et al. (1996) and Jordan et al. (1996) that paclitaxel can efficiently arrest cell in mitosis. However, our results suggest that PDS and paclitaxel's synergy does not influence the cell fraction accumulated in mitosis. Consistent with Swanton et al. (2007) we found that paclitaxel causes an increase in cells with an abnormal chromosomal content. These cells have less than 1 pair of chromosomes (2n) or more than 2 pairs when in mitosis (4n). This is a consequence of cells escaping the mitotic block with failed chromosomal segregation (Jordan et al., 1996; Swanton et al., 2007; Kang et al., 2009). However, the combination of PDS and paclitaxel did not increase the percentage of cells with abnormal chromosomal content. As we did not observe a difference with the combination treatment compared to the single treatment of paclitaxel, we increased the PDS concentration from 5 µM to 10 µM. This did not have a substantial effect on the results we obtained, and we were not able to make a better distinction between single and combination treatments for H1299 shBRCA2$^{\mathrm{DOX}}$. In contrast, in MDA-MB-436, the cell fraction of polyploid cells is higher than in H1299, and also control and PDS treated samples showed an increase in the number of ">G2/M" cells. However, the combination treatment did not affect "<G1" or ">G2/M" differently than other treatments in MDA-MB-436 BRCA1$^{5396\mathrm{G>A}}$. Unfortunately, due to time shortage, majorly caused by COVID-19, we were not able to do more experiments to optimise the combination treatment of PDS and paclitaxel. Nevertheless, we observed that the combination treatment could activate the innate immune response. However, it has no additional influence on blocking cells in mitosis nor causing cells with abnormal chromosomal numbers.

5.4 Unsuccessful BRCA2 knockout in HAP1

Characterisation of the new HAP1 *TP53*$^{-/-}$ *BRCA2*$^{-/-}$ cell line was a continuation of the collaboration that we have with the lab of Dr Serena Nik-Zainal (University of Cambridge). In the past, other members of our lab characterised their HAP1 *TP53*$^{-/-}$ *BRCA1*$^{-/-}$ variant. These cell lines were

developed as the BRCA1 or BRCA2 knockout models in the field of study are currently limited. Furthermore, no model with both BRCA1 and BRCA2 knockout is available, restricting accurate comparison of the effect of BRCA1 and BRCA2 knock out. The sensitivity of HAP1 *TP53*$^{-/-}$ cells, with or without BRCA1 and BRCA2 knockout, to olaparib were investigated to confirm that the cells were functionally BRCA-deficient as BRCA-deficient cells are sensitive to PARP inhibitors (Figure 4.10) (Tutt et al., 2009, 2010). Strikingly, HAP1 *TP53*$^{-/-}$ *BRCA2*$^{-/-}$ did not show sensitivity for olaparib treatment and grew similarily to HAP1 *TP53*$^{-/-}$ in the presence of olaparib. Verification of the BRCA2 status by Western blot showed the absence of full-length BRCA2. An immunofluorescence experiment that was done as a confirmation of functionally inactive BRCA2 demonstrated the presence of RAD51 foci in irradiated HAP1 *TP53*$^{-/-}$ *BRCA2*$^{-/-}$ in Figure 4.12. This implies that HR is still active in the cell, and therefore BRCA2 is not (entirely) knocked out. This was confirmed after the Nik-Zainal lab did next-generation sequencing. The in frame deletion introduced by CRISPR-Cas9 resulted in a truncated BRCA2 that was functionally active in HR resulting in resistance to olaparib treatment.

6 Conclusions

The discovery of G4s has allowed the development of novel anti-cancer therapy based on the stabilisation of these secondary structures. Despite the number of developed ligands, insight into the mechanism of action is required to develop a more effective G4 ligand. We confirmed that PDS could specifically kill BRCA1 and BRCA2-deficient cells and tumours as known from previous studies. Subsequently, we discovered that PDS activates the innate immune response, likely via micronuclei formation, which contributes to the induction of apoptosis in these cells. Furthermore, the combination of PDS with paclitaxel demonstrated a synergistic effect on tumour growth suppression. Combination of other G4 ligands with paclitaxel has shown similar results emphasising the importance of continuing the exploration of this new anti-cancer combination therapy. Despite the promising results, further investigation is required to identify how PDS triggers DNA damage through innate immune activation and what drives the synergy of the combination of PDS and paclitaxel.

7 Future perspectives

The combination of PDS and paclitaxel has high therapeutical potential, and further work is required to gain mechanistic insight into this treatment's synergy. First of all, an optimisation of the treatment conditions is essential. A viability for PDS and paclitaxel combination in H1299 shBRCA2^{DOX} cells is required to determine the range of doses that induces synergy *in vitro*. As we hypothesise this combination leads to the induction of micronuclei. An immunofluorescence-based experiment is required to confirm that micronuclei are induced upon combination treatment. Further characterisation of the accumulation of polyploid cells by staining with DAPI will allow the identification of multinucleated cells. Live-cell imaging for cells treated with single or combination treatment of PDS and paclitaxel could also reveal the length of time required for the cell to go into apoptosis or is able to escape the induced mitotic block. Experiments with temporal knockdown of cGAS and STING are required to confirm the dependence of PDS or combination treatment induced cell death on activation of the innate immune response. Subsequently, investigating xenograft material for innate immune response activation via Western blot and RT-qPCR can give more accurate insights into the drugs' synergism on activating the innate immune response. Whilst work is still required to determine the mechanism of action of the PDS and paclitaxel combination, our work indicates a link between DNA-damage and innate immune response activation may be critical in driving the synergy of these compounds.

References

Aaltonen, L., Johns, L., Järvinen, H., Mecklin, J. P., and Houlston, R. (2007). Explaining the familial colorectal cancer risk associated with mismatch repair (MMR)-deficient and MMR-stable tumors. *Clinical Cancer Research*, 13(1):356–361.

Ahrabi, S., Sarkar, S., Pfister, S. X., Pirovano, G., Higgins, G. S., Porter, A. C. G., and Humphrey, T. C. (2016). A role for human homologous recombination factors in suppressing microhomology-mediated end joining. *Nucleic Acids Research*, 44(12):5743–5757.

Arnaudeau, C., Lundin, C., and Helleday, T. (2001). DNA double-strand breaks associated with replication forks are predominantly repaired by homologous recombination involving an exchange mechanism in mammalian cells. *Journal of Molecular Biology*, 307(5):1235–1245.

Asamitsu, S., Obata, S., Yu, Z., Bando, T., and Sugiyama, H. (2019). Recent Progress of Targeted G-Quadruplex-Preferred Ligands Toward Cancer Therapy. *Molecules*, 24(3):429.

Attardi, L. D. (2005). The role of p53-mediated apoptosis as a crucial anti-tumor response to genomic instability: Lessons from mouse models.

Aylon, Y., Liefshitz, B., and Kupiec, M. (2004). The CDK regulates repair of double-strand breaks by homologous recombination during the cell cycle. *The EMBO Journal*, 23(24):4868–4875.

Baumann, P. and West, S. C. (1998). Role of the human RAD51 protein in homologous recombination and double- stranded-break repair.

Bennardo, N., Cheng, A., Huang, N., and Stark, J. M. (2008). Alternative-NHEJ is a mechanistically distinct pathway of mammalian chromosome break repair. *PLoS Genetics*, 4(6).

Besnard, E., Babled, A., Lapasset, L., Milhavet, O., Parrinello, H., Dantec, C., Marin, J. M., and Lemaitre, J. M. (2012). Unraveling cell type-specific and reprogrammable human replication origin signatures associated with G-quadruplex consensus motifs. *Nature Structural and Molecular Biology*, 19(8):837–844.

Bétous, R., Goullet de Rugy, T., Pelegrini, A. L., Queille, S., de Villartay, J.-P., and Hoffmann, J.-S. (2018). DNA replication stress triggers rapid DNA replication fork breakage by Artemis and XPF. *PLOS Genetics*, 14(7):e1007541.

Bidzinska, J., Cimino-Reale, G., Zaffaroni, N., and Folini, M. (2013). G-quadruplex structures in the human genome as novel therapeutic targets.

Blagosklonny, M. V. and Fojo, T. (1999). Molecular effects of paclitaxel: Myths and reality (a critical review).

Blajeski, A. L., Kottke, T. J., and Kaufmann, S. H. (2001). A multistep model for paclitaxel-induced apoptosis in human breast cancer cell lines. *Experimental Cell Research*, 270(2):277–288.

Bryan, T. M. (2019). Mechanisms of DNA replication and repair: Insights from the study of G-quadruplexes. *Molecules*, 24(19).

Campbell, N. H., Karim, N. H., Parkinson, G. N., Gunaratnam, M., Petrucci, V., Todd, A. K., Vilar, R., and Neidle, S. (2012). Molecular basis of structure-activity relationships between salphen metal complexes and human telomeric DNA quadruplexes. *Journal of Medicinal Chemistry*, 55(1):209–222.

Canman, C. E., Lim, D. S., Cimprich, K. A., Taya, Y., Tamai, K., Sakaguchi, K., Appella, E., Kastan, M. B., and Siliciano, J. D. (1998). Activation of the ATM kinase by ionizing radiation and phosphorylation of p53. *Science*, 281(5383):1677–1679.

Carr, A. M. (2002). Checking that replication breakdown is not terminal.

Carvalho, J., Mergny, J. L., Salgado, G. F., Queiroz, J. A., and Cruz, C. (2020). G-quadruplex, Friend or Foe: The Role of the G-quartet in Anticancer Strategies.

Cerbinskaite, A., Mukhopadhyay, A., Plummer, E. R., Curtin, N. J., and Edmondson, R. J. (2012). Defective homologous recombination in human cancers.

Chabalier, C., Lamare, C., Racca, C., Privat, M., Valette, A., and Larminat, F. (2006). BRCA1 downregulation leads to premature inactivation of spindle checkpoint and confers paclitaxel resistance. *Cell Cycle*, 5(9):1001–1007.

Chang, H. H., Pannunzio, N. R., Adachi, N., and Lieber, M. R. (2017). Non-homologous DNA end joining and alternative pathways to double-strand break repair.

Chatzinikolaou, G., Karakasilioti, I., and Garinis, G. A. (2014). DNA damage and innate immunity: Links and trade-offs.

Chawla-Sarkar, M., Lindner, D. J., Liu, Y. F., Williams, B. R., Sen, G. C., Silverman, R. H., and Borden, E. C. (2003). Apoptosis and interferons: Role of interferon-stimulated genes as mediators of apoptosis.

Chen, M. C., Murat, P., Abecassis, K., Ferre-D'Amare, A. R., and Balasubramanian, S. (2015). Insights into the mechanism of a G-quadruplex-unwinding DEAH-box helicase. *Nucleic Acids Research*, 43(4):2223–2231.

Ciccia, A., McDonald, N., and West, S. C. (2008). Structural and Functional Relationships of the XPF/MUS81 Family of Proteins. *Annual Review of Biochemistry*, 77(1):259–287.

Civril, F., Deimling, T., De Oliveira Mann, C. C., Ablasser, A., Moldt, M., Witte, G., Hornung, V., and Hopfner, K. P. (2013). Structural mechanism of cytosolic DNA sensing by cGAS. *Nature*, 498(7454):332–337.

Cocco, M. J., Hanakahi, L. A., Huber, M. D., and Maizels, N. (2003). Specific interactions of distamycin with G-quadruplex DNA. *Nucleic acids research*, 31(11):2944–2951.

Cookson, J. C., Dai, F., Smith, V., Heald, R. A., Laughton, C. A., Stevens, M. F., and Burger, A. M. (2005). Pharmacodynamics of the G-quadruplex-stabilizing telomerase inhibitor 3,11-difluoro-6,8,13-trimethyl-8H-quino[4,3,2-kl]acridinium methosulfate (RHPS4) in vitro: Activity in human tumor cells correlates with telomere length and can be enhanced, or antagonized, with cytotoxic agents. *Molecular Pharmacology*, 68(6):1551–1558.

Črnugelj, M., Šket, P., and Plavec, J. (2003). Small change in a G-rich sequence, a dramatic change in topology: New dimeric G-quadruplex folding motif with unique loop orientations. *Journal of the American Chemical Society*, 125(26):7866–7871.

Dalton, W. B. and Yang, V. W. (2009). Role of prolonged mitotic checkpoint activation in the formation and treatment of cancer.

Daly, M. B., Axilbund, J. E., Buys, S., Crawford, B., Farrell, C. D., Friedman, S., Garber, J. E., Goorha, S., Gruber, S. B., Hampel, H., Kaklamani, V., Kohlmann, W., Kurian, A., Litton, J., Marcom, P. K., Nussbaum, R., Offit, K., Pal, T., Pasche, B., Pilarski, R., Reiser, G., Shannon, K. M., Smith, J. R., Swisher, E., and Weitzel, J. N. (2010). Genetic/familial high-risk assessment: Breast and ovarian - Clinical practice guidelines in oncology™.

De Laat, W. L., Jaspers, N. G., and Hoeijmakers, J. H. (1999). Molecular mechanism of nucleotide excision repair.

De Magis, A., Manzo, S. G., Russo, M., Marinello, J., Morigi, R., Sordet, O., and Capranico, G. (2019). DNA damage and genome instability by G-quadruplex ligands are mediated by R loops in human cancer cells. *Proceedings of the National Academy of Sciences of the United States of America*, 116(3):816–825.

De Veer, M. J., Sim, H., Whisstock, J. C., Devenish, R. J., and Ralph, S. J. (1998). IFI60/ISG60/IFIT4, a new member of the human IFI54/IFIT2 family of interferon-stimulated genes. *Genomics*, 54(2):267–277.

Delia, D., Mizutani, S., Panigone, S., Tagliabue, E., Fontanella, E., Asada, M., Yamada, T., Taya, Y., Prudente, S., Saviozzi, S., Frati, L., Pierotti, M. A., and Chessa, L. (2000). ATM protein and p53-serine 15 phosphorylation in ataxia-telangiectasia (AT) patients and at heterozygotes. *British Journal of Cancer*, 82(12):1938–1945.

Diamond, M. S., Kinder, M., Matsushita, H., Mashayekhi, M., Dunn, G. P., Archambault, J. M., Lee, H., Arthur, C. D., White, J. M., Kalinke, U., Murphy, K. M., and Schreiber, R. D. (2011).

Type I interferon is selectively required by dendritic cells for immune rejection of tumors. *Journal of Experimental Medicine*, 208(10):1989–2003.

Dickey, J. S., Redon, C. E., Nakamura, A. J., Baird, B. J., Sedelnikova, O. A., and Bonner, W. M. (2010). Stress and γ-H2AX. In *Handbook of Cell Signaling, 2/e*, volume 3, pages 2273–2282. Elsevier Inc.

Ding, L., Kim, H. J., Wang, Q., Kearns, M., Jiang, T., Ohlson, C. E., Li, B. B., Xie, S., Liu, J. F., Stover, E. H., Howitt, B. E., Bronson, R. T., Lazo, S., Roberts, T. M., Freeman, G. J., Konstantinopoulos, P. A., Matulonis, U. A., and Zhao, J. J. (2018). PARP Inhibition Elicits STING-Dependent Antitumor Immunity in Brca1-Deficient Ovarian Cancer. *Cell Reports*, 25(11):2972–2980.

Dobbs, N., Burnaevskiy, N., Chen, D., Gonugunta, V. K., Alto, N. M., and Yan, N. (2015). STING activation by translocation from the ER is associated with infection and autoinflammatory disease. *Cell Host and Microbe*, 18(2):157–168.

Drygin, D., Siddiqui-Jain, A., O'Brien, S., Schwaebe, M., Lin, A., Bliesath, J., Ho, C. B., Proffitt, C., Trent, K., Whitten, J. P., Lim, J. K., Von Hoff, D., Anderes, K., and Rice, W. G. (2009). Anticancer activity of CX-3543: A direct inhibitor of rRNA biogenesis. *Cancer Research*, 69(19):7653–7661.

Dueva, R. and Iliakis, G. (2013). Alternative pathways of non-homologous end joining (NHEJ) in genomic instability and cancer. *Translational Cancer Research*, 2(3):163–177.

Dynan, W. S. and Yoo, S. (1998). Interaction of Ku protein and DNA-dependent protein kinase catalytic subunit with nucleic acids. *Nucleic Acids Research*, 26(7):1551–1559.

Eden, E., Geva-Zatorsky, N., Issaeva, I., Cohen, A., Dekel, E., Danon, T., Cohen, L., Mayo, A., and Alon, U. (2011). Proteome half-life dynamics in living human cells. *Science*, 331(6018):764–768.

Essers, J., Van Steeg, H., De Wit, J., Swagemakers, S. M., Vermeij, M., Hoeijmakers, J. H., and

Kanaar, R. (2000). Homologous and non-homologous recombination differentially affect DNA damage repair in mice. *EMBO Journal*, 19(7):1703–1710.

Featherstone, C. and Jackson, S. P. (1999). DNA double-strand break repair. *Current Biology*, 9(20):R759–R761.

Fedor, Y., Vignard, J., Nicolau-Travers, M. L., Boutet-Robinet, E., Watrin, C., Salles, B., and Mirey, G. (2013). From single-strand breaks to double-strand breaks during S-phase: A new mode of action of the Escherichia coli Cytolethal Distending Toxin. *Cellular Microbiology*, 15(1):1–15.

Fenech, M., Kirsch-Volders, M., Natarajan, A. T., Surralles, J., Crott, J. W., Parry, J., Norppa, H., Eastmond, D. A., Tucker, J. D., and Thomas, P. (2011). Molecular mechanisms of micronucleus, nucleoplasmic bridge and nuclear bud formation in mammalian and human cells. *Mutagenesis*, 26(1):125–132.

Feng, W. and Jasin, M. (2017). Homologous Recombination and Replication Fork Protection: BRCA2 and More! *Cold Spring Harbor symposia on quantitative biology*, 82:329–338.

Ferlini, C., Cicchillitti, L., Raspaglio, G., Bartollino, S., Cimitan, S., Bertucci, C., Mozzetti, S., Gallo, D., Persico, M., Fattorusso, C., Campiani, G., and Scambia, G. (2009). Paclitaxel directly binds to Bcl-2 and functionally mimics activity of Nur77. *Cancer Research*, 69(17):6906–6914.

Friedberg, E. C. (2008). A brief history of the DNA repair field. *Cell Research*, 18(1):3–7.

Gaillard, H., García-Muse, T., and Aguilera, A. (2015). Replication stress and cancer. *Nature Reviews Cancer 2015 15:5*, 15(5):276–289.

Gascoigne, K. E. and Taylor, S. S. (2008). Cancer Cells Display Profound Intra- and Interline Variation following Prolonged Exposure to Antimitotic Drugs. *Cancer Cell*, 14(2):111–122.

Gauthier, L. R., Granotier, C., Hoffschir, F., Etienne, O., Ayouaz, A., Desmaze, C., Mailliet, P., Biard, D. S., and Boussin, F. D. (2012). Rad51 and DNA-PKcs are involved in the generation of specific telomere aberrations induced by the quadruplex ligand 360A that impair mitotic cell progression and lead to cell death. *Cellular and Molecular Life Sciences*, 69(4):629–640.

Gisselsson, D., Björk, J., Höglund, M., Mertens, F., Dal Cin, P., Åkerman, M., and Mandahl, N. (2001). Abnormal nuclear shape in solid tumors reflects mitotic instability. *American Journal of Pathology*, 158(1):199–206.

Glück, S., Guey, B., Gulen, M. F., Wolter, K., Kang, T. W., Schmacke, N. A., Bridgeman, A., Rehwinkel, J., Zender, L., and Ablasser, A. (2017). Innate immune sensing of cytosolic chromatin fragments through cGAS promotes senescence. *Nature Cell Biology*, 19(9):1061–1070.

Gonzalo, S. and Coll-Bonfill, N. (2019). Genomic instability and innate immune responses to self-DNA in progeria.

Gowan, S. M., Harrison, J. R., Patterson, L., Valenti, M., Read, M. A., Neidle, S., and Kelland, L. R. (2002). A G-quadruplex-interactive potent small-molecule inhibitor of telomerase exhibiting in vitro and in vivo antitumor activity. *Molecular Pharmacology*, 61(5):1154–1162.

Gudmundsdottir, K. and Ashworth, A. (2006). The roles of BRCA1 and BRCA2 and associated proteins in the maintenance of genomic stability.

Günthert, A. R., Pilz, S., Kuhn, W., Emons, G., and Meden, H. (1999). Docetaxel is effective in the treatment of metastatic endometrial cancer. *Anticancer Research*, 19(4 C):3459–3461.

Hanahan, D. and Weinberg, R. A. (2000). The hallmarks of cancer. *Cell*, 100(1):57–70.

Hänsel-Hertsch, R., Di Antonio, M., and Balasubramanian, S. (2017). DNA G-quadruplexes in the human genome: Detection, functions and therapeutic potential. *Nature Reviews Molecular Cell Biology*, 18(5):279–284.

Harding, S. M., Benci, J. L., Irianto, J., Discher, D. E., Minn, A. J., and Greenberg, R. A. (2017). Mitotic progression following DNA damage enables pattern recognition within micronuclei. *Nature*, 548(7668):466–470.

Hatch, E. M., Fischer, A. H., Deerinck, T. J., and Hetzer, M. W. (2013). Catastrophic Nuclear Envelope Collapse in Cancer Cell Micronuclei. *Cell*, 154(1):47.

Heyer, W.-D., Ehmsen, K. T., and Liu, J. (2010). Regulation of Homologous Recombination in Eukaryotes.

Hoeijmakers, J. H. J. (2001). Genome maintenance mechanisms for preventing cancer. *Nature*, 411(6835):366–374.

Hoffelder, D. R., Luo, L., Burke, N. A., Watkins, S. C., Gollin, S. M., and Saunders, W. S. (2004). Resolution of anaphase bridges in cancer cells. *Chromosoma*, 112(8):389–397.

Hollaender, A. and Curtis, J. T. (1935). Effect of Sublethal Doses of Monochromatic Ultraviolet Radiation on Bacteria in Liquid Suspensions. *Proceedings of the Society for Experimental Biology and Medicine*, 33(1):61–62.

Horwitz, S. B. (1992). Mechanism of action of taxol. *Trends in Pharmacological Sciences*, 13(April):134 – 136.

Huppert, J. L. (2010). Structure, location and interactions of G-quadruplexes. *FEBS Journal*, 277(17):3452–3458.

Huppert, J. L. and Balasubramanian, S. (2005). Prevalence of quadruplexes in the human genome. *Nucleic Acids Research*, 33(9):2908–2916.

Hustedt, N. and Durocher, D. (2017). The control of DNA repair by the cell cycle.

Im, J. Y., Lee, K. W., Won, K. J., Kim, B. K., Ban, H. S., Yoon, S. H., Lee, Y. J., Kim, Y. J., Song, K. B., and Won, M. (2016). DNA damage-induced apoptosis suppressor (DDIAS), a novel target of NFATc1, is associated with cisplatin resistance in lung cancer. *Biochimica et Biophysica Acta - Molecular Cell Research*, 1863(1):40–49.

Ira, G., Pellicioll, A., Balijja, A., Wang, X., Florani, S., Carotenuto, W., Liberi, G., Bressan, D., Wan, L., Hollingsworth, N. M., Haber, J. E., and Folani, M. (2004). DNA end resection, homologous recombination and DNA damage checkpoint activation require CDK1. *Nature*, 431(7011):1011–1017.

Jazayeri, A., Falck, J., Lukas, C., Bartek, J., Smith, G. C., Lukas, J., and Jackson, S. P. (2006). ATM- and cell cycle-dependent regulation of ATR in response to DNA double-strand breaks. *Nature Cell Biology*, 8(1):37–45.

Jordan, M. A., Wendell, K., Gardiner, S., Brent Derry, W., Copp, H., and Wilson, L. (1996). Mitotic Block Induced in HeLa Cells by Low Concentrations of Paclitaxel (Taxol) Results in Abnormal Mitotic Exit and Apoptotic Cell Death. *Cancer Research*, 56(4).

Kang, H. J., Lee, S. H., Price, J. E., and Kim, L. S. (2009). Curcumin Suppresses the Paclitaxel-Induced Nuclear Factor-κB in Breast Cancer Cells and Potentiates the Growth Inhibitory Effect of Paclitaxel in a Breast Cancer Nude Mice Model. *The Breast Journal*, 15(3):223–229.

Kapuscinski, J. (1995). DAPI: A DMA-Specific fluorescent probe. *Biotechnic and Histochemistry*, 70(5):220–233.

Karanja, K. K., Cox, S. W., Duxin, J. P., Stewart, S. A., and Campbell, J. L. (2012). DNA2 and EXO1 in replication-coupled, homology-directed repair and in the interplay between HDR and the FA/BRCA network. *Cell Cycle*, 11(21):3983–3996.

Khandare, J. J., Jayant, S., Singh, A., Chandna, P., Wang, Y., Vorsa, N., and Minko, T. (2006). Dendrimer versus linear conjugate: Influence of polymeric architecture on the delivery and anti-cancer effect of paclitaxel. *Bioconjugate Chemistry*, 17(6):1464–1472.

Khanna, K. K. and Jackson, S. P. (2001). DNA double-strand breaks: Signaling, repair and the cancer connection. *Nature Genetics*, 27(3):247–254.

Khosravi, R., Maya, R., Gottlieb, T., Oren, M., Shiloh, Y., and Shkedy, D. (1999). Rapid ATM-dependent phosphorylation of MDM2 precedes p53 accumulation in response to DNA damage. *Proceedings of the National Academy of Sciences of the United States of America*, 96(26):14973–14977.

Kim, C., Wang, X. D., and Yu, Y. (2020). Parp1 inhibitors trigger innate immunity via parp1 trapping-induced DNA damage response. *eLife*, 9:1–47.

Kim, G., Ison, G., McKee, A. E., Zhang, H., Tang, S., Gwise, T., Sridhara, R., Lee, E., Tzou, A., Philip, R., Chiu, H. J., Ricks, T. K., Palmby, T., Russell, A. M., Ladouceur, G., Pfuma, E., Li, H., Zhao, L., Liu, Q., Venugopal, R., Ibrahim, A., and Pazdur, R. (2015). FDA approval summary: Olaparib monotherapy in patients with deleterious germline BRCA-mutated advanced ovarian cancer treated with three or more lines of chemotherapy. *Clinical Cancer Research*, 21(19):4257–4261.

Kozlov, S. V., Graham, M. E., Jakob, B., Tobias, F., Kijas, A. W., Tanuji, M., Chen, P., Robinson, P. J., Taucher-Scholz, G., Suzuki, K., So, S., Chen, D., and Lavin, M. F. (2011). Autophosphorylation and ATM activation: Additional sites add to the complexity. *Journal of Biological Chemistry*, 286(11):9107–9119.

Krogh, B. O. and Symington, L. S. (2004). Recombination Proteins in Yeast. *Annual Review of Genetics*, 38(1):233–271.

Krokan, H. E. and Bjørås, M. (2013). Base excision repair. *Cold Spring Harbor Perspectives in Biology*, 5(4):1–22.

Kunkel, T. A. and Erie, D. A. (2005). DNA MISMATCH REPAIR. *Annual Review of Biochemistry*, 74(1):681–710.

Lai, X., Broderick, R., Bergoglio, V., Zimmer, J., Badie, S., Niedzwiedz, W., Hoffmann, J. S., and Tarsounas, M. (2017). MUS81 nuclease activity is essential for replication stress tolerance and chromosome segregation in BRCA2-deficient cells. *Nature Communications*, 8(1):1–13.

Lam, E. Y. N., Beraldi, D., Tannahill, D., and Balasubramanian, S. (2013). G-quadruplex structures are stable and detectable in human genomic DNA. *Nature Communications*, 4(1):1–8.

Levine, A. J. (1997). p53, the cellular gatekeeper for growth and division.

Lieber, M. R. (2010). The Mechanism of Double-Strand DNA Break Repair by the Nonhomologous DNA End-Joining Pathway. *Annual Review of Biochemistry*, 79(1):181–211.

Lin, W., Sampathi, S., Dai, H., Liu, C., Zhou, M., Hu, J., Huang, Q., Campbell, J., Shin-Ya, K., Zheng, L., Chai, W., and Shen, B. (2013). Mammalian DNA2 helicase/nuclease cleaves G-quadruplex DNA and is required for telomere integrity. *EMBO Journal*, 32(10):1425–1439.

Lindahl, T. and Barnes, D. E. (2000). Repair of endogenous DNA damage. In *Cold Spring Harbor Symposia on Quantitative Biology*, volume 65, pages 127–133. Cold Spring Harbor Laboratory Press.

Lohse, I., Borgida, A., Cao, P., Cheung, M., Pintilie, M., Bianco, T., Holter, S., Ibrahimov, E., Kumareswaran, R., Bristow, R. G., Tsao, M. S., Gallinger, S., and Hedley, D. W. (2015). BRCA1 and BRCA2 mutations sensitize to chemotherapy in patient-derived pancreatic cancer xenografts. *British Journal of Cancer*, 113(3):425–432.

Mackenzie, K. J., Carroll, P., Martin, C.-A., Murina, O., Fluteau, A., Simpson, D. J., Olova, N., Sutcliffe, H., Rainger, J. K., Leitch, A., Osborn, R. T., Wheeler, A. P., Nowotny, M., Gilbert, N., Chandra, T., Reijns, M. A. M., and Jackson, A. P. (2017). cGAS surveillance of micronuclei links genome instability to innate immunity. *Nature*, 548(7668):461–465.

Masuda-Sasa, T., Polaczek, P., Peng, X. P., Chen, L., and Campbell, J. L. (2008). Processing of G4 DNA by Dna2 helicase/nuclease and replication protein A (RPA) provides insights into the mechanism of Dna2/RPA substrate recognition. *Journal of Biological Chemistry*, 283(36):24359–24373.

McLuckie, K. I., Di Antonio, M., Zecchini, H., Xian, J., Caldas, C., Krippendorff, B. F., Tannahill, D., Lowe, C., and Balasubramanian, S. (2013). G-quadruplex DNA as a molecular target for induced synthetic lethality in cancer cells. *Journal of the American Chemical Society*, 135(26):9640–9643.

Miglietta, G., Russo, M., and Capranico, G. (2020). G-quadruplex–R-loop interactions and the mechanism of anticancer G-quadruplex binders. *Nucleic Acids Research*, 48(21):11942–11957.

Mills, K. D., Ferguson, D. O., and Alt, F. W. (2003). The role of DNA breaks in genomic instability and tumorigenesis. *Immunological Reviews*, 194(1):77–95.

Milross, C. G., Mason, K. A., Hunter, N. R., Chung, W.-K., Peters, L. J., and Milas, L. (1996). Relationship of Mitotic Arrest and Apoptosis to Antitumor Effect of Paclitaxel. *JNCI Journal of the National Cancer Institute*, 88(18):1308–1314.

Mori, M., Yoneyama, M., Ito, T., Takahashi, K., Inagaki, F., and Fujita, T. (2004). Identification of Ser-386 of Interferon Regulatory Factor 3 as Critical Target for Inducible Phosphorylation That Determines Activation. *Journal of Biological Chemistry*, 279(11):9698–9702.

Motwani, M., Pesiridis, S., and Fitzgerald, K. A. (2019). DNA sensing by the cGAS–STING pathway in health and disease.

Negritto, M. C. (2010). Repairing Double-Strand DNA Breaks. *Nature Education*, 3(9):26.

Nguyen, T. Q. N., Lim, K. W., and Phan, A. T. (2017). A Dual-Specific Targeting Approach Based on the Simultaneous Recognition of Duplex and Quadruplex Motifs. *Scientific Reports*, 7(1):1–7.

Nimonkar, A. V., Özsoy, A. Z., Genschel, J., Modrich, P., and Kowalczykowski, S. C. (2008). Human exonuclease 1 and BLM helicase interact to resect DNA and initiate DNA repair. *Proceedings of the National Academy of Sciences of the United States of America*, 105(44):16906–16911.

Pampalona, J., Soler, D., Genescà, A., and Tusell, L. (2010). Telomere dysfunction and chromosome structure modulate the contribution of individual chromosomes in abnormal nuclear morphologies. *Mutation Research - Fundamental and Molecular Mechanisms of Mutagenesis*, 683(1-2):16–22.

Panvichian, R., Orth, K., Day, M. L., Day, K. C., Pilat, M. J., and Pienta, K. J. (1998). Paclitaxel-associated Multimininucleation Is Permitted by the Inhibition of Caspase Activation: A Potential Early Step in Drug Resistance. *Cancer Research*, 58(20).

Pâques, F. and Haber, J. E. (1999). Multiple Pathways of Recombination Induced by Double-Strand Breaks in Saccharomyces cerevisiae. *Microbiology and Molecular Biology Reviews*, 63(2):349–404.

Patel, K. J., Yu, V. P., Lee, H., Corcoran, A., Thistlethwaite, F. C., Evans, M. J., Colledge, W. H., Friedman, L. S., Ponder, B. A., and Venkitaraman, A. R. (1998). Involvement of Brca2 in DNA repair. *Molecular Cell*, 1(3):347–357.

Pepe, A. and West, S. C. (2014). MUS81-EME2 promotes replication fork restart. *Cell Reports*, 7(4):1048–1055.

Perkhofer, L., Schmitt, A., Carrasco, M. C. R., Ihle, M., Hampp, S., Ruess, D. A., Hessmann, E., Russell, R., Lechel, A., Azoitei, N., Lin, Q., Liebau, S., Hohwieler, M., Bohnenberger, H., Lesina, M., Algül, H., Gieldon, L., Schröck, E., Gaedcke, J., Wagner, M., Wiesmüller, L., Sipos, B., Seufferlein, T., Reinhardt, H. C., Frappart, P.-O., and Kleger, A. (2017). ATM Deficiency Generating Genomic Instability Sensitizes Pancreatic Ductal Adenocarcinoma Cells to Therapy-Induced DNA Damage. *Cancer Research*, 77(20):5576–5590.

Porteus, M. (2007). Using homologous recombination to manipulate the genome of human somatic cells. *Biotechnology and Genetic Engineering Reviews*, 24(1):195–212.

Reisländer, T., Groelly, F. J., and Tarsounas, M. (2020). DNA Damage and Cancer Immunotherapy: A STING in the Tale.

Reisländer, T., Lombardi, E. P., Groelly, F. J., Miar, A., Porru, M., Di Vito, S., Wright, B., Lockstone, H., Biroccio, A., Harris, A., Londoño-Vallejo, A., and Tarsounas, M. (2019). BRCA2 abrogation triggers innate immune responses potentiated by treatment with PARP inhibitors. *Nature Communications*, 10(1).

Rickman, K. and Smogorzewska, A. (2019). Advances in understanding DNA processing and protection at stalled replication forks.

Riffell, J. L., Zimmerman, C., Khong, A., McHardy, L. M., and Roberge, M. (2009). Effects of chemical manipulation of mitotic arrest and slippage on cancer cell survival and proliferation. *Cell Cycle*, 8(18):3029–3042.

Rizzo, A., Salvati, E., Porru, M., D'Angelo, C., Stevens, M. F., D'Incalci, M., Leonetti, C., Gilson, E., Zupi, G., and Biroccio, A. (2009). Stabilization of quadruplex DNA perturbs telomere replication leading to the activation of an ATR-dependent ATM signaling pathway. *Nucleic Acids Research*, 37(16):5353–5364.

Rodriguez, R., Miller, K. M., Forment, J. V., Bradshaw, C. R., Nikan, M., Britton, S., Oelschlaegel, T., Xhemalce, B., Balasubramanian, S., and Jackson, S. P. (2012). Small-molecule-induced DNA damage identifies alternative DNA structures in human genes. *Nature Chemical Biology*, 8(3):301–310.

Rowinsky, E. K., Eisenhauer, E. A., Chaudhry, V., Arbuck, S. G., and Donehower, R. C. (1993). Clinical toxicities encountered with paclitaxel (TAXOL®). In *Seminars in Oncology*, volume 20, pages 1–15. W.B. Saunders Ltd.

Rowinsky, E. K. M. and Donehower, R. C. M. (1995). Paclitaxel (Taxol). *New England Journal of Medicine*, 333(1):75–75.

Saitoh, T., Fujita, N., Hayashi, T., Takahara, K., Satoh, T., Lee, H., Matsunaga, K., Kageyama, S., Omori, H., Noda, T., Yamamoto, N., Kawai, T., Ishii, K., Takeuchi, O., Yoshimori, T., and Akira, S. (2009). Atg9a controls dsDNA-driven dynamic translocation of STING and the innate immune response. *Proceedings of the National Academy of Sciences of the United States of America*, 106(49):20842–20846.

Schärer, O. D. (2013). Nucleotide excision repair in Eukaryotes.

Schiff, P. B., Fant, J., and Horwitz, S. B. (1979). Promotion of microtubule assembly in vitro by taxol [19].

Schultze, P., Hud, N. V., Smith, F. W., and Feigon, J. (1999). The effect of sodium, potassium and ammonium ions on the conformation of the dimeric quadruplex formed by the Oxytricha nova telomere repeat oligonucleotide d(G 4 T 4 G 4). *Nucleic Acids Research*, 27(15):3018–3028.

Sen, T., Rodriguez, B. L., Chen, L., Della Corte, C. M., Morikawa, N., Fujimoto, J., Cristea, S., Nguyen, T., Diao, L., Li, L., Fan, Y., Yang, Y., Wang, J., Glisson, B. S., Wistuba, I. I., Sage, J., Heymach, J. V., Gibbons, D. L., and Byers, L. A. (2019). Targeting DNA damage response promotes antitumor immunity through STING-mediated T-cell activation in small cell lung cancer. *Cancer Discovery*, 9(5):646–661.

Servant, M. J., Grandvaux, N., TenOever, B. R., Duguay, D., Lin, R., and Hiscott, J. (2003). Identification of the minimal phosphoacceptor site required for in vivo activation of interferon regulatory factor 3 in response to virus and double-stranded RNA. *Journal of Biological Chemistry*, 278(11):9441–9447.

Sharan, S. K., Morimatsu, M., Albrecht, U., Lim, D. S., Regel, E., Dinh, C., Sands, A., Eichele, G., Hasty, P., and Bradley, A. (1997). Embryonic lethality and radiation hypersensitivity mediated by Rad51 in mice lacking Brca2. *Nature*, 386(6627):804–810.

Siddik, Z. H. (2003). Cisplatin: Mode of cytotoxic action and molecular basis of resistance.

Singla, A. K., Garg, A., and Aggarwal, D. (2002). Paclitaxel and its formulations. *International Journal of Pharmaceutics*, 235(1-2):179–192.

Spivak, G. (2015). Nucleotide excision repair in humans.

Stewart, Z. A., Mays, D., and Pietenpol, J. A. (1999). Defective G1-S Cell Cycle Checkpoint Function Sensitizes Cells to Microtubule Inhibitor-induced Apoptosis. *Cancer Research*, 59(15).

Stracker, T. H. and Petrini, J. H. (2011). The MRE11 complex: Starting from the ends.

Sun, L., Wu, J., Du, F., Chen, X., and Chen, Z. J. (2013). Cyclic GMP-AMP synthase is a cytosolic DNA sensor that activates the type I interferon pathway. *Science*, 339(6121):786–791.

Sun, Z. Y., Wang, X. N., Cheng, S. Q., Su, X. X., and Ou, T. M. (2019). Developing novel G-quadruplex ligands: From interaction with nucleic acids to interfering with nucleic acid–protein interaction.

Swanton, C., Marani, M., Pardo, O., Warne, P. H., Kelly, G., Sahai, E., Elustondo, F., Chang, J., Temple, J., Ahmed, A. A., Brenton, J. D., Downward, J., and Nicke, B. (2007). Regulators of Mitotic Arrest and Ceramide Metabolism Are Determinants of Sensitivity to Paclitaxel and Other Chemotherapeutic Drugs. *Cancer Cell*, 11(6):498–512.

Symington, L. S. and Gautier, J. (2011). Double-Strand Break End Resection and Repair Pathway Choice. *Annual Review of Genetics*, 45(1):247–271.

Tahara, H., Shin-ya, K., Seimiya, H., Yamada, H., Tsuruo, T., and Ide, T. (2006). G-Quadruplex stabilization by telomestatin induces TRF2 protein dissociation from telomeres and anaphase bridge formation accompanied by loss of the 3 telomeric overhang in cancer cells. *Oncogene*, 25(13):1955–1966.

Tanaka, Y. and Chen, Z. J. (2012). STING specifies IRF3 phosphorylation by TBK1 in the cytosolic DNA signaling pathway. *Science signaling*, 5(214):ra20.

Ten Tije, A. J., Smorenburg, C. H., Seynaeve, C., Sparreboom, A., Schothorst, K. L., Kerkhofs, L. G., Van Reisen, L. G., Stoter, G., Bontenbal, M., and Verweij, J. (2004). Weekly paclitaxel as first-line chemotherapy for elderly patients with metastatic breast cancer. A multicentre phase II trial. *European Journal of Cancer*, 40(3):352–357.

Tippana, R., Xiao, W., and Myong, S. (2014). G-quadruplex conformation and dynamics are determined by loop length and sequence. *Nucleic Acids Research*, 42(12):8106–8114.

Todd, A. K., Johnston, M., and Neidle, S. (2005). Highly prevalent putative quadruplex sequence motifs in human DNA. *Nucleic Acids Research*, 33(9):2901–2907.

Truong, L. N., Li, Y., Shi, L. Z., Hwang, P. Y. H., He, J., Wang, H., Razavian, N., Berns, M. W., and Wu, X. (2013). Microhomology-mediated End Joining and Homologous Recombination share the initial end resection step to repair DNA double-strand breaks in mammalian cells. *Proceedings of the National Academy of Sciences of the United States of America*, 110(19):7720–7725.

Tubbs, A. and Nussenzweig, A. (2017a). Endogenous DNA Damage as a Source of Genomic Instability in Cancer.

Tubbs, A. and Nussenzweig, A. (2017b). Leading Edge Review Endogenous DNA Damage as a Source of Genomic Instability in Cancer. *Cell*, 168:644–656.

Turner, N., Tutt, A., and Ashworth, A. (2005). Targeting the DNA repair defect of BRCA tumours.

Tutt, A. and Ashworth, A. (2002). The relationship between the roles of BRCA genes in DNA repair and cancer predisposition.

Tutt, A., Bertwistle, D., Valentine, J., Gabriel, A., Swift, S., Ross, G., Griffin, C., Thacker, J., and Ashworth, A. (2001). Mutation in Brca2 stimulates error-prone homology-directed repair of DNA double-strand breaks occurring between repeated sequences. *The EMBO Journal*, 20(17):4704–4716.

Tutt, A., Robson, M., Garber, J. E., Domchek, S., Audeh, M. W., Weitzel, J. N., Friedlander, M., and Carmichael, J. (2009). Phase II trial of the oral PARP inhibitor olaparib in BRCA-deficient advanced breast cancer. *Journal of Clinical Oncology*, 27(18_suppl):CRA501–CRA501.

Tutt, A., Robson, M., Garber, J. E., Domchek, S. M., Audeh, M. W., Weitzel, J. N., Friedlander, M., Arun, B., Loman, N., Schmutzler, R. K., Wardley, A., Mitchell, G., Earl, H., Wickens, M., and Carmichael, J. (2010). Oral poly(ADP-ribose) polymerase inhibitor olaparib in patients with BRCA1 or BRCA2 mutations and advanced breast cancer: A proof-of-concept trial. *The Lancet*, 376(9737):235–244.

van Oosterom, A. T. (1995). Docetaxel (Taxotere): an effective agent in the management of second-line breast cancer. *Seminars in oncology*, 22(6 Suppl 13):22–8.

Vanpouille-Box, C., Demaria, S., Formenti, S. C., and Galluzzi, L. (2018). Cytosolic DNA Sensing in Organismal Tumor Control.

Venkitaraman, A. R. (1999). Breast cancer genes and DNA repair.

Verweij, J., Clavel, M., and Chevalier, B. (1994). Paclitaxel (Taxol™) and docetaxel (Taxotere™): Not simply two of a kind. *Annals of Oncology*, 5(6):495–505.

Vousden, K. H. and Lu, X. (2002). Live or let die: The cell's response to p53.

Wall, M. E. and Warn, M. C. (1995). Camptothecin and Taxol: Discovery to Clinic - Thirteenth Bruce F. Cain Memorial Award Lecture'. Technical report.

Walsh, V. and Goodman, J. (2002). The billion dollar molecule: Taxol in historical and theoretical perspective. *Clio medica (Amsterdam, Netherlands)*, 66:245–267.

Wang, H., Shi, L. Z., Wong, C. C., Han, X., Hwang, P. Y. H., Truong, L. N., Zhu, Q., Shao, Z., Chen, D. J., Berns, M. W., Yates, J. R., Chen, L., and Wu, X. (2013). The Interaction of CtIP and Nbs1 Connects CDK and ATM to Regulate HR-Mediated Double-Strand Break Repair. *PLoS Genetics*, 9(2).

Wang, Y., Yang, J., Wild, A. T., Wu, W. H., Shah, R., Danussi, C., Riggins, G. J., Kannan, K., Sulman, E. P., Chan, T. A., and Huse, J. T. (2019). G-quadruplex DNA drives genomic instability and represents a targetable molecular abnormality in ATRX-deficient malignant glioma. *Nature Communications*, 10(1):1–14.

Wani, M. C., Taylor, H. L., Wall, M. E., Coggon, P., and Mcphail, A. T. (1971). Plant Antitumor Agents.VI.The Isolation and Structure of Taxol, a Novel Antileukemic and Antitumor Agent from Taxus brevifolia2. *Journal of the American Chemical Society*, 93(9):2325–2327.

Weaver, B. A. (2014). How Taxol/paclitaxel kills cancer cells.

Weitzmann, M. N., Woodford, K. J., and Usdin, K. (1996). The development and use of a DNA polymerase arrest assay for the evaluation of parameters affecting intrastrand tetraplex formation. *Journal of Biological Chemistry*, 271(34):20958–20964.

Whitby, M. C. (2007). Holliday junction resolution. pages 169–199. Springer, Berlin, Heidelberg.

White, D. E., Negorev, D., Peng, H., Ivanov, A. V., Maul, G. G., and Rauscher, F. J. (2006). KAP1, a novel substrate for PIKK family members, colocalizes with numerous damage response factors at DNA lesions. *Cancer Research*, 66(24):11594–11599.

Williams, R. S., Dodson, G. E., Limbo, O., Yamada, Y., Williams, J. S., Guenther, G., Classen, S., Glover, J. N., Iwasaki, H., Russell, P., and Tainer, J. A. (2009). Nbs1 Flexibly Tethers Ctp1 and Mre11-Rad50 to Coordinate DNA Double-Strand Break Processing and Repair. *Cell*, 139(1):87–99.

Woo, S. R., Corrales, L., and Gajewski, T. F. (2015). The STING pathway and the T cell-inflamed tumor microenvironment.

Xu, H., Di Antonio, M., McKinney, S., Mathew, V., Ho, B., O'Neil, N. J., Santos, N. D., Silvester, J., Wei, V., Garcia, J., Kabeer, F., Lai, D., Soriano, P., Banáth, J., Chiu, D. S., Yap, D., Le, D. D., Ye, F. B., Zhang, A., Thu, K., Soong, J., Lin, S. C., Tsai, A. H. C., Osako, T., Algara, T., Saunders, D. N., Wong, J., Xian, J., Bally, M. B., Brenton, J. D., Brown, G. W., Shah, S. P., Cescon, D., Mak, T. W., Caldas, C., Stirling, P. C., Hieter, P., Balasubramanian, S., and Aparicio, S. (2017). CX-5461 is a DNA G-quadruplex stabilizer with selective lethality in BRCA1/2 deficient tumours. *Nature Communications*, 8(1):1–18.

Yan, S., Xuan, J., Brajanovski, N., Tancock, M. R., Madhamshettiwar, P. B., Simpson, K. J., Ellis, S., Kang, J., Cullinane, C., Sheppard, K. E., Hannan, K. M., Hannan, R. D., Sanij, E., Pearson, R. B., and Chan, K. T. (2020). The RNA polymerase I transcription inhibitor CX-5461 cooperates with topoisomerase 1 inhibition by enhancing the DNA damage response in homologous recombination-proficient high-grade serous ovarian cancer. *British Journal of Cancer*, pages 1–12.

Yang, H., Wang, H., Ren, U., Chen, Q., and Chena, Z. J. (2017). CGAS is essential for cellular senescence. *Proceedings of the National Academy of Sciences of the United States of America*, 114(23):E4612–E4620.

Yao, Y. X., Xu, B. H., and Zhang, Y. (2018). CX-3543 Promotes Cell Apoptosis through Down-regulation of CCAT1 in Colon Cancer Cells. *BioMed Research International*, 2018.

Zeman, M. K. and Cimprich, K. A. (2014). Causes and consequences of replication stress.

Zhao, W., Steinfeld, J. B., Liang, F., Chen, X., Maranon, D. G., Jian Ma, C., Kwon, Y., Rao, T., Wang, W., Sheng, C., Song, X., Deng, Y., Jimenez-Sainz, J., Lu, L., Jensen, R. B., Xiong, Y., Kupfer, G. M., Wiese, C., Greene, E. C., and Sung, P. (2017a). BRCA1-BARD1 promotes RAD51-mediated homologous DNA pairing. *Nature*, 550(7676):360–365.

Zhao, X., Wei, C., Li, J., Xing, P., Li, J., Zheng, S., and Chen, X. (2017b). Cell cycle-dependent control of homologous recombination. *Acta Biochim Biophys Sin*, (8):655–668.

Zharkov, D. O. (2008). Base excision DNA repair.

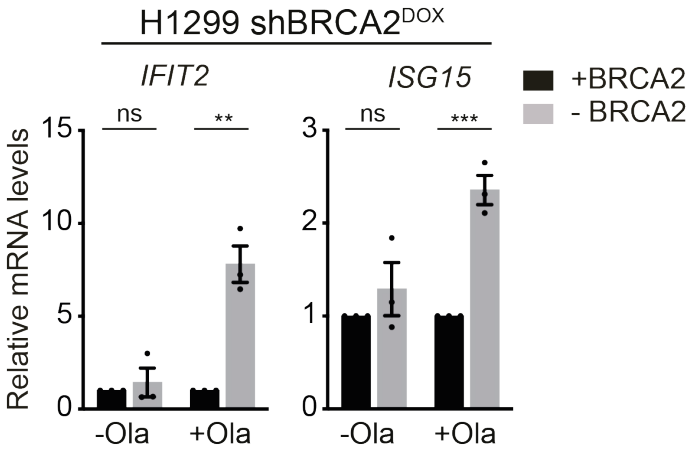
Zhong, B., Yang, Y., Li, S., Wang, Y. Y., Li, Y., Diao, F., Lei, C., He, X., Zhang, L., Tien, P., and Shu, H. B. (2008). The Adaptor Protein MITA Links Virus-Sensing Receptors to IRF3 Transcription Factor Activation. *Immunity*, 29(4):538–550.

Zierhut, C., Yamaguchi, N., Paredes, M., Luo, J. D., Carroll, T., and Funabiki, H. (2019). The Cytoplasmic DNA Sensor cGAS Promotes Mitotic Cell Death. *Cell*, 178(2):302–315.

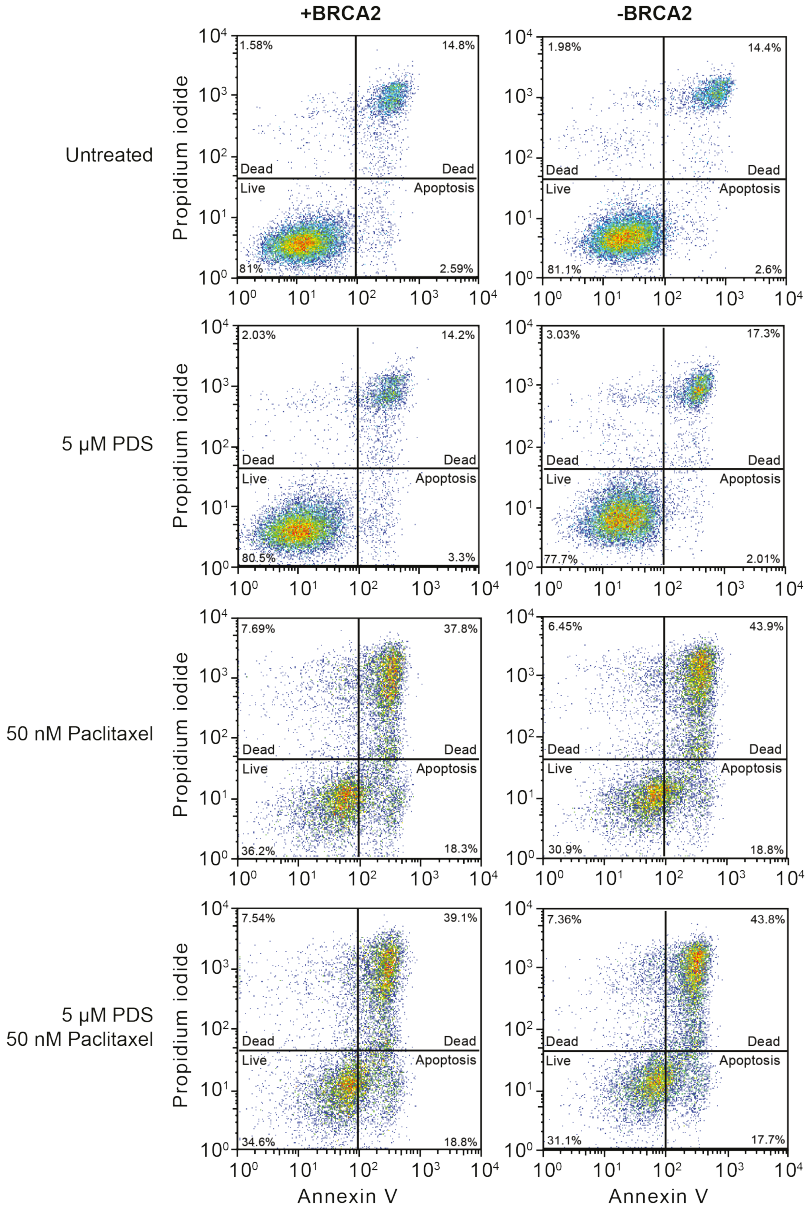
Zimmer, J., Tacconi, E. M., Folio, C., Badie, S., Porru, M., Klare, K., Tumiati, M., Markkanen, E., Halder, S., Ryan, A., Jackson, S. P., Ramadan, K., Kuznetsov, S. G., Biroccio, A., Sale, J. E., and Tarsounas, M. (2016). Targeting BRCA1 and BRCA2 Deficiencies with G-Quadruplex-Interacting Compounds. *Molecular Cell*, 61(3):449–460.

Zuffo, M., Guédin, A., Leriche, E. D., Doria, F., Pirota, V., Gabelica, V., Mergny, J. L., and Freccero, M. (2018). More is not always better: Finding the right trade-off between affinity and selectivity of a G-quadruplex ligand. *Nucleic Acids Research*, 46(19):115.

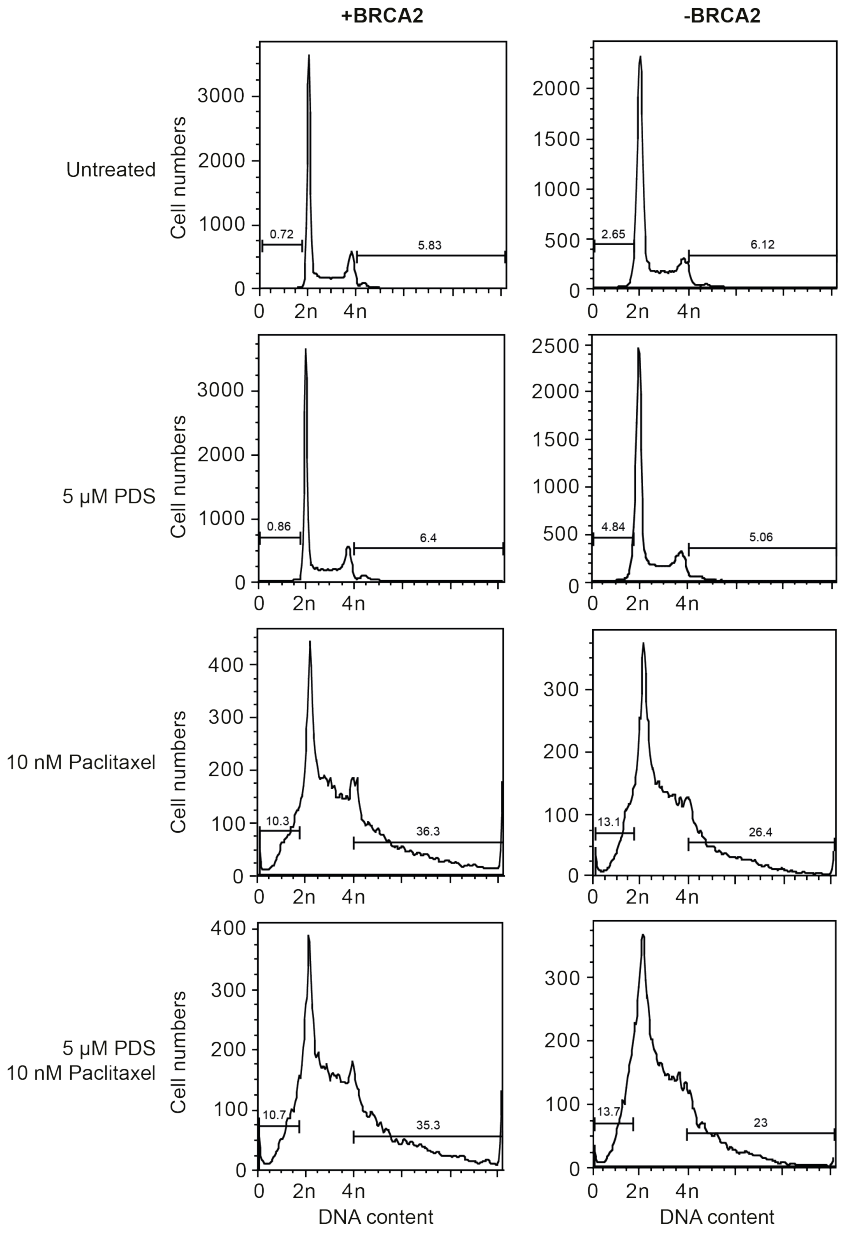
8 Appendix



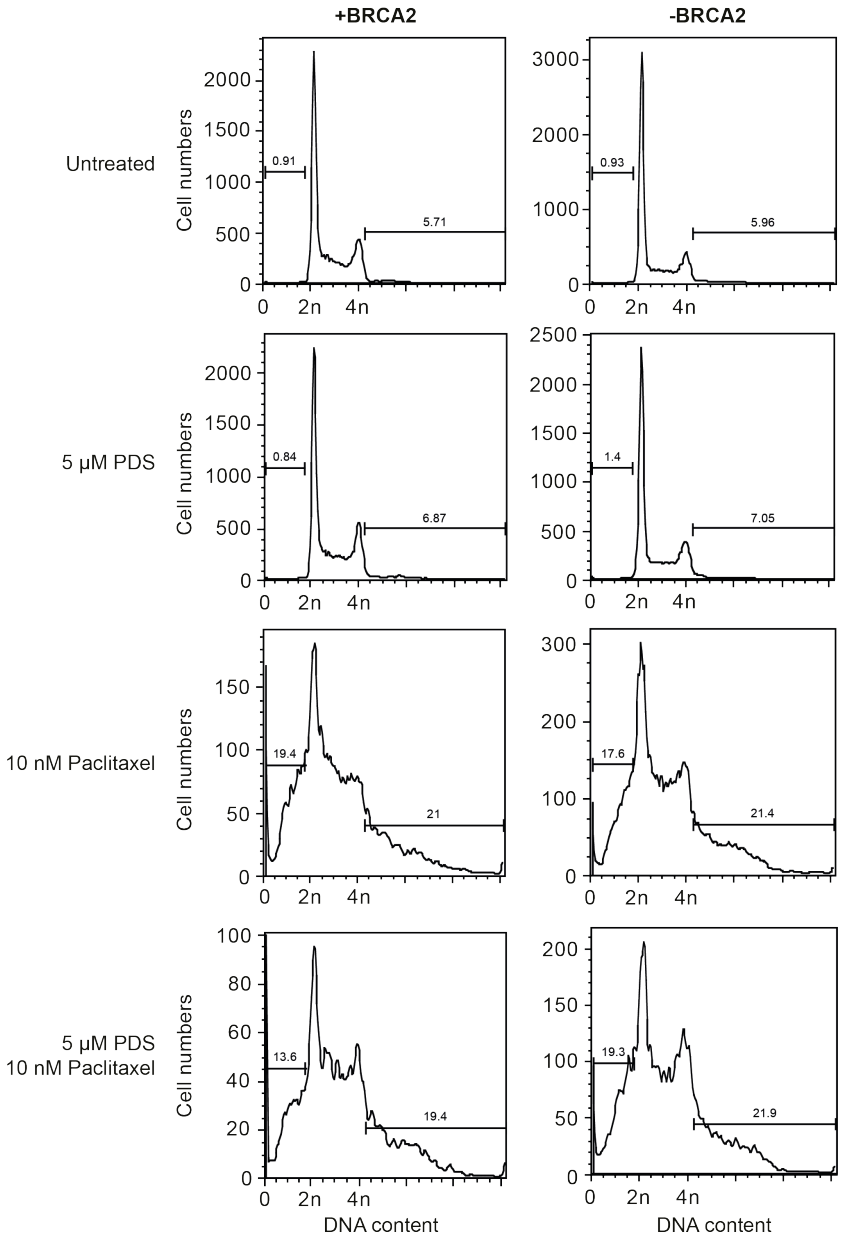
Supplementary Figure 1: Innate immune response activation in H1299 upon treatment with olaparib. H1299 shBRCA2^{DOX} were pre-treated for 4 days with or without 2 µg/mL DOX prior to further treatment. Subsequently, the cells were cultured in the absence (-Ola) of olaparib or with 5 µM (+Ola) for 3 days. RNA was extracted, reverse transcribed to cDNA and used for qPCR analysis using specific primers for the indicated genes. The mRNA levels were normalised to the mRNA levels of GAPDH and the -BRCA2 samples. The graphs represent the $2^{-\Delta\Delta C^t}$ value. Error bars represent standard error of the mean (SEM) of n = 3 technical replicates. NS: $p > 0.05$; *: $p < 0.05$; **: $p \leq 0.01$; ***: $p \leq 0.001$ (unpaired two-tailed t-test).



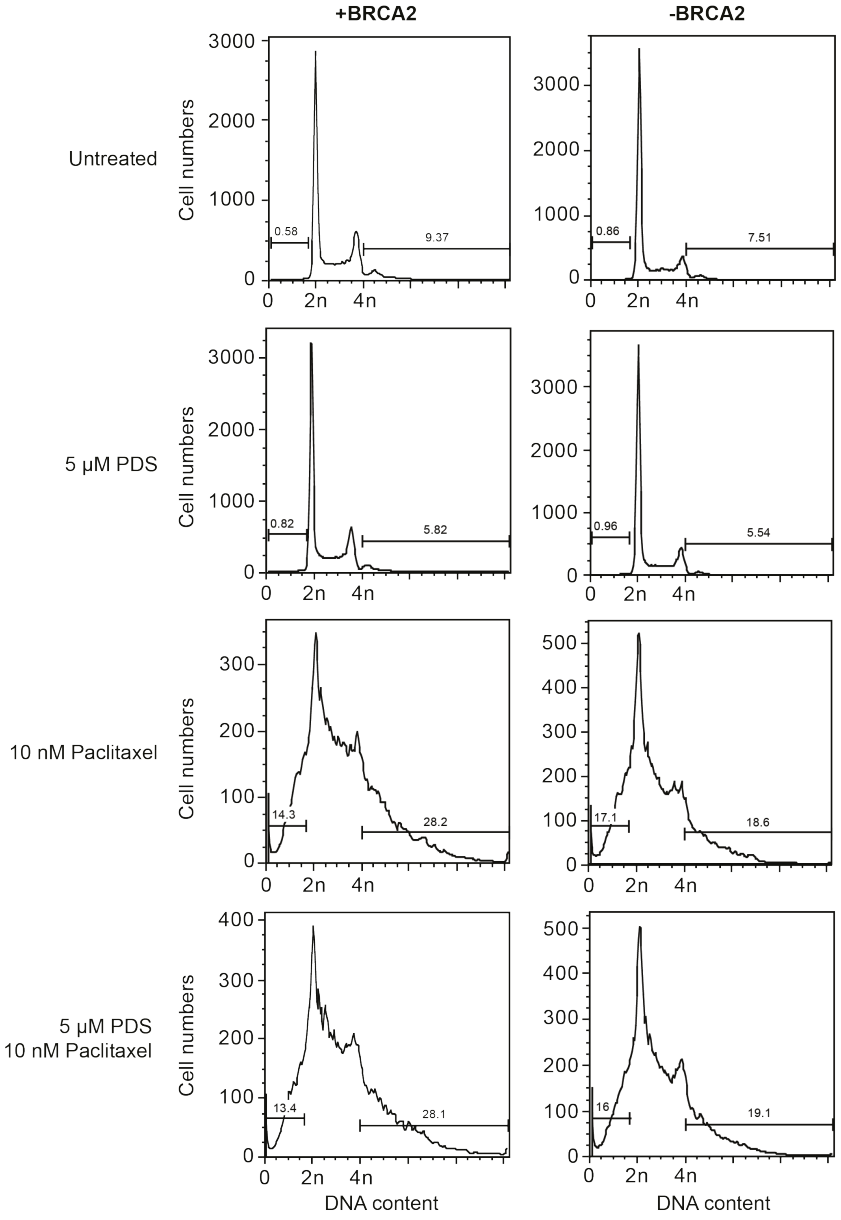
Supplementary Figure 2: No synergistic effect on triggering apoptosis *in vitro* upon combination treatment. Apoptotic cell fraction induced by single or combination treatment with PDS and paclitaxel in *BRCA2*$^{+/+}$ and *BRCA2*$^{-/-}$. Cells were pre-treated with 2 µg/mL DOX for 4 days prior to further treatment. Subsequently, the cells were treated for 3 days with 5 µM PDS and/or 10 nM of paclitaxel and 2 µg/mL DOX as indicated. The Dead Cell Apoptosis Kit with Annexin V Alexa Fluor™ 488 was used to stain the cells and DNA was stained with propidium iodide. The percentage of living, dead or apoptotic cells was determined via flow cytometry analysis. n = 1 independent experiments.



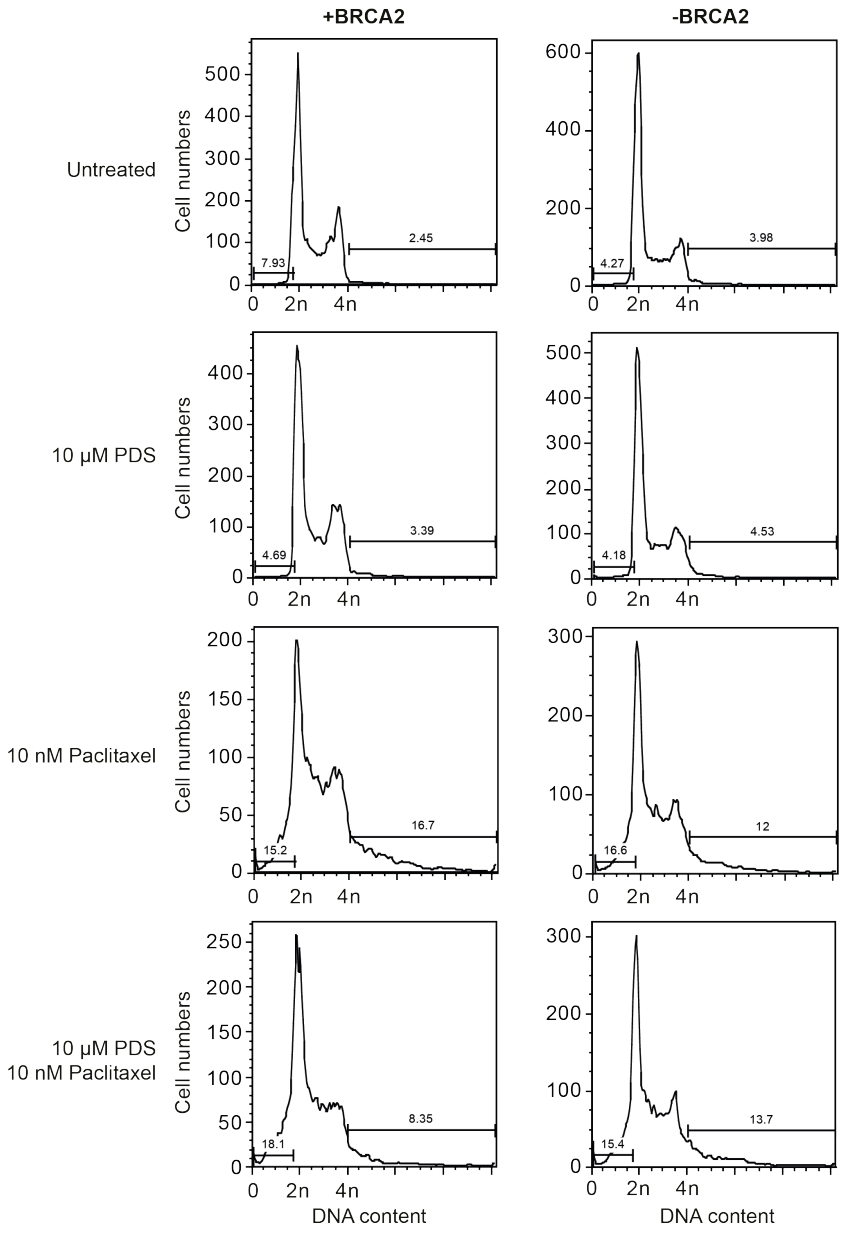
Supplementary Figure 3: The influence of single and combination treatment on the cell cycle and DNA content of H1299 - Replicate 1. H1299 shBRCA2^{DOX} were pre-treated for 2 days with or without 2 µg/mL DOX prior to further treatment. Subsequently, the cells were treated for 3 days with 5 µM PDS and/or 10 nM of paclitaxel and 2 µg/mL DOX as indicated. Cells were labelled with EdU for 30 minutes prior to harvesting and the DNA was stained with propidium iodide. The cell cycle distribution was determined via flow cytometry analysis.



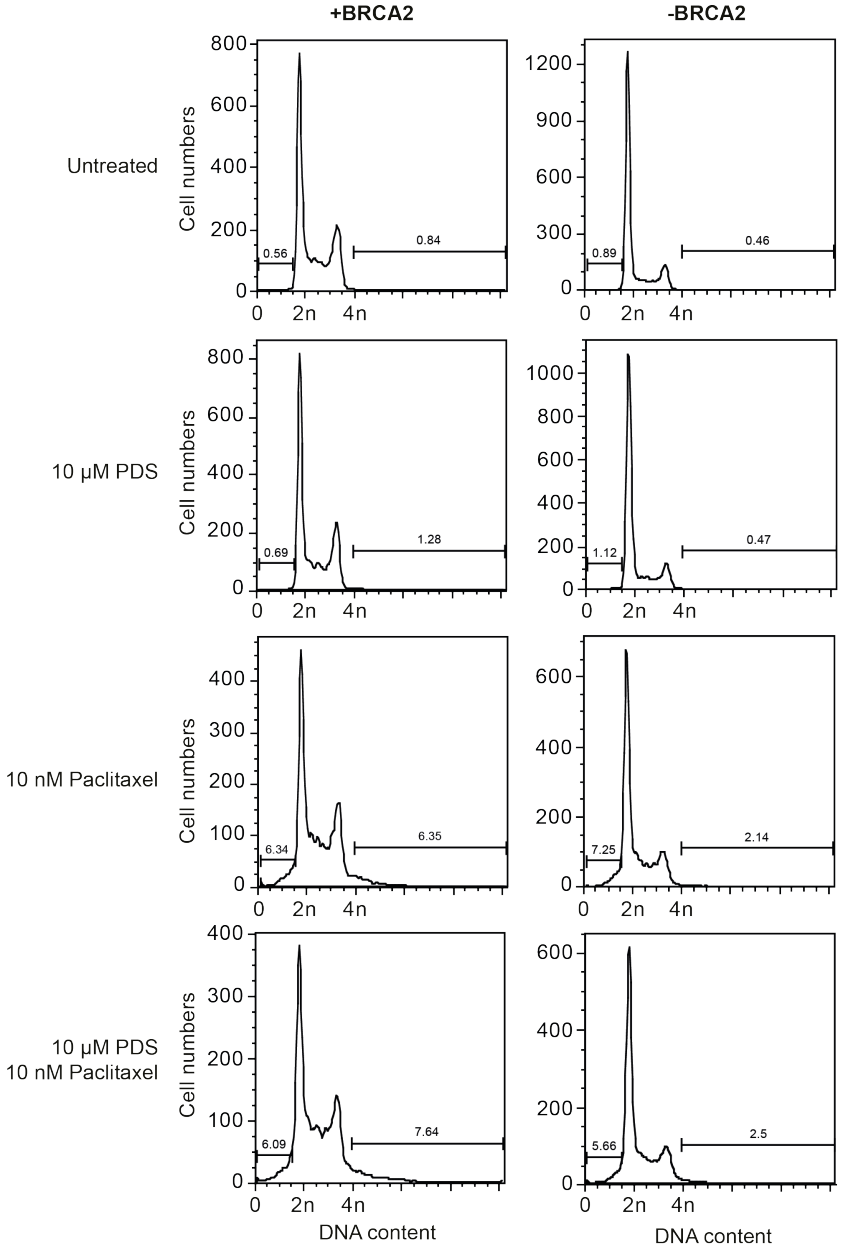
Supplementary Figure 4: The influence of single and combination treatment on the cell cycle and chromosomal content of H1299 - Replicate 2. H1299 shBRCA2^{DOX} were pre-treated for 2 days with or without 2 µg/mL DOX prior to further treatment. Subsequently, the cells were treated for 3 days with 5 µM PDS and/or 10 nM of paclitaxel and 2 µg/mL DOX as indicated. Cells were labelled with EdU for 30 minutes prior to harvesting and the DNA was stained with propidium iodide. The cell cycle distribution was determined via flow cytometry analysis.



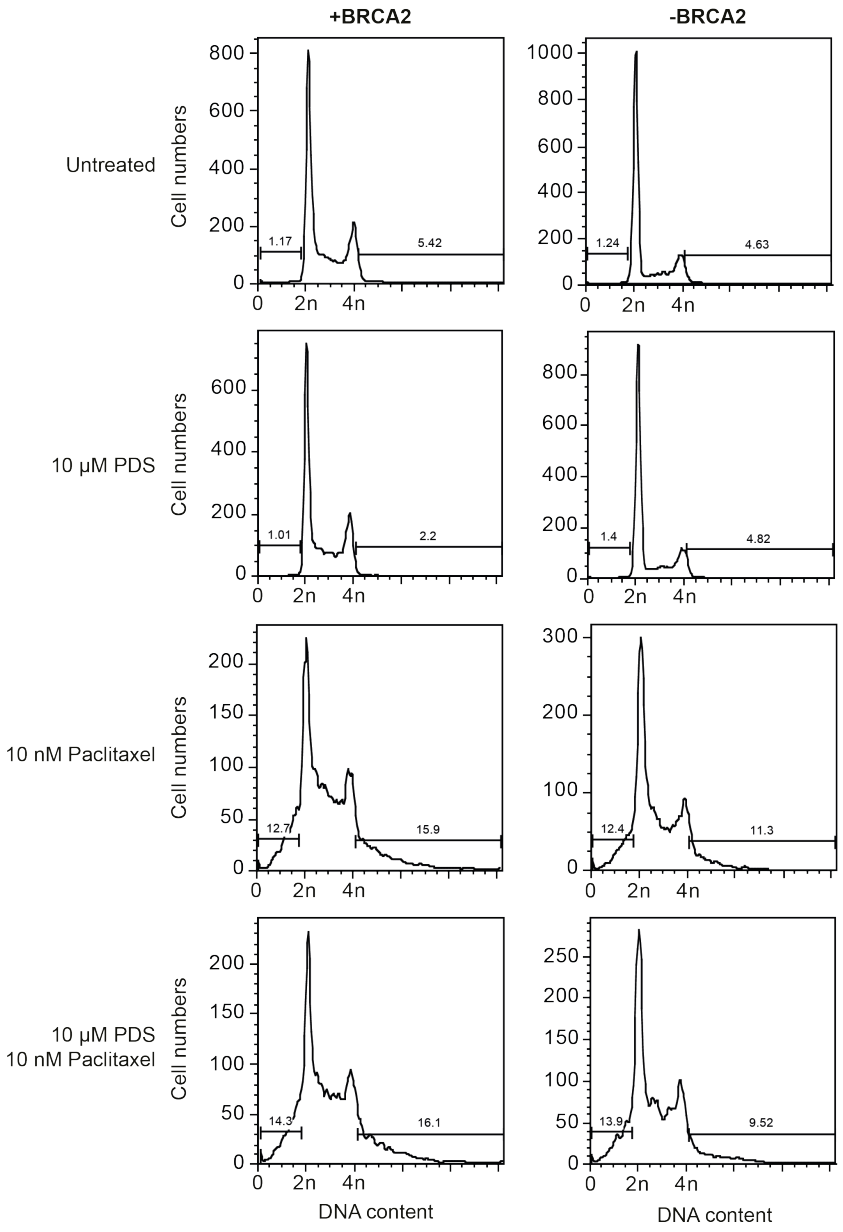
Supplementary Figure 5: The influence of single and combination treatment on the cell cycle and chromosomal content of H1299 - Replicate 3. H1299 shBRCA2^{DOX} were pre-treated for 2 days with or without 2 µg/mL DOX prior to further treatment. Subsequently, the cells were treated for 3 days with 5 µM PDS and/or 10 nM of paclitaxel and 2 µg/mL DOX as indicated. Cells were labelled with EdU for 30 minutes prior to harvesting and the DNA was stained with propidium iodide. The cell cycle distribution was determined via flow cytometry analysis.



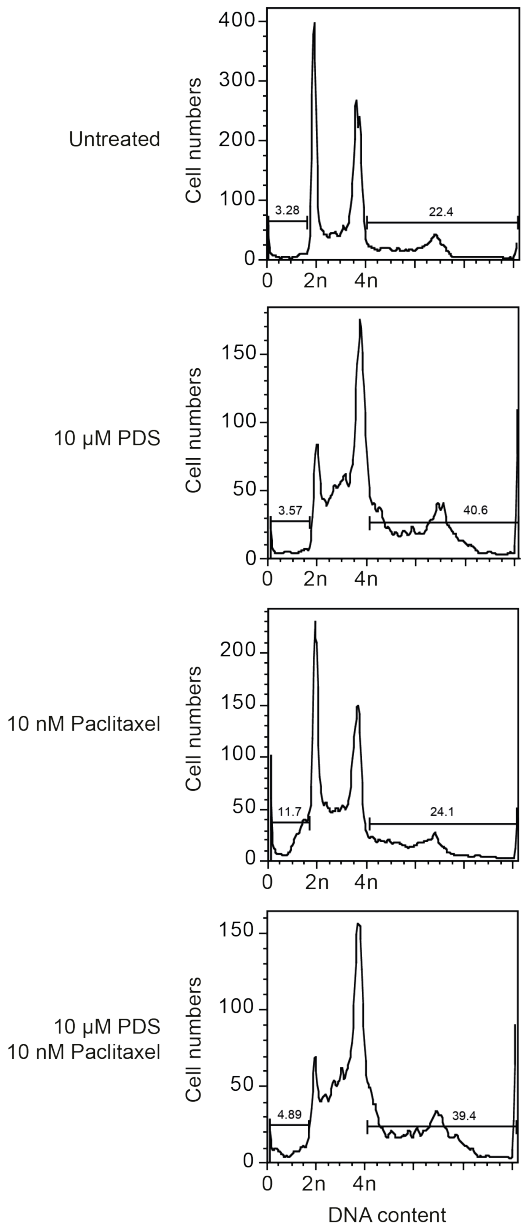
Supplementary Figure 6: The influence of single or combination treatment on the chromosomal content of H1299 - Replicate 1. H1299 shBRCA2^{DOX} were pre-treated for 2 days with or without 2 µg/mL DOX prior to further treatment. Subsequently, the cells were treated for 3 days with 10 µM PDS and/or 10 nM of paclitaxel and 2 µg/mL DOX as indicated. The DNA was stained with propidium iodide. The percentage "<G1" and ">G2/M" was determined via flow cytometry analysis.



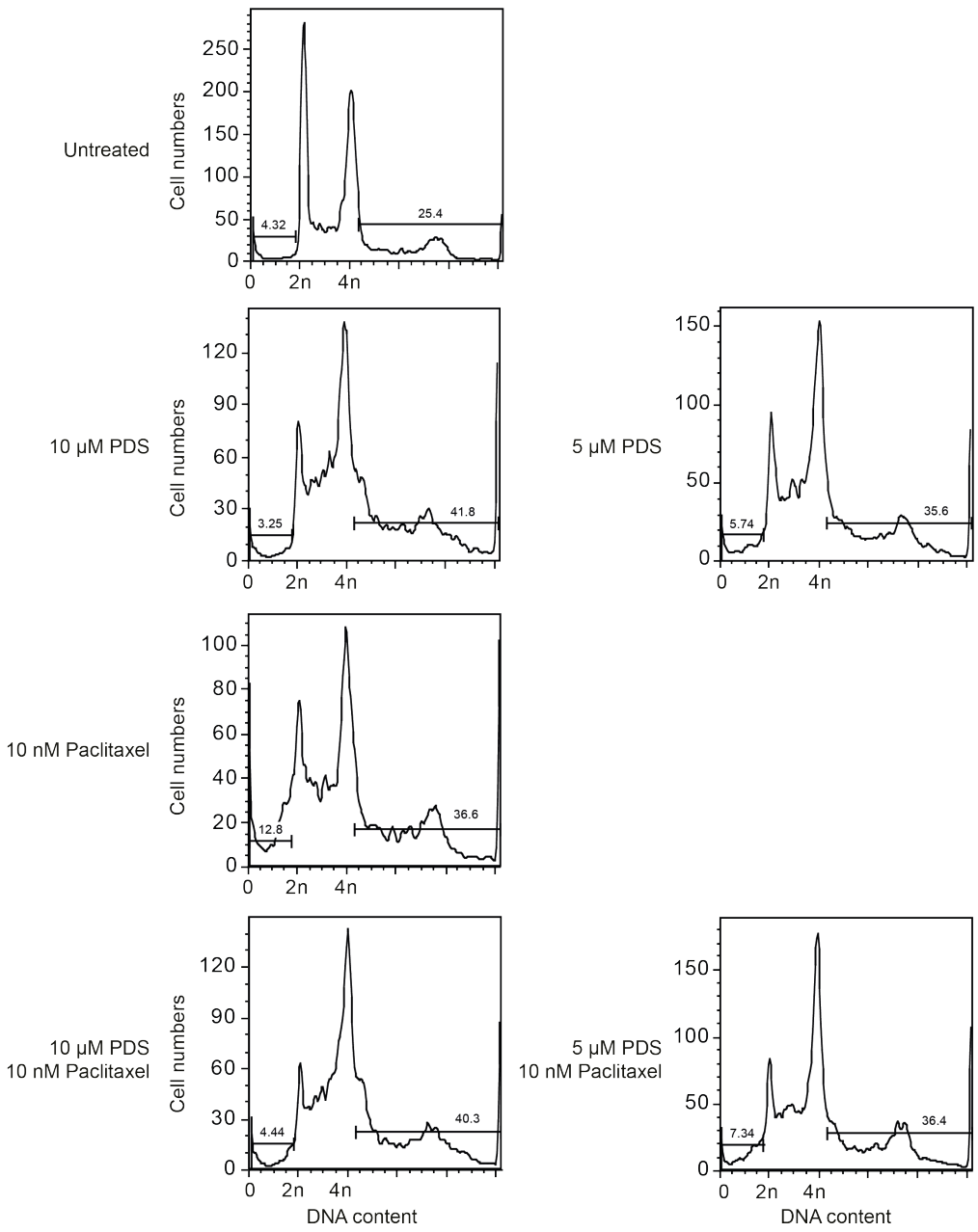
Supplementary Figure 7: The influence of single or combination treatment on the chromosomal content of H1299 - Replicate 2. H1299 shBRCA2^{DOX} were pre-treated for 2 days with or without 2 µg/mL DOX prior to further treatment. Subsequently, the cells were treated for 3 days with 10 µM PDS and/or 10 nM of paclitaxel and 2 µg/mL DOX as indicated. The DNA was stained with propidium iodide. The percentage "<G1" and ">G2/M" was determined via flow cytometry analysis.



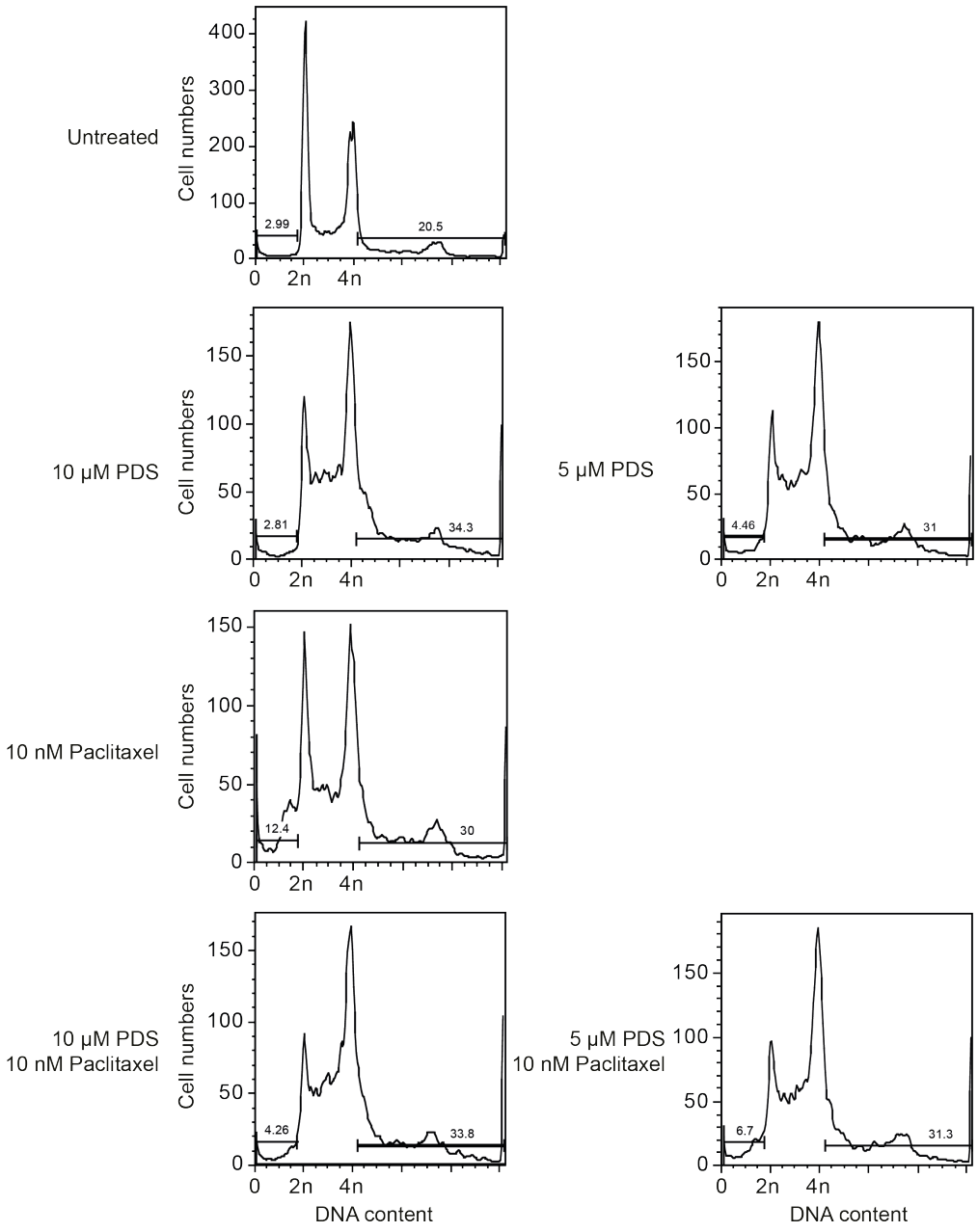
Supplementary Figure 8: The influence of single or combination treatment on the chromosomal content of H1299 - Replicate 3. H1299 shBRCA2^{DOX} were pre-treated for 2 days with or without 2 µg/mL DOX prior to further treatment. Subsequently, the cells were treated for 3 days with 10 µM PDS and/or 10 nM of paclitaxel and 2 µg/mL DOX as indicated. The DNA was stained with propidium iodide. The percentage "<G1" and ">G2/M" was determined via flow cytometry analysis.



Supplementary Figure 9: The influence of single or combination treatment on the chromosomal content of MDA-MB-436 - Replicate 1. MDA-MB-436 BRCA1$^{5396G>A}$ were treated for 3 days with 10 µM PDS and/or 10 nM of paclitaxel. The DNA was stained with propidium iodide. The percentage "<G1" and ">G2/M" was determined via flow cytometry analysis.



Supplementary Figure 10: The influence of single or combination treatment on the chromosomal content of MDA-MB-436 - Replicate 2. MDA-MB-436 BRCA1$^{5396G>A}$ were treated for 3 days with 5 or 10 µM PDS and/or 10 nM of paclitaxel. The DNA was stained with propidium iodide. The percentage "<G1" and ">G2/M" was determined via flow cytometry analysis.



Supplementary Figure 11: The influence of single or combination treatment on the chromosomal content of MDA-MB-436 - Replicate 3. MDA-MB-436 BRCA1$^{5396G>A}$ were treated for 3 days with 5 or 10 µM PDS and/or 10 nM of paclitaxel. The DNA was stained with propidium iodide. The percentage "<G1" and ">G2/M" was determined via flow cytometry analysis.